

NASA CR-101942

FLAW GROWTH BEHAVIOR OF INCONEL 718 AT ROOM AND CRYOGENIC TEMPERATURE

By

D. E. Pettit, C. E. Feddersen, H. Mindlin

Prepared for

THE BENDIX CORPORATION

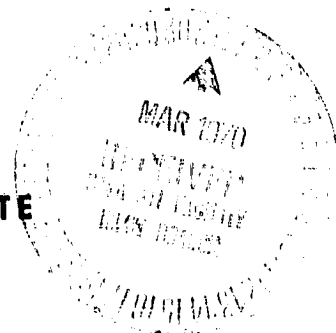
under

Prime Contract NAS 9-7689

with

NATIONAL AERONAUTICS & SPACE ADMINISTRATION

BATTELLE MEMORIAL INSTITUTE
Columbus Laboratories



N7U-23013

FAULTY FORM 900

| | |
|-------------------------------|------------|
| (THRU) | (CODE) |
| 96 | 17 |
| (ACCESSION NUMBER) | (PAGES) |
| NASA-CR-101942 | |
| (NASA CR OR TMX OR AD NUMBER) | (CATEGORY) |

This report was prepared as an account of Government sponsored work. Neither the United States, nor the National Aeronautics and Space Administration (NASA), nor any person acting on behalf of NASA:

- A.) Makes any warranty or representation, expressed or implied, with respect to the accuracy, completeness, or usefulness of the information contained in this report, or that the use of any information, apparatus, method, or process disclosed in this report may not infringe privately owned rights; or
- B.) Assumes any liabilities with respect to the use of, or for damages resulting from the use of any information, apparatus, method or process disclosed in this report.

As used above, "person acting on behalf of NASA" includes any employee or contractor of NASA, or employee of such contractor, to the extent that such employee or contractor of NASA, or employee of such contractor prepares, disseminates, or provides access to, any information pursuant to his employment or contract with NASA, or his employment with such contractor.

Requests for copies of this report should be referred to

National Aeronautics and Space Administration
Office of Scientific and Technical Information
Attention: AFSS-A
Washington, D. C. 20546

NASA CR 10/1942

FINAL REPORT

FLAW GROWTH BEHAVIOR OF INCONEL 718
AT ROOM AND CRYOGENIC TEMPERATURE

by

D. E. Pettit, C. E. Feddersen, H. Mindlin

BATTELLE MEMORIAL INSTITUTE
Columbus Laboratories
Columbus, Ohio

prepared for

THE BENDIX CORPORATION
INSTRUMENTS & LIFE SUPPORT DIVISION
DAVENPORT, IOWA

under

Prime Contract NAS 9-7689

with

NATIONAL AERONAUTICS & SPACE ADMINISTRATION
MANNED SPACECRAFT CENTER
HOUSTON, TEXAS

FLAW GROWTH BEHAVIOR OF INCONEL 718
AT ROOM AND CRYOGENIC TEMPERATURE

by

D. E. Pettit, C. E. Feddersen, H. Mindlin

ABSTRACT

The flaw growth characteristics of parent and welded Inconel 718 sheet and inter-
granularly formed material were determined at room and cryogenic temperatures for
surface-flawed specimens. Fracture tests, sustained-load tests, and fatigue-crack
propagation tests were conducted for these conditions in various environments including
trichlorofluoroethane (Ucon 113), liquid nitrogen, liquid oxygen, and liquid hydrogen.
The resulting data were then analyzed within the framework of linear elastic fracture
mechanics.

KEY WORDS

Inconel 718

Cryogenic temperature

Fracture

Sustained-load flaw growth

Fatigue-crack propagation rate

FOREWORD

In conjunction with Contract NAS 9-7689 between NASA-MSC and The Bendix Corporation, Instruments & Life Support Division, to supply Cryogenic Gas Storage Systems (CGSS) for the Apollo Applications Program, NASA required the use of Inconel 718 for pressure vessel applications. This requirement prompted NASA/MSC, Houston, Texas, to request Bendix to undertake a study of the flaw growth characteristics of Inconel 718 at room and cryogenic temperatures. The resulting program was conducted by the Columbus Laboratories of Battelle Memorial Institute acting as a subcontractor to the Instruments & Life Support Division of The Bendix Corporation. The results of this program, as reported herein, were completed between April 29, 1968, and October 31, 1969. The work was administered under the direction of Mr. C. R. Stone at Bendix, and technical cognizance of Mr. R. G. Forman at NASA/MSC as allocated by the prime contract technical monitor, Mr. Gordon Rysavy of NASA/MSC.

This work was performed by the Structural Materials Engineering Division of Battelle Memorial Institute, H. Mindlin, Division Chief, under the technical supervision of D. E. Pettit and C. E. Foddersen.

SUMMARY

The objective of this program was to determine the fracture, fatigue-crack propagation, and sustained-load flaw growth characteristics of surface-flawed base and tungsten inert gas (TIG) welded Inconel 718 sheet material for cryogenic tankage applications. Using linear elastic fracture mechanics, results of tests conducted on flat sheet specimens (Phase I) were analyzed and correlated with results from tests of specimens machined from a fabricated pressure vessel (Phase II).

The results of tests to determine the best of three heat treatments indicated that a 1360 F direct-age heat treatment of the flat sheet offered slightly better fracture and tensile properties at both room and liquid hydrogen temperatures. The specimens for the remainder of the program were then given this heat treatment by Bendix.

In Phase I, two possible proof-test environments, trichlorofluoroethane (Ucon 113) and liquid nitrogen, and two service environments, liquid oxygen and liquid hydrogen, were used for the flaw growth studies. The liquid nitrogen and liquid hydrogen had the most critical effect on fracture behavior of precracked surface-flawed specimens. That is, the lowest critical stress-intensity factor, K_{Ic} , was obtained in these environments. Liquid nitrogen and liquid hydrogen also were found to be the most critical on the fracture strength of welded specimens having flaws located on and parallel to the weld centerline. Additional fracture tests of similarly flawed weld specimens in liquid hydrogen indicated that the lack of a postweld heat treatment substantially reduced the critical stress-intensity factor.

In the tests conducted to determine the effect of environment on the flaw growth under sustained load, it was observed that the liquid-oxygen and liquid-hydrogen environments with the flaw located on the weld centerline were the most severe conditions.

In both liquid oxygen and liquid hydrogen environments, the results of fatigue-crack propagation tests of specimens with flaws located in the parent material and at the weld centerline indicated good correlation with the equation proposed by Forman^{(1)*}. However, two specimens tested under high mean-load and very small alternating stress conditions (simulating the pressure fluctuations that a tank could experience under operating conditions) exhibited a fatigue-crack propagation rate an order of magnitude higher than predicted by Forman's equation. It appears a more detailed examination of this problem is necessary.

In Phase II of the program, specimens cut from a fabricated pressure vessel were tested under certain similar (to Phase I) conditions to permit comparison with the results obtained from sheet specimens.

Room-temperature and liquid-hydrogen tensile test results on the parent and welded vessel material indicated no effect of location of the test specimen in the actual vessel. In general, the yield strengths and the ultimate strengths of the parent and welded vessel material were from 4 to 20 ksi lower than those observed for the flat sheet material. The one exception to this was the welded material tensile results in liquid hydrogen where the yield strength was equivalent to that of the flat sheet material and the average ultimate tensile strength was 32 ksi higher.

*Numbers in parentheses refer to references listed on page 71.

The results of liquid-oxygen and liquid-hydrogen fracture tests of flawed weld (vessel) specimens indicated an average stress-intensity factor of $61 \text{ ksi } \sqrt{\text{in.}}$ (at the tip of the flaw, maximum depth) for both environments. The corresponding stress-intensity factor at the surface was $85 \text{ ksi } \sqrt{\text{in.}}$. The analysis of this data did include a bending moment correction for the specimen curvature; however, since the surface material, in all cases, yielded prior to fracture, the stress-intensity factor computed at the tip of the flaw is believed to be more valid for the curved welded vessel material. The value of $61 \text{ ksi } \sqrt{\text{in.}}$ is considerably higher than the stress intensity factor, $52 \text{ ksi } \sqrt{\text{in.}}$, found for a flaw in a similar location in the welded flat sheet tested in the same cryogenic environments. Thus, within the limits of the bending corrections, the welded vessel material has at least equivalent and possibly superior fracture characteristics than has the flat sheet material.

The results of liquid-oxygen and liquid-hydrogen fatigue-crack propagation tests (at $R = 0$) on welded vessel material indicated a slightly lower propagation rate than predicted by Forman's equation. Thus, for a given stress-intensity factor at the tip of the crack, the fatigue-crack propagation rate will be lower in the welded vessel material than in the welded flat sheet material.

TABLE OF CONTENTS

| | <u>Page</u> |
|---|-------------|
| 1.0 INTRODUCTION | 1 |
| 2.0 TECHNICAL DISCUSSION | 3 |
| 2.1 Background | 3 |
| 2.2 Stress-Intensity Factors for Surface Flaws In Flat Plates | 3 |
| 2.3 The Effect of Curvature on Tensile Properties | 6 |
| 2.4 The Effect of Curvature on the Surface Flaw Stress- Intensity Factor | 7 |
| 3.0 MATERIALS | 11 |
| 3.1 Phase I Sheet Material | 11 |
| 3.2 Phase II Vessel Material | 11 |
| 4.0 PHASE I PROCEDURES | 13 |
| 4.1 Specimen Fabrication | 13 |
| 4.2 Tensile Test Procedures | 13 |
| 4.3 Fracture Test Procedures | 18 |
| 4.4 Sustained-Load Flaw Growth Test Procedures | 18 |
| 4.5 Fatigue-Crack Propagation Procedures | 23 |
| 5.0 PHASE II PROCEDURES | 25 |
| 5.1 Specimen Preparation | 25 |
| 5.2 Tensile and Fracture Test Procedures | 25 |
| 5.3 Fatigue Test Procedures | 25 |
| 6.0 PHASE I TEST RESULTS | 27 |
| 6.1 Selection of Heat Treatment for Inconel 718 Sheet Material | 27 |
| 6.2 Tensile Test Results | 27 |
| 6.3 Fracture Test Results | 32 |
| 6.4 Sustained-Load Flaw-Growth Results | 38 |
| 6.5 Fatigue-Crack Propagation Results (R = 0) | 50 |
| 6.6 Fatigue-Crack Propagation Rates Under High Mean-Stress Conditions | 62 |
| 7.0 PHASE II TEST RESULTS | 63 |
| 7.1 Tensile Test Results | 63 |
| 7.2 Fracture Test Results | 63 |
| 7.3 Fatigue-Crack Propagation Results | 66 |

TABLE OF CONTENTS
(Continued)

| | <u>Page</u> |
|---|-------------|
| 8.0 CONCLUDING DISCUSSION | 69 |
| References | 71 |
| APPENDIX A. ANALYSIS OF CURVATURE EFFECTS FOR VESSEL- MATERIAL SPECIMENS | A-1 |
| APPENDIX B. LIST OF SYMBOLS. | B-1 |

LIST OF ILLUSTRATIONS

| <u>Figure</u> | | <u>Page</u> |
|---------------|--|-------------|
| 1. | Procedure Used to Determine the Magnification Factor, M_K' | 5 |
| 2. | Schematic of Load Values Typically Associated With the Fracture Process. | 7 |
| 3. | Tensile Specimen Configuration | 14 |
| 4. | Specimen Configuration for Flaw Growth Studies | 15 |
| 5. | Baldwin Test Equipment With Cryogenic Dewar in Position | 16 |
| 6. | Extensometer Used During the Tensile Tests | 17 |
| 7. | Compliance Gage Used for the Fracture Tests | 19 |
| 8. | Sustained-Load Equipment Used for Liquid-Oxygen and Liquid-Hydrogen Tests | 20 |
| 9. | Control Console and Hydraulic System of the Battelle Cryogenic Testing Machine | 21 |
| 10. | Loading Chamber and Cryogenic Dewar of the Battelle Cryogenic Testing Machine | 22 |
| 11. | Sustained-Load Test Results for Welded Inconel 718 in Ucon 113 at Room Temperature | 41 |
| 12. | Sustained-Load Test Results for Parent Inconel 718 in Ucon 113 at Room Temperature | 42 |
| 13. | Sustained-Load Test Results for Welded Inconel 718 in Liquid Oxygen | 43 |
| 14. | Sustained-Load Test Results for Parent Inconel 718 in Liquid Oxygen | 44 |
| 15. | Sustained-Load Test Results for Welded Inconel 718 in Liquid Nitrogen | 45 |
| 16. | Sustained-Load Test Results for Parent Inconel 718 in Liquid Nitrogen | 46 |
| 17. | Typical Sustained-Load Flaw-Growth Specimen After Testing | 47 |
| 18. | Sustained-Load Flaw-Growth Rate for Inconel 718 Sheet Material in Liquid Hydrogen | 48 |
| 19. | Sustained-Load Flaw-Growth Results for Inconel 718 Material (Heat Affected Zone) Tested in Liquid Oxygen | 51 |

LIST OF ILLUSTRATIONS
(Continued)

| <u>Figure</u> | | <u>Page</u> |
|---------------|--|-------------|
| 20. | Sustained-Load Flaw-Growth Rates for Inconel 718 Sheet Material in Liquid Hydrogen | 52 |
| 21. | Welded Inconel 718 Sheet Material Fatigue Results in Liquid Oxygen, R = 0 | 54 |
| 22. | Measured Fatigue-Crack Propagation Rates for Parent Inconel 718 Tested in Liquid Oxygen and Liquid Hydrogen, R = 0 | 57 |
| 23. | Alternate Presentation of the Fatigue Results for Welded Inconel 718 Tested in Liquid Oxygen, R = 0 | 59 |
| 24. | Normalized Flaw Depth Versus K_{II}/K_{IC} for Welded Inconel 718 Specimens Fatigue Tested in Liquid Oxygen | 60 |
| 25. | Fatigue-Crack Propagation Rates for Welded Inconel 718 Tested in Liquid Oxygen and Liquid Hydrogen | 61 |
| 26. | Fatigue-Crack Propagation Rates for Welded Vessel Material Based on the Corrected Stress-Intensity Factor at $\alpha = 0$ | 68 |
| 27. | Schematic of the Effect of the Critical Stress-Intensity Factor on the Maximum Possible Flaw Size After Proof Testing | 70 |
| A-1. | Idealized Fixture Arrangements for Curved Specimens | A-2 |
| A-2. | Resulting Bending Moment in a Curved Specimen Subjected to Tension Loading | A-5 |
| A-3. | Load-Strain Profile for Curved Specimens Under Tension Loading | A-6 |

LIST OF TABLES

| <u>Table</u> | | <u>Page</u> |
|--------------|--|-------------|
| 1. | Phases of the Experimental Investigation | 1 |
| 2. | Stress-Intensity Magnification Factors for Surface Flaws as Per Reference (3) | 6 |
| 3. | Weld Parameters for Inconel 718 Sheet Material 0.113-Inch Thick . . | 11 |
| 4. | Room Temperature Tensile Results for Three Different Heat Treatments of Inconel 718 Sheet | 28 |
| 5. | Liquid Hydrogen Tensile Results for Three Different Heat Treatments of Inconel 718 Sheet | 29 |
| 6. | Preliminary Inconel 718 Weld Material Fracture Test Results in Liquid Hydrogen | 30 |
| 7. | Room Temperature and Liquid Hydrogen Tensile Results for Inconel 718 Sheet Material | 31 |
| 8. | Comparison of Average Tensile Properties for Inconel 718 Sheet Material | 31 |
| 9. | Tensile Test Results for Welded and Annealed Sheet Material in Liquid Nitrogen | 32 |
| 10. | Inconel 718 Parent Material Fracture Results in Ucon 113 | 33 |
| 11. | Inconel 718 Welded Material Fracture Results in Ucon 113 | 33 |
| 12. | Inconel 718 Parent Material Fracture Results in Liquid Oxygen . . . | 33 |
| 13. | Inconel 718 Welded Material Fracture Results in Liquid Oxygen . . . | 34 |
| 14. | Inconel 718 Parent Material Fracture Results in Liquid Nitrogen . . . | 34 |
| 15. | Inconel 718 Welded Material Fracture Results in Liquid Nitrogen . . . | 34 |
| 16. | Inconel 718 Parent Material Fracture Results in Liquid Hydrogen . . . | 35 |
| 17. | Inconel 718 Welded Material Fracture Results in Liquid Hydrogen . . . | 35 |
| 18. | Inconel 718 Weld (HAZ) Material Fracture Results in Liquid Nitrogen . | 36 |
| 19. | Inconel 718 Weld (HAZ) Material Fracture Results in Liquid Hydrogen . | 36 |
| 20. | Inconel 718 As-Welded Material Fracture Results in Liquid Hydrogen . | 36 |

LIST OF TABLES
(Continued)

| <u>Table</u> | | <u>Page</u> |
|--------------|--|-------------|
| 21. | Summary of Fracture Toughness Results for Parent and Weld Inconel 718 Sheet Material | 37 |
| 22. | Summary of the Average Fracture Results for Inconel 718 Sheet Material | 38 |
| 23. | Sustained-Load Flaw Growth Results for Inconel 718 Sheet Material Tested in Ucon 113 at Room Temperature. | 39 |
| 24. | Sustained-Load Flaw Growth Results for Inconel 718 Sheet Material Tested in Liquid Oxygen | 39 |
| 25. | Sustained-Load Flaw Growth Results for Inconel 718 Sheet Material Tested in Liquid Nitrogen | 40 |
| 26. | Sustained-Load Flaw Growth Results for Inconel 718 Sheet Material Tested in Liquid Hydrogen. | 49 |
| 27. | Summary of the Sustained-Load Flaw Growth Results for Inconel 718 Sheet Material. | 49 |
| 28. | Sustained-Load Flaw Growth Results in Liquid Oxygen for Specimens With the Flaw in the Heat-Affected Zone | 50 |
| 29. | Welded Inconel 718 Sheet Material Fatigue Results in Liquid Oxygen. | 53 |
| 30. | Fatigue-Crack Propagation Results for Parent Inconel 718 Tested in Liquid Oxygen | 55 |
| 31. | Fatigue-Crack Propagation Results for Parent Inconel 718 Tested in Liquid Hydrogen | 55 |
| 32. | Fatigue-Crack Propagation Results for Welded Inconel 718 Tested in Liquid Hydrogen | 56 |
| 33. | Computed Fatigue-Crack Propagation Rates for Welded Inconel 718 Tested in Liquid Oxygen | 58 |
| 34. | High Mean-Load Fatigue-Crack Propagation Results for Welded Inconel 718 Tested in Liquid Oxygen, Stress = 72 ± 8 ksi. | 62 |
| 35. | Room-Temperature Tensile Test Results for Pressure Vessel Material | 63 |
| 36. | Tensile Test Results for Pressure Vessel Material in Liquid Hydrogen. | 63 |

LIST OF TABLES
(Continued)

| <u>Table</u> | | <u>Page</u> |
|--------------|---|-------------|
| 37. | Uncorrected Inconel 718 Vessel Weld Material Fracture Results in Liquid Oxygen | 65 |
| 38. | Uncorrected Inconel 718 Vessel Weld Material Fracture Results in Liquid Hydrogen | 65 |
| 39. | Welded Pressure Vessel Material Fracture Results Corrected for Curvature | 65 |
| 40. | Fatigue-Crack Propagation Results for Welded Vessel Material Tested in Liquid Oxygen and in Liquid Hydrogen | 66 |

1.0 INTRODUCTION

This program was initiated to determine the flaw growth characteristics of Inconel 718 at room and cryogenic temperatures. The investigation was conducted in two phases as shown in Table 1. Phase I involved a comprehensive investigation of the flaw growth behavior of parent and TIG-welded Inconel 718 sheet material in trichlorofluoroethane (hereinafter referred to as Ucon 113), liquid nitrogen, liquid oxygen, and liquid hydrogen. In Phase II, the specimens were fabricated from TIG-welded Inconel 718 hemispheres formed by the Bendix Inturgescent Forming process. Selected flaw growth behavior tests were then conducted on the Phase II specimens in liquid oxygen and liquid hydrogen. The results of the Phase I and the Phase II tests were then compared to determine if the sheet material results correlated with those of the Phase II inturgescently formed material.

The results of this study are presented in the format of the current concepts of linear elastic fracture mechanics. When combined with the results from other NASA/ MSC programs, these data will form a basis for the determination of the reliability of individual pressure vessels. The following sections of this report present the technical framework and results for each of the two phases of the investigation.

TABLE 1. PHASES OF THE EXPERIMENTAL INVESTIGATION

| Condition | Environment | Test Result | | | |
|--|-----------------------------|-------------|----------|----------------|---------------------------|
| | | Tensile | Fracture | Sustained Load | Fatigue-Crack Propagation |
| <u>Phase I: Inconel 718 Sheet Material</u> | | | | | |
| Parent | Room Temperature Air | X | -- | -- | -- |
| | Ucon 113 (Room Temperature) | -- | X | X | -- |
| | LN ₂ (-320 F) | -- | X | X | -- |
| | LO ₂ (-297 F) | -- | X | X | X |
| | LH ₂ (-423 F) | X | X | X | X |
| Welded | Ucon 113 (Room Temperature) | X | X | X | -- |
| | LN ₂ (-320 F) | -- | X | X | -- |
| | LO ₂ (-297 F) | -- | X | X | X |
| | LH ₂ (1423 F) | X | X | X | X |
| | | | | | |
| <u>Phase II: Inturgescently Formed Inconel 718</u> | | | | | |
| Parent | Room Temperature Air | X | -- | -- | -- |
| | LO ₂ (-297 F) | -- | -- | -- | -- |
| | LH ₂ (-423 F) | X | -- | -- | -- |
| Welded | Room Temperature Air | X | -- | -- | -- |
| | LO ₂ (297 F) | -- | X | -- | X |
| | LH ₂ (-423 F) | X | X | -- | X |

2.0 TECHNICAL DISCUSSION

2.1 Background

In many cases, the use of high-strength materials in space hardware has been dictated by the weight limitations of the complete vehicle. The structural design must utilize the material to its maximum strength within the severe limitations of reliability and safety. In general, presently accepted design techniques have permitted the consideration of several of the more common strength criteria, such as ultimate tensile strength, yield strength, or fatigue. The required use of higher and higher strength materials has introduced the need for further considerations - such as notch sensitivity and effects of flaws introduced during fabrication or in-service use. In any critical application, the possible existence of flaws such as weld defects, fabrication or material defects, or corrosion-related cracking can seriously affect the service reliability of the structure.

In the past, nondestructive test techniques have been used to detect and screen out many of these defects. However, methods such as radiography and ultrasonics have limitations that may prevent the detection of defects below the sensitivity of the method being used. These undetected flaws, however, may still be large enough to endanger the integrity of the vessel.

Therefore, it is of prime importance to ask what is the maximum size defect the vessel can tolerate and still perform its service function? This means that the entire life must be considered - from material through welding, postweld forming and heat treatment, proof testing, actual in-service loading, and the various environments related to fabrication, testing, and/or service.

One procedure to obtain verification of structural integrity through the definition of critical flaw size is by the application of the current concepts of linear elastic fracture mechanics to data carefully generated in the laboratory to simulate service conditions. To be relative and useful, any such program must provide information on the effect of flaw size on fracture strength, the rate of flaw growth (crack propagation) under cyclic loading, and the rate of flaw growth under sustained-load conditions. This program was designed to generate such information.

At the onset of the program, it was recognized that the high cost of fabricated pressure vessels prohibited the use of specimens cut from vessel material for the entire program. Subsequently, Inconel 718 sheet material was used for Phase I of the evaluation. In Phase II, the sheet material results were then correlated with results for specimens cut from a fabricated Inconel 718 pressure vessel.

2.2 Stress-Intensity Factors for Surface Flaws in Flat Plates

In the past 10 years, several analytical expressions have been proposed for the stress-intensity factor associated with a surface flaw in a finite size specimen. Since the objective of this program is to generate information to be used by NASA-MSD and Bendix in the analysis of Inconel 718 pressure vessels, the procedures used in this program were those recommended by NASA-MSD.

The basic equation used to compute the stress-intensity factor for Phase I was:

$$K = 1.1 \sigma \sqrt{\pi a} / Q M'_k \quad (1)$$

where

a = flaw depth

σ = gross stress

M'_k = magnification factor

Q = Irwin plasticity correction = $\Phi^2 - 0.212 \left\{ \frac{\sigma}{\sigma_y} \right\}^2$

Φ = elliptic integral of the second kind

σ_y = 0.2 percent yield stress.

In this equation, the magnification factor, M'_k , is a function of the $a/2c$ ratio and the a/t ratio, where $2c$ is the surface crack length, and t is the specimen thickness. The value of M'_k for a particular specimen is determined by an interpolation procedure that is illustrated in Figure 1. This procedure is based on the following considerations:

- (1) The values of M'_k at $a/2c = 0$ correspond to Kobayashi's⁽²⁾ magnification factor evaluated at a σ/σ_y ratio of 0.4, or

$$[M'_k]_{a/2c = 0} = [M'_k]_{(\sigma/\sigma_y = 0.4)} = M_{kf} \cdot [M_{kp}]_{\sigma/\sigma_y = 0.4} \quad (2)$$

where

M_{kf} = Kobayashi's magnification factor for flaw depth

M_{kp} = Kobayashi's plasticity correction

Kobayashi's plasticity correction is a function of σ/σ_y , so the condition of $\sigma/\sigma_y = 0.4$ employed is a significant restriction. These values, as listed in Table 3 of Reference (3), were incorporated into the computer analysis and are listed in Table 2.

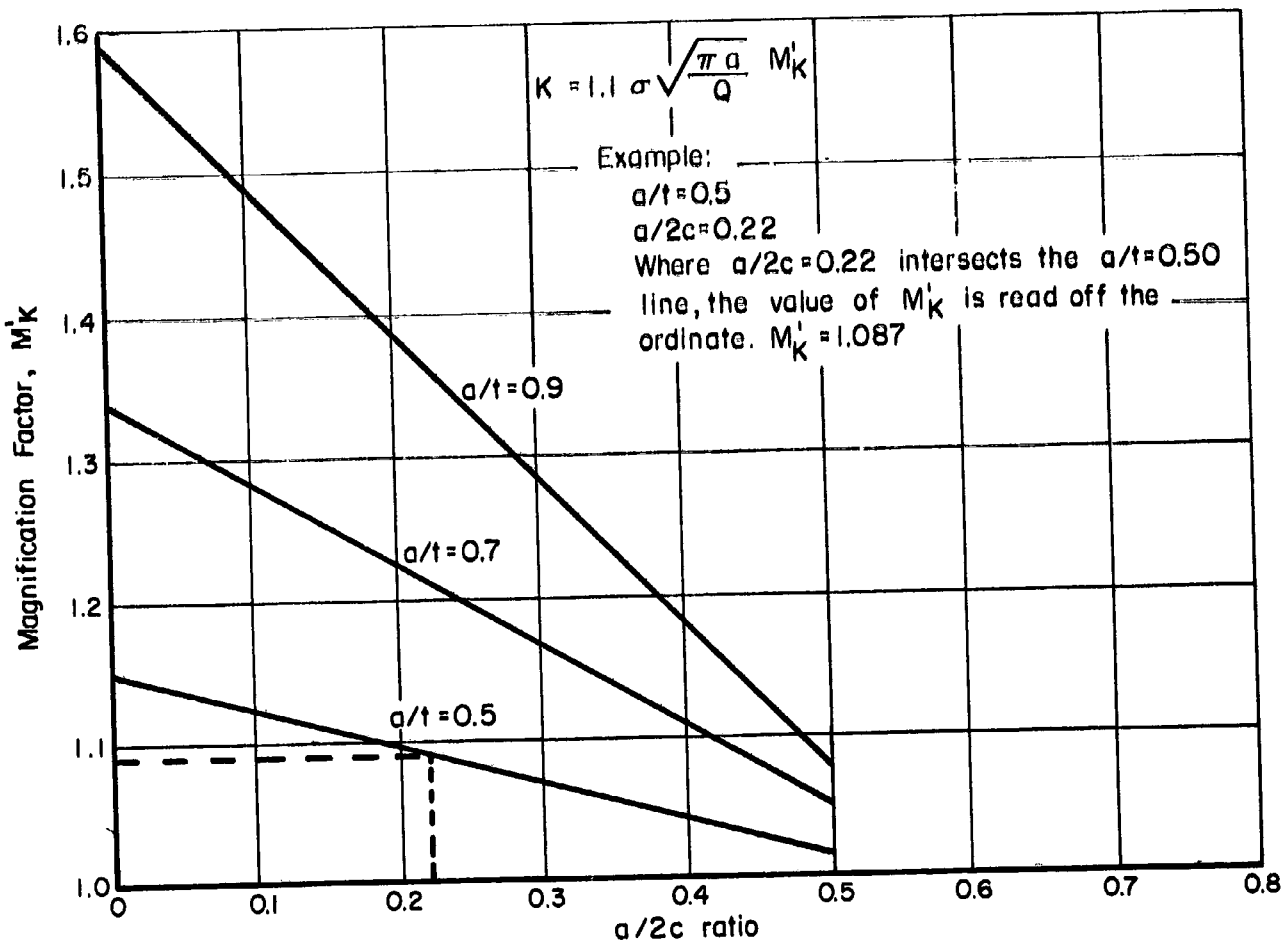
- (2) The values of M'_k at $a/2c = 0.5$ are set equal to the magnification factor proposed by Smith⁽⁴⁾ for semicircular flaws. These values are closely approximated by

$$[M'_k]_{(a/2c = 0.5)} = 1 + (a/t)^2 / 10. \quad (3)$$

This expression also was incorporated into the computer analysis.

- (3) The values of M'_k that have been determined for a specific a/t ratio at $a/2c = 0$ and at $a/2c = 0.5$ serve as end points for a linear interpolation between the two values; i. e., the points are connected with a straight line as shown in Figure 1. The value of M'_k corresponds to the intercept of the actual $a/2c$ ratio with the line corresponding to the actual a/t ratio for a given specimen.

- (4) An example of this procedure is shown graphically in Figure 1.



$M'_K = M_{kf} \cdot (M_{kp}) \sigma / \sigma_y = 0.4$
 (Kobayashi's expression limited to $\sigma / \sigma_y = 0.4$)

Smith's
 elastic solution
 $M'_K = 1 + (a/t)^2 / 10$

FIGURE 1. PROCEDURE USED TO DETERMINE THE MAGNIFICATION FACTOR, M'_K

TABLE 2. STRESS INTENSITY MAGNIFICATION FACTORS FOR SURFACE FLAWS AS PER REFERENCE (3)

| Flaw Depth Thickness a/t | Ratio, | Magnification Factor, M_K | Flaw Depth Thickness a/t | Ratio, | Magnification Factor, M_K |
|--------------------------------|--------|-----------------------------------|--------------------------------|--------|-----------------------------------|
| 0.075 or less | | 1.00 | 0.550 | | 1.20 |
| 0.100 | | 1.01 | 0.575 | | 1.22 |
| 0.125 | | 1.01 | 0.600 | | 1.24 |
| 0.150 | | 1.01 | 0.625 | | 1.26 |
| 0.175 | | 1.02 | 0.650 | | 1.28 |
| 0.200 | | 1.02 | 0.675 | | 1.30 |
| 0.225 | | 1.02 | 0.700 | | 1.33 |
| 0.250 | | 1.03 | 0.725 | | 1.36 |
| 0.275 | | 1.04 | 0.750 | | 1.39 |
| 0.300 | | 1.05 | 0.775 | | 1.42 |
| 0.325 | | 1.06 | 0.800 | | 1.45 |
| 0.350 | | 1.07 | 0.825 | | 1.48 |
| 0.375 | | 1.08 | 0.850 | | 1.51 |
| 0.400 | | 1.09 | 0.875 | | 1.53 |
| 0.425 | | 1.10 | 0.900 | | 1.55 |
| 0.450 | | 1.12 | 0.925 | | 1.57 |
| 0.475 | | 1.14 | 0.950 | | 1.58 |
| 0.500 | | 1.16 | 0.975 | | 1.59 |
| 0.525 | | 1.18 | 1.000 | | 1.60 |

In the analysis of fracture data, the three load levels normally associated with the fracture process were determined when possible. These loads are illustrated in Figure 2 and are denoted as the maximum load, P_1 ; the "pop-in" load, P_2 ; and the arbitrary selection of a 5-percent offset load, P_3 . For the relatively thin materials (0.114 inch for this program) used in aerospace pressure vessel applications, pop-in usually does not occur, so K_{Ic} is generally based on the stress at failure. It should be recognized, however, that there is considerable evidence⁽⁵⁾ that some form of slow flaw growth may occur in thin materials during a fracture test, i. e., during a proof cycle. A study of this phenomena, however, is beyond the scope of the present program, so the conventional analysis procedure of using the stress at failure (or pop-in, if observed) is used throughout this report.

2.3 The Effect of Curvature on Tensile Properties

The curved configuration of the vessel material specimens introduced an additional bending stress component into the analysis. Since it was not realistic to straighten the specimens prior to testing, an initial load eccentricity existed. As the load increases, however, the specimen tends to straighten and the loading eccentricity decreases. A discussion of the relative magnitude of this effect is presented in Appendix A. For the conditions of these tests, the resulting ultimate tensile strength and elongation values should not be significantly affected, but the yield strength values would be slightly depressed. However, as shown in Appendix A, the error in yield strength for this material and configuration should be small.

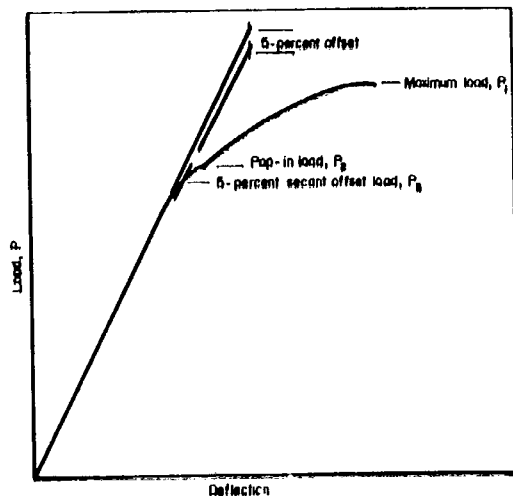


FIGURE 2. SCHEMATIC OF LOAD VALUES TYPICALLY ASSOCIATED WITH THE FRACTURE PROCESS

2.4 The Effect of Curvature on the Surface Flaw Stress-Intensity Factor

The cumulative nature of the stress-intensity factor, K , was employed to combine by superposition the axial load and bending moment flaw models into a resultant stress-intensity factor. Thus, the axial-load stress-intensity factor, K_A , and the bending-moment stress-intensity factor, K_B , may be expressed as

$$K = K_A + K_B \quad (4)$$

The axial load component as described previously is:

$$K_A = 1.1 M_K \sigma_A \sqrt{\pi a / Q} \quad (5)$$

However, the more general format of this expression, which must be considered in the cases of load interactions, is

$$K_A = f(\alpha) M_K \sigma_A \sqrt{\pi a / Q} \quad (6)$$

where

$f(\alpha)$ = free surface correction as a function of position on the perimeter of the flaw front

α = polar angle measured from the axis of symmetry.

For the special case of idealized axial loading,

$$f(\alpha) = 1.1$$

at $\alpha = \pi/2$, and Equation (5) is obtained.

The bending moment contribution to the total stress-intensity factor has been developed by Smith⁽⁴⁾ for the case of bending where the flaw is located on the tension side of the neutral axis or, as in our case, the flaw is located on the concave surface of the specimen. Smith's expression can be written as

$$K_B = M_B \sigma_B \sqrt{\pi a / Q} \quad , \quad (7)$$

where

M_B = bending magnification factor

σ_B = extreme fiber bending stress component.

This expression is valid for the range $a/t < 0.7$, which includes the results of this program. Expression (4) then becomes

$$K = f(\alpha) M_K \sigma_A \sqrt{\pi a / Q} + M_B \sigma_B \sqrt{\pi a / Q} = K_A \left[1 + \left(\frac{M_B}{f(\alpha)} \right) \cdot \frac{\sigma_B}{\sigma_A} \cdot \frac{1}{M_K} \right] \quad (8)$$

Depending on the relative combination of axial and bending loads, the critical resultant stress-intensity factor may occur at some location other than $\alpha = 0$. In fact, at very high stress gradients (i. e., when bending effects greatly over-ride axial load levels), the critical stress intensity factor occurs on the flaw front adjacent to the free surface. While it would be desirable to map the conditions on the entire flaw front, it is considered sufficient to determine the limiting values at $\alpha = 0$, and $\alpha = \pi/2$. For the normal range of flaw shapes ($0.2 < a/2c < 0.5$) and the normal range of flaw depth ($a \leq 0.7t$), the following expressions are applicable:

at $\alpha = 0$ (flaw tip)

$$M_B \approx 0.4$$

$$f(\alpha) \approx 1.1$$

at $\alpha = \pi/2$ (free surface)

$$M_B \approx 0.9$$

$$f(\alpha) \approx 1.0$$

For these points, Expression (8) becomes, at $\alpha = 0$,

$$K = K_A \left(1 + 0.36 \frac{\sigma_B}{\sigma_A} \cdot \frac{1}{M_K} \right) \quad (9)$$

and, at $\alpha = \pi/2$,

$$K = K_A \left(1 + 0.9 \frac{\sigma_B}{\sigma_A} \cdot \frac{1}{M_K} \right) \quad (10)$$

The obvious approximations which are inherent to the generalization and mixing of these models suggest that the conservative simplification of Expressions (9) and (10) to

$$K = K_A \left(1 + 0.3 \frac{\sigma_B}{\sigma_A} \right), \text{ at } \alpha = 0 \quad (11)$$

and

$$K = K_A \left(1 + 0.8 \frac{\sigma_B}{\sigma_A} \right), \text{ at } \alpha = \pi/2 \quad , \quad (12)$$

is in order. For the case of the simple pin-end conditions used for the fracture tests, the stress ratio as derived in Appendix A becomes

$$\sigma_B / \sigma_A = \frac{(0.75)(L/R)(L/t)}{1 + \frac{12\sigma_A}{K_1 E} (L/t)^2} \quad (13)$$

Since the fatigue test specimens are tightly clamped in special gripping fixtures (no rotation results during clamping) to avoid localized fretting, the specimens' ends were subject to rotational restraint. Thus the stress ratio is expressed as

$$\sigma_B / \sigma_A = (b/t)a = \frac{(0.75)(L/R)(L/t)}{1 + \frac{12\sigma_A}{k_2 E} (L/t)^2} \quad (14)$$

as shown in Appendix A.

In calibrating the fatigue machine and gripping arrangement for these specimens, it was noted that an 800-pound preload was required to achieve an initial zero bending moment at the critical section. This was determined by using calibration specimens with strain gages mounted on opposite sides of the critical test section. Denoting σ_0 as the initial preload stress, the stress ratio of Expression (14) above is thus modified to

$$\sigma_B / \sigma_A = \frac{\sigma_A - \sigma_0}{\sigma_A} \cdot \frac{\sigma_B}{\sigma_A - \sigma_0} = \left(1 - \frac{\sigma_0}{\sigma_A}\right) \frac{(0.75)(L/R)(L/T)}{1 + \frac{12(\sigma_A - \sigma_0)}{k_2 E} (L/T)^2} \quad (15)$$

This latter stress ratio expression is then used to compute the stress-intensity factor at the maximum flaw depth, K_0 , and the stress-intensity factor at the specimen surface, $K_{\pi/2}$.

3.0 MATERIALS

3.1 Phase I Sheet Material

The material used in this phase of the program was purchased from Pacific Metals Division of A. M. Castle and Company by the Bendix Corporation in the form of 0.125 x 48 x 120-inch sheet with the following composition:

| <u>Heat No.</u> | <u>%C</u> | <u>%Mn</u> | <u>%Fe</u> | <u>%S</u> | <u>%Si</u> | <u>%Cu</u> | <u>%Ni</u> | <u>%Cr</u> | <u>%Al</u> | <u>%Ti</u> | <u>%Mg</u> | <u>%Co</u> | <u>%Mo</u> |
|-----------------|-----------|------------|------------|-----------|------------|------------|------------|------------|------------|------------|------------|------------|------------|
| HT18A8E | 0.04 | 0.10 | 17.99 | 0.007 | 0.24 | 0.05 | 52.75 | 19.12 | 0.40 | 0.83 | -- | 0.06 | 3.03 |

All welded specimens were tungsten inert gas (TIG) welded, using the weld parameters presented in Table 3. The welded specimens were heat treated after welding. All specimens were supplied to Battelle in the form of heat-treated specimen blanks of 0.113-inch thick sheet material.

TABLE 3. WELD PARAMETERS FOR INCONEL 718 SHEET MATERIAL 0.113-INCH THICK

| <u>Parameters</u> | <u>Quantitation</u> |
|----------------------|--|
| Volts | 13 |
| Amperes | 90 |
| Electrode | 1/16-inch diameter, 1% thoriated tungsten, 30° included angle, 0.015-inch flat |
| Weld Speed | 5 inches/minute |
| Filler Wire | 0.035-inch diameter Inconel |
| Wire Speed | 18-1/2 inches/minute |
| Torch Gas | 75% He, 25% Ar @ cfh (with Ar meter) |
| Backing Gas | Argon with 131 ppm O ₂ |
| Backing Gas Pressure | 0.9 inch water |
| Preweld Purge | 30 cfh with backing gas for 10 minutes |

3.2 Phase II Vessel Material

In Phase II of this program, specimens were cut from a completely fabricated pressure vessel produced by Bendix Corporation. The vessel was 39 inches in diameter with wall thickness from 0.125 inch in the wall to 0.175 inch at the welds. The material

used to fabricate this vessel was secured by Bendix from Allvac in the form of 0.187- x 56- x 56-inch Allvac 718 sheet. The material was from Heat No. 6754 and had the following chemical composition:

| | | | | | | | | |
|-----------|------------|------------|------------|------------|----------------|------------|------------|------------|
| <u>%C</u> | <u>%S</u> | <u>%Mn</u> | <u>%Si</u> | <u>%Cr</u> | <u>%Mo</u> | <u>%Co</u> | <u>%Ti</u> | <u>%Al</u> |
| 0.038 | 0.004 | 0.10 | 0.14 | 19.05 | 3.05 | 0.20 | 0.86 | 0.55 |
| <u>%B</u> | <u>%Fe</u> | <u>%Cu</u> | <u>%Ni</u> | <u>%P</u> | <u>Cb + Ta</u> | | | |
| 0.003 | Bal. | 0.02 | 52.2 | 0.003 | 5.08 | | | |
| | | | | | -.02. | | | |

Bendix Corporation then inturgesciently formed the material into hemispheres which were TIG welded together to form the pressure vessel. The welding schedule used was the same as previously described for the Phase I sheet material.

4.0 PHASE I PROCEDURES

4.1 Specimen Fabrication

Two basic specimen configurations were used in this phase. The tensile specimens were machined to the configuration illustrated in Figure 3. This specimen size was dictated by the size limitation of the available liquid-hydrogen dewar. All welded tensile specimens were tested with the weld bead on. Specimens for the flaw growth portion of the study (fracture, sustained-load, and fatigue tests) were machined to the configuration shown in Figure 4. For these tests, the weld bead was machined flush with the parent metal except where noted.

The initial flaw studied consisted of a fatigue crack propagated from an Electric Discharge Machine (EDM) slot 0.25-inch long by 0.070-inch deep and located at the desired flaw position. Flaw locations studied were (1) the parent material, (2) the center of the root side of the weld, or (3) the heat-affected zone on the root side of the weld. The initial fatigue crack was introduced into the specimens by the following cantilever bending fatigue stress cycle:

| <u>Flaw Location</u> | <u>Maximum Bending Stress, psi</u> |
|---|--|
| Parent Material | ±50,000 |
| Weld material and heat affected zone (weld bead off) | ±45,000 |
| Weld Material (weld bead on) | { +36,500 -19,000 |

At these stresses, the desired initial fatigue crack was generated in 30,000 to 60,000 cycles. In all cases the maximum bending stress was reduced to values less than the expected test stress during the last 0.050 inch of crack growth. This reduction in cracking stress reduced the potential of a residual plastic zone at the crack tip larger than would occur on the first load cycle of the subsequent test. The specimens were then ready for testing.

4.2 Tensile Test Procedures

All tensile tests were conducted in accordance with Federal Test Standard No. 151 except for a slightly smaller sized specimen. Each test was conducted in a Baldwin 200,000-pound-capacity Universal testing machine equipped with a removable cryogenic dewar as shown in Figure 5. A Baldwin strain-follower extensometer with a 1-inch gage length was installed on the specimen as shown in Figure 6, and the specimen inserted into the test environment. For the cryogenic tests, the specimen was inserted into the closed cryogenic dewar and held at zero load while the dewar was filled. The specimen was then allowed to soak in the environment for 15 minutes prior to test to assure that the

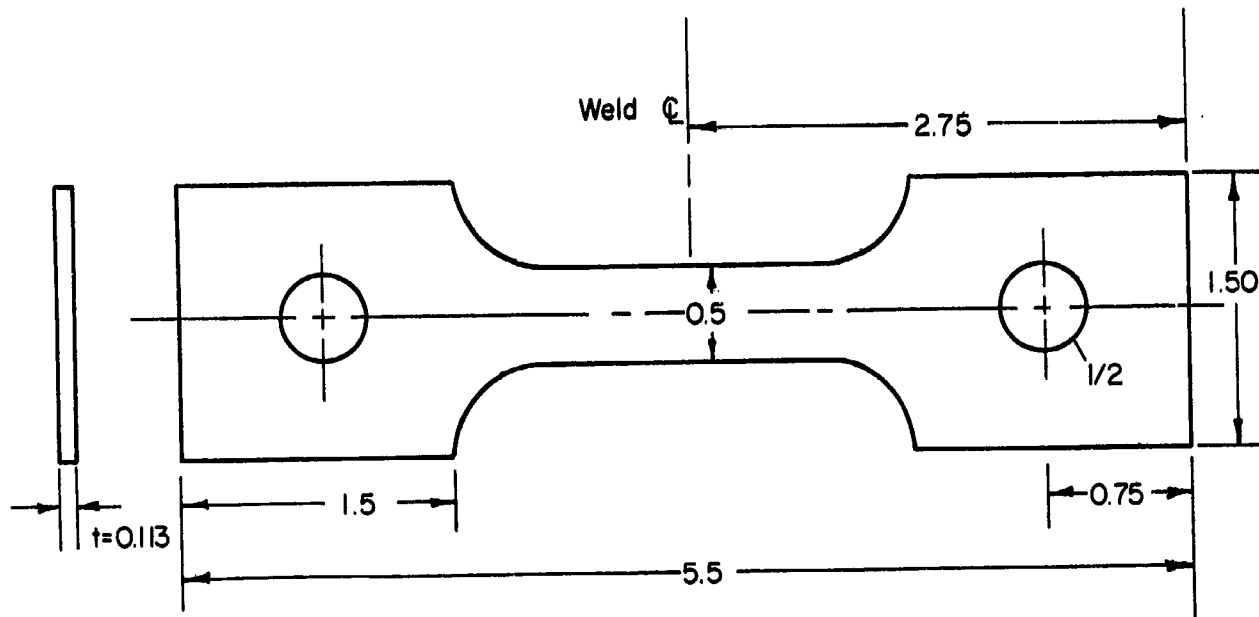


FIGURE 3. TENSILE SPECIMEN CONFIGURATION
 Dimensions in inches.

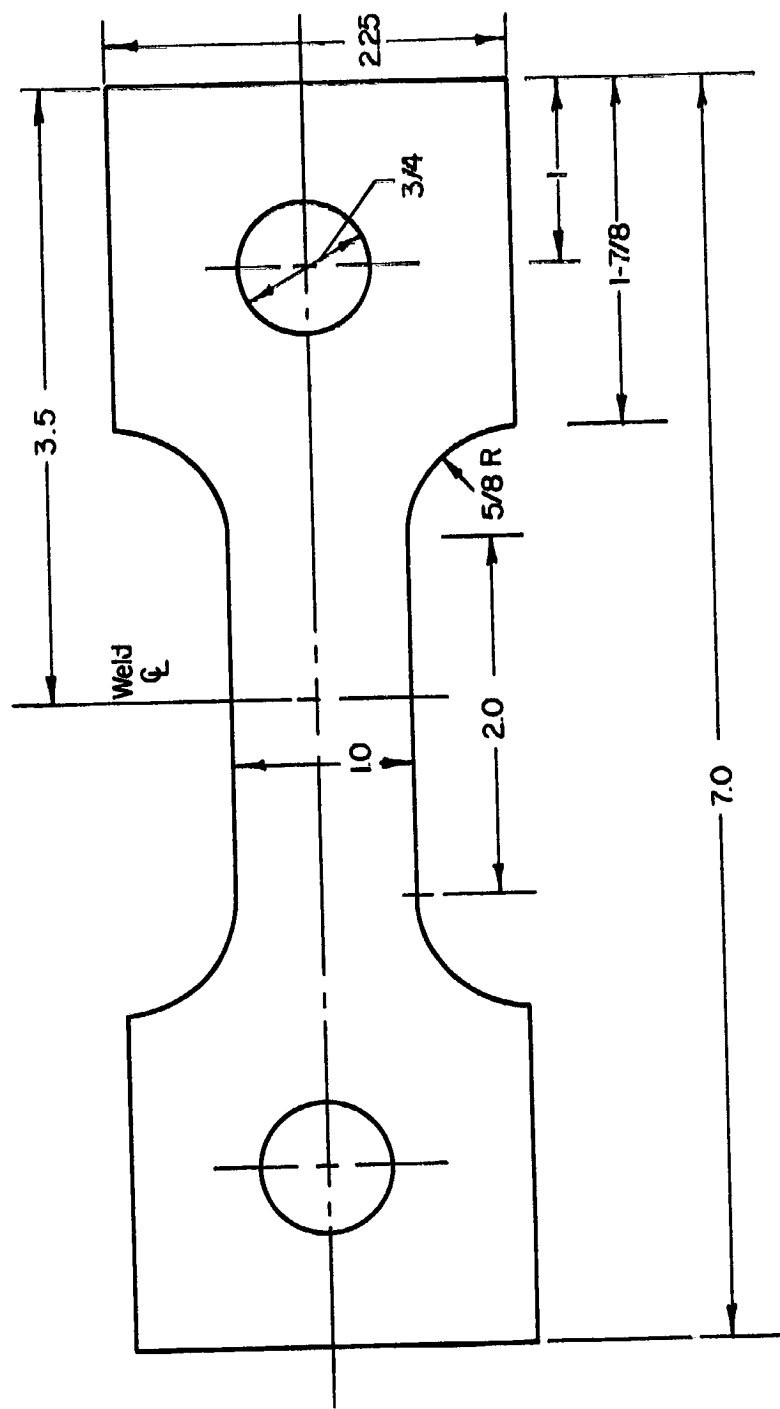
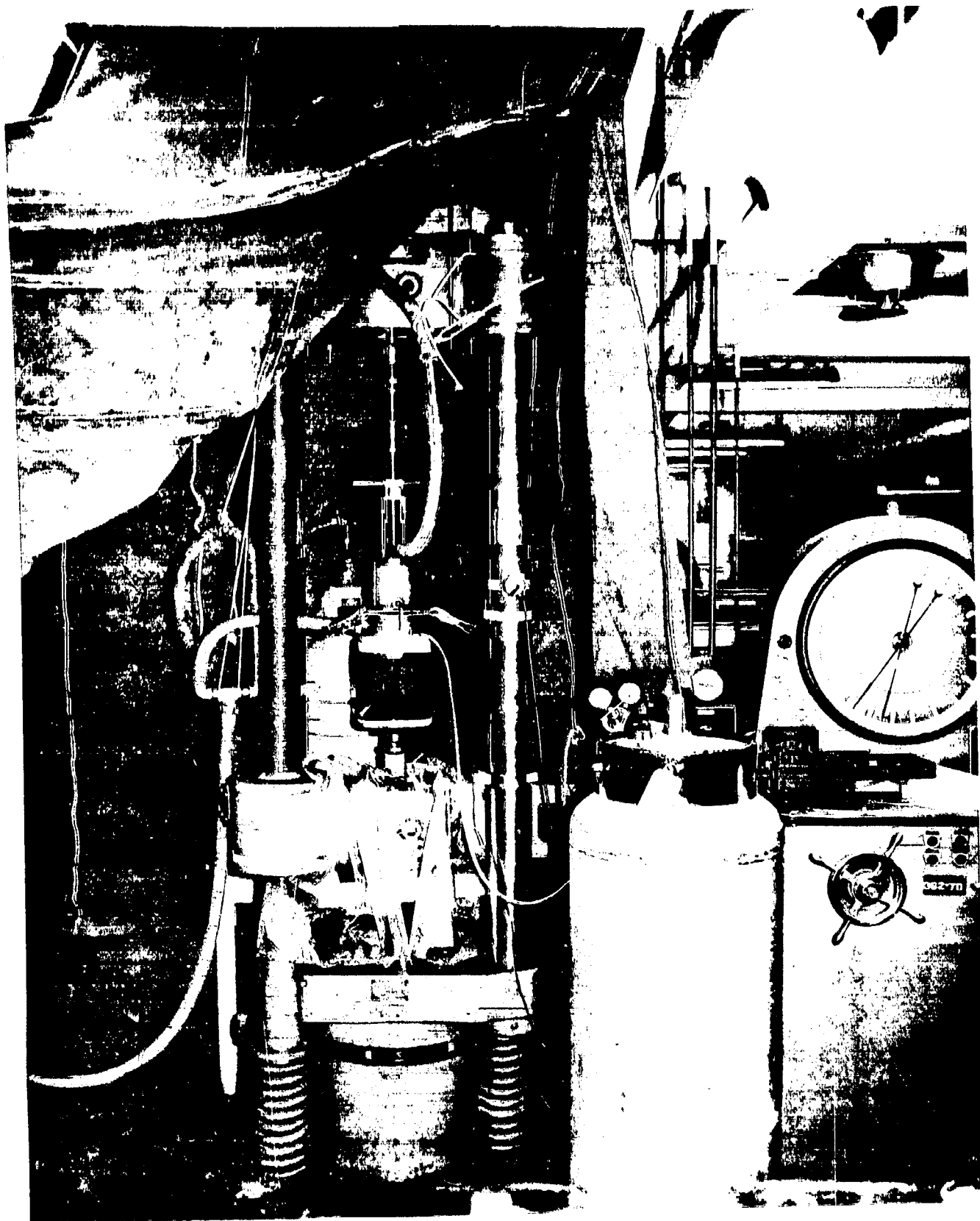


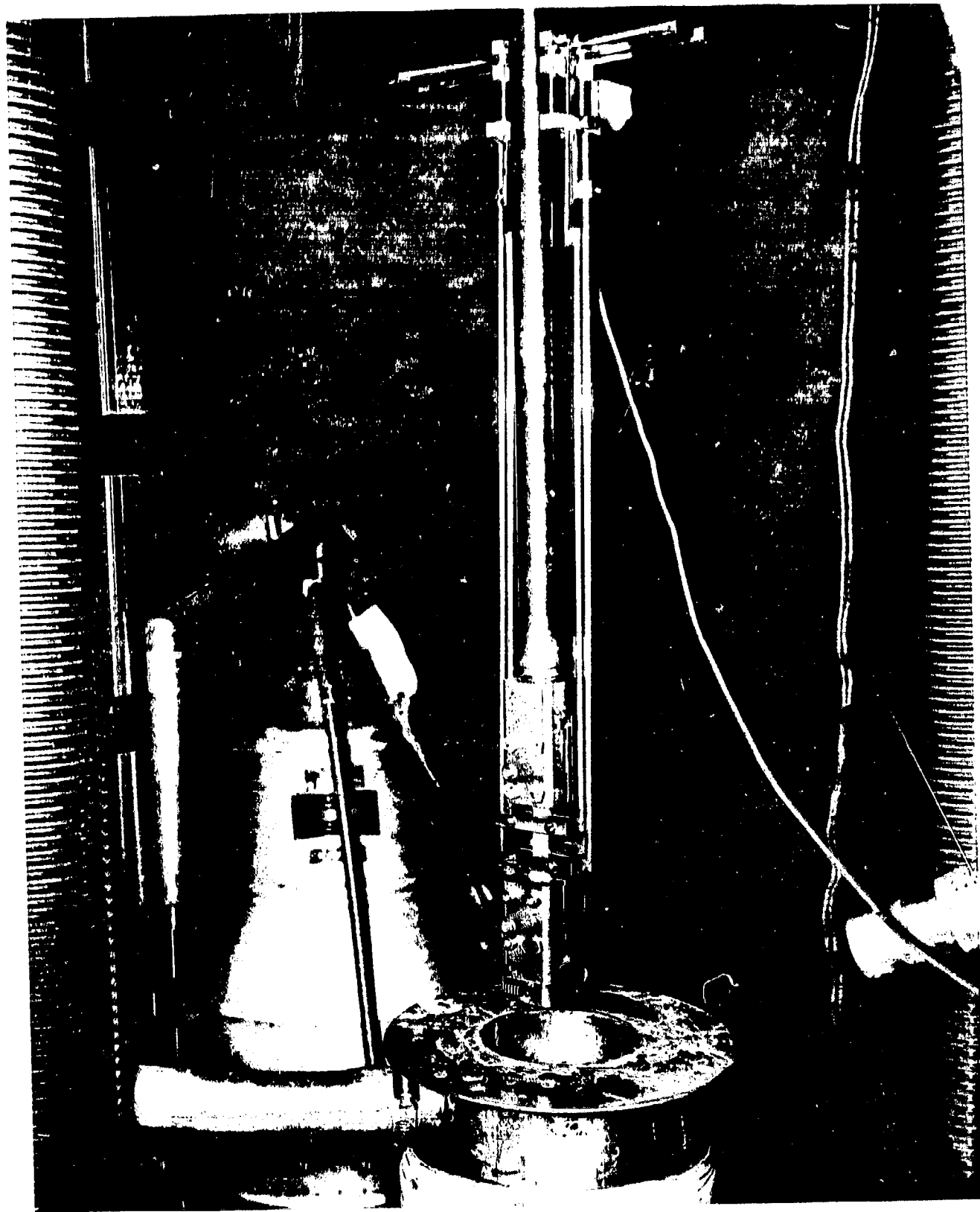
FIGURE 4. SPECIMEN CONFIGURATION FOR FLAW GROWTH STUDIES

Dimensions in inches.



42794

FIGURE 5. BALDWIN TEST EQUIPMENT WITH CRYOGENIC DEWAR IN POSITION



42792

FIGURE 6. EXTENSOMETER USED DURING THE TENSILE TESTS

test temperature had been reached. The test was then conducted to failure at a strain rate of 0.005 in./in./min. An autographic record of the load versus extensometer deflection was recorded and the normal tensile properties determined.

4.3 Fracture Test Procedures

All fracture tests were conducted in the 200,000-pound-capacity Baldwin Universal testing machine used for the tensile tests. A cryogenic dewar was used to submerge the flaw in the test environment for the three cryogenic liquids. The Ucon 113 environment was contained in a plexiglass box that was attached at the bottom of the specimen so that the flaw was submerged in the Ucon 113. Each specimen was placed in the test environment, the temperature allowed to equilibrate, and the specimen then was loaded to failure at an indicated strain rate of 0.005 in./in./min./as measured by the machine cross-head travel. A record of load versus compliance was made throughout each test.

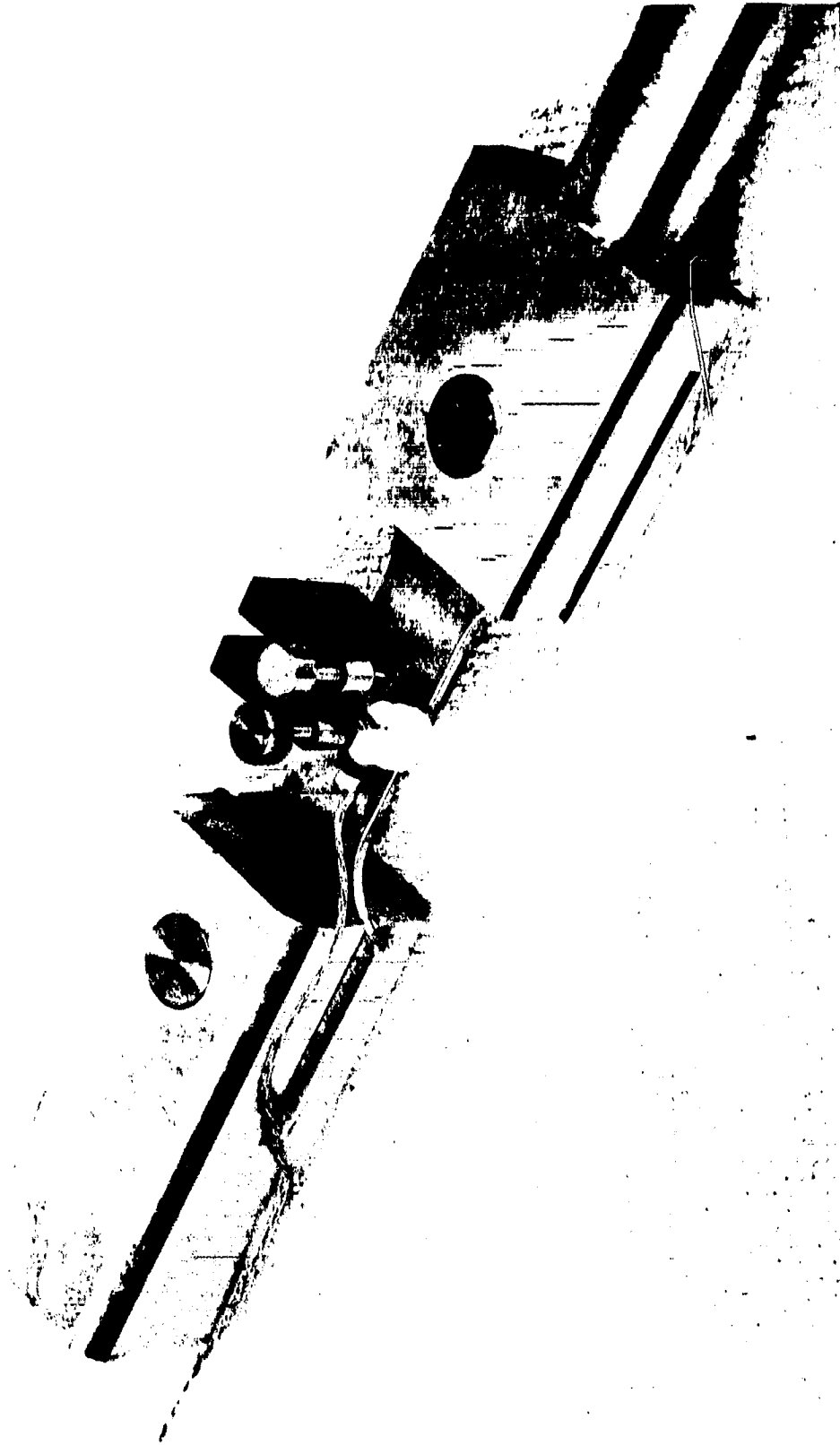
For the nine preliminary welded fracture tests used in the heat treatment study, the weld bead was not machined off and the compliance was measured with the Baldwin strain-follower extensometer with a 0.5-inch gage length centered over the flaw. For the rest of the fracture tests, the weld bead was machined off and a more sensitive double cantilever compliance gage, shown in Figure 7, was used. No significant variation in the load-compliance record was observed as measured by the two techniques.

4.4 Sustained-Load Flaw-Growth Test Procedures

The sustained-load tests on parent material specimens in Ucon 113, liquid nitrogen, and liquid oxygen and on welded specimens in Ucon 113 were conducted in a standard 9:1-ratio lever-arm creep machine with a 20,000-pound load capacity. A plexiglass container filled with Ucon 113 was fitted around the specimen for the Ucon 113 tests; whereas the specimen was submerged in a cryogenic dewar for the cryogenic environments. The cryogenic liquid levels were automatically maintained at a level above the flaw by means of cryogenic level probes that controlled the fluid flow from the reservoir by operating a solenoid valve.

The welded material tests in liquid oxygen and in liquid hydrogen were conducted in a 10,000-pound capacity (Satec) creep machine equipped with a cryogenic dewar with automatic level controls. This equipment shown in Figure 8 was located in an explosion-proof room.

The parent material tests in liquid hydrogen were conducted under load control in Battelle's cryogenic electrohydraulic universal testing machine shown in Figures 9 and 10. The cryogenic test chamber of this 25,000-pound capacity machine is located inside the explosion-proof room, the hydraulic power plant unit and electric controls being located outside the room. In this machine, the load is applied through a load cell to a cantilever beam which transfers the load to a loading rod extending through a pressurized bellows system into the cryogenic dewar. As before, the cryogenic liquid level was maintained with automatic level controls. This arrangement results in a completely sealed and spark-free laboratory room. The load accuracy of this machine at the specimen was ± 2 percent.



43673

FIGURE 7. COMPLIANCE GAGE USED FOR THE FRACTURE TESTS

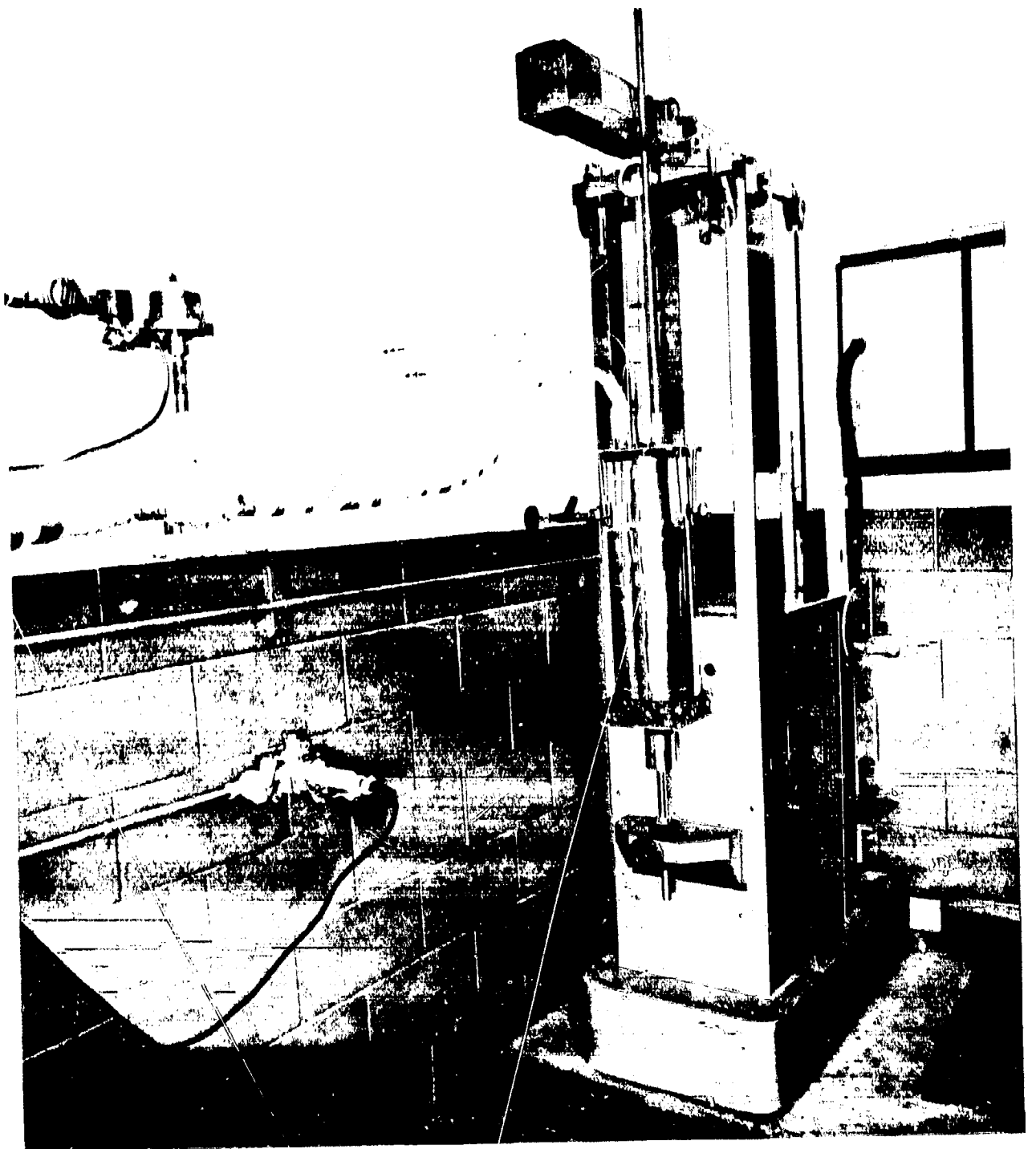
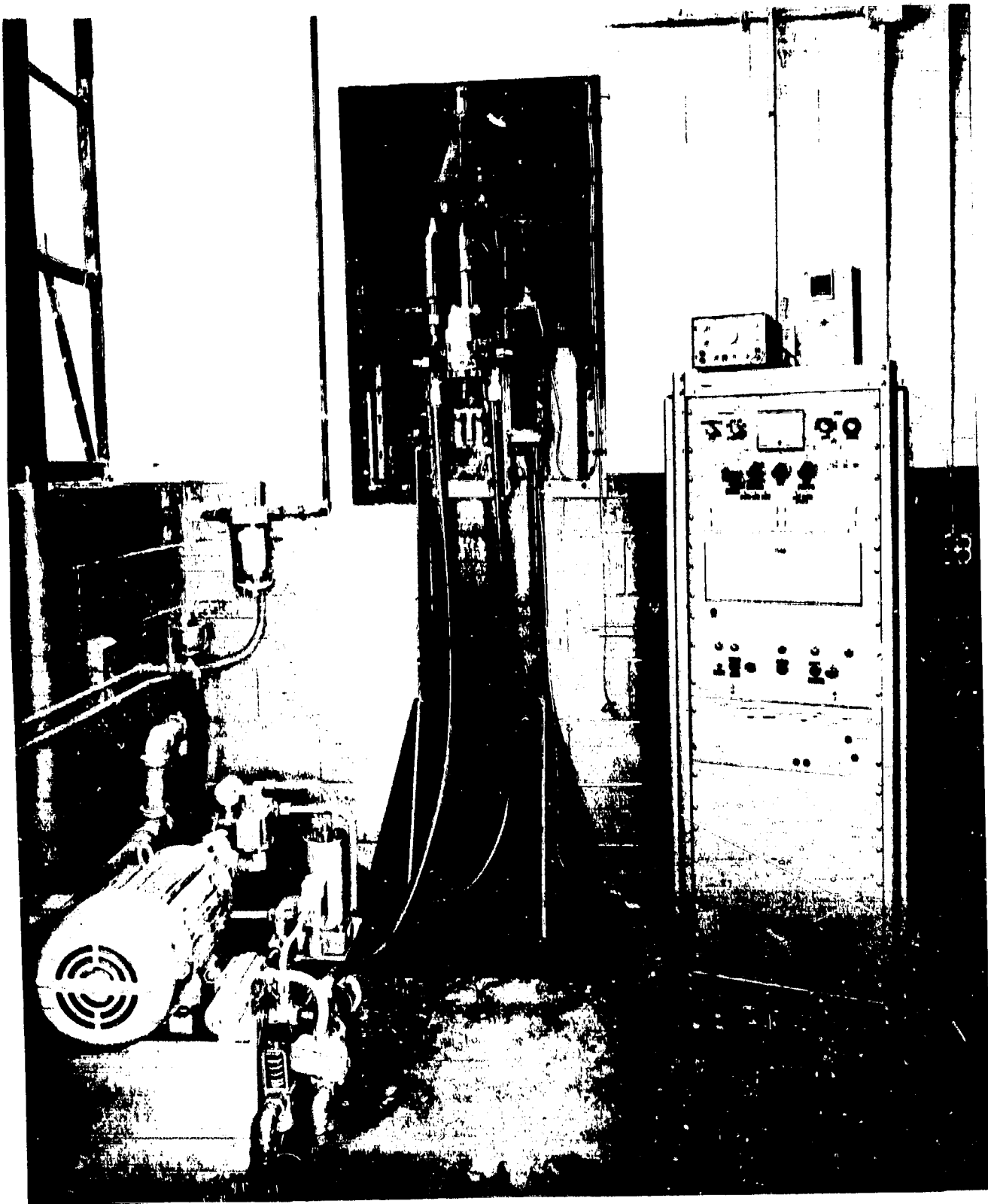
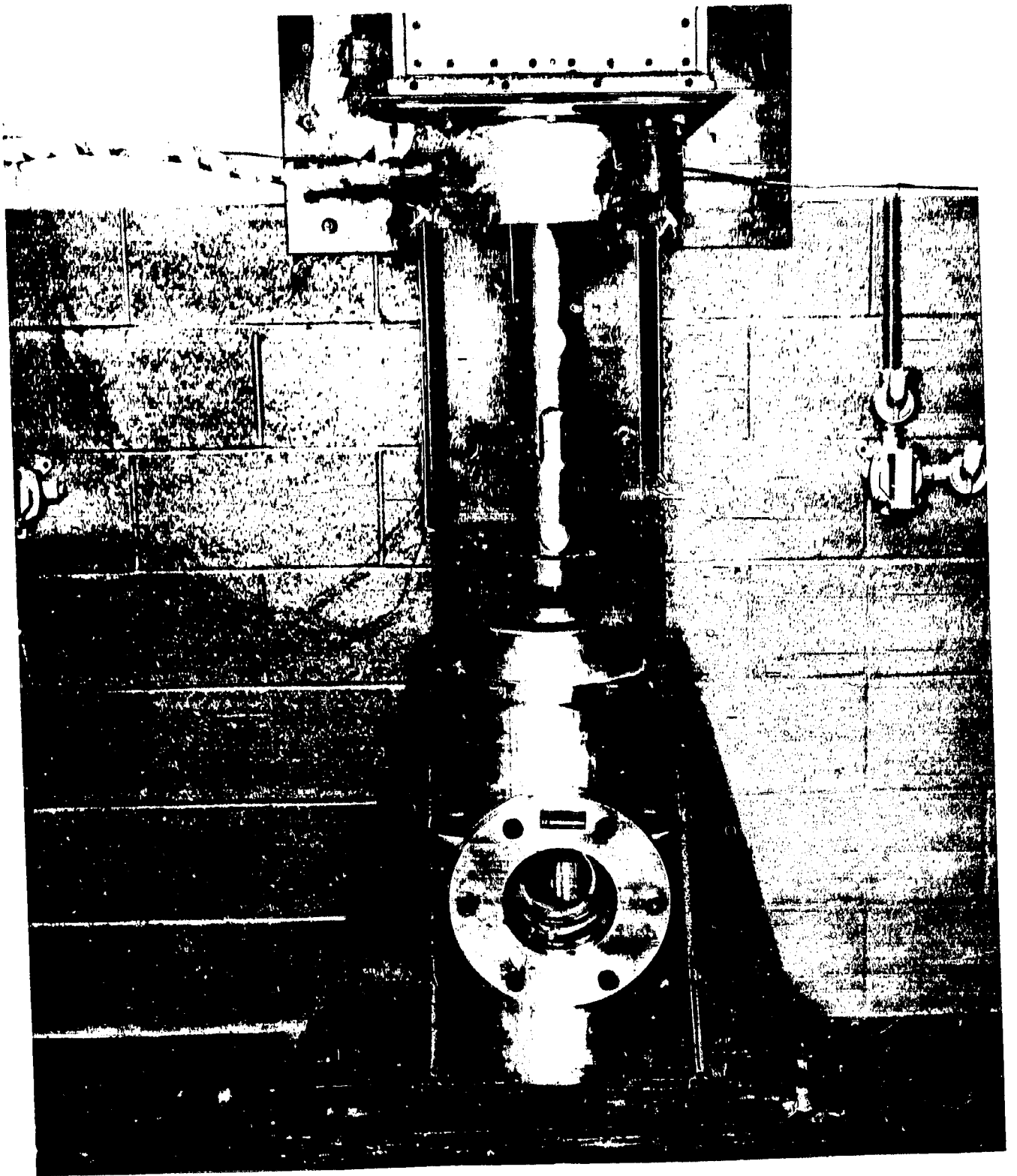


FIGURE 8. SUSTAINED-LOAD EQUIPMENT USED FOR LIQUID OXYGEN AND LIQUID HYDROGEN TESTS



44356

FIGURE 9. CONTROL CONSOLE AND HYDRAULIC SYSTEM OF THE BATTELLE CRYOGENIC TESTING MACHINE



44358

FIGURE 10. LOADING CHAMBER AND CRYOGENIC DEWAR OF THE BATTELLE CRYOGENIC TESTING MACHINE

Each sustained-load specimen was inserted into the appropriate test machine, allowed to equilibrate at the test temperature, and the load applied. If failure did not occur during the test duration, the specimen was removed and fatigue cycled to mark the extent of flaw growth that occurred under sustained loading. The specimen was then fractured and the initial and final flaw sizes measured on the fracture surface with a toolmakers microscope.

4.5 Fatigue-Crack Propagation Procedures

All of the fatigue-crack propagation tests were conducted in load control in the Battelle cryogenic electrohydraulic test system described in the previous subsection. Each specimen was inserted into the machine and held at zero load while the cryogenic dewar was filled with the proper cryogen for the test. Fifteen minutes were then allowed for the specimen temperature to equilibrate. With the exception of the welded material tests in liquid oxygen (that were cycled until failure occurred), each specimen was fatigue cycled a number of cycles estimated to produce from 0.005 to 0.010 inch of flaw growth in the thickness direction. The test was then stopped, the number of cycles recorded, and the specimen fractured. Subsequently, the initial and final flaw sizes were measured from the fracture surface with a toolmakers microscope. The average fatigue-crack propagation rate was then determined for each specimen.

5.0 PHASE II PROCEDURES

5.1 Specimen Preparation

All tensile and flaw growth specimens were machined from curved blanks supplied by Bendix Corporation to the same projected configuration used for the respective sheet material tests. All of the fracture and fatigue specimens were cut from the girth weld with the weld lying perpendicular to the specimen longitudinal axis. The tensile specimens were cut from the locations listed in the tensile results section. No attempt was made to straighten the specimens prior to testing, so all tests were conducted on curved specimens. As for the sheet material, the weld bead was left on the tensile specimens and machined flush with the base metal for the flaw growth specimens. The initial fatigue cracks were produced from an EDM flaw located at the center of the weld on the concave side of the specimen by using a cantilever bending fatigue cycle of $\pm 50,000$ psi.

5.2 Tensile and Fracture Test Procedures

All tensile and fracture tests were conducted using the same procedures and equipment previously described for the sheet material tests. The only modification was the addition of several chain links to the upper grip load train. This allowed the specimens to be gripped in the machine without inducing any bending stress at zero load.

5.3 Fatigue Test Procedures

The vessel material fatigue tests were conducted in the Battelle cryogenic testing machine previously described and using the same procedures used for the sheet material. The only equipment modification was the addition of contoured shims in the machine grips. These shims allowed the grips to be clamped to the specimen so that the specimen ends were not free to rotate and no bending was introduced in the specimen at zero load. The resulting grip end conditions are analyzed in more detail in Appendix A.

6.0 PHASE I TEST RESULTS

6.1 Selection of Heat Treatment for Inconel 718 Sheet Material

The first step in evaluating the Inconel 718 sheet material was the selection of a heat treatment suitable for cryogenic applications. Specifically, specimens from three candidate heat treatments were evaluated on the basis of room temperature and liquid-hydrogen tensile results and liquid-hydrogen fracture test results on welded specimens. The three heat treatments examined were 1400 F direct age (D. A.), 1360 F D. A. , and 1850 F anneal + 1360 F age.

The results of tensile tests at room temperature and in liquid hydrogen are presented in Tables 4 and 5 for the three heat-treat conditions. The only significant variation in properties observed was in the yield and ultimate strengths of the weld material, both at room temperature and in liquid hydrogen. In both environments the 1850 F anneal + 1360 F age welded specimens exhibited a yield strength approximately 7 ksi higher than the 1360 F D. A. specimens and from 11 to 16 ksi higher than the 1400 F D. A. specimens.

Next, a series of fracture toughness tests were conducted in liquid hydrogen on three welded specimens for each heat treatment. However, the presence of the weld bead resulted in the premature failure of two specimens during precracking. These failures occurred at the weld bead-parent metal interface and resulted from the geometric stress raiser at the corner of the interface. As a result of this secondary cracking, a posttest examination of each specimen was conducted. The results of these tests are presented in Table 6 where the specimens with secondary flaws are identified by an asterisk and, therefore, do not represent valid stress-intensity factors.

For the valid tests results in Table 6, the critical stress-intensity factor for specimens with the 1400 F D. A. and 1360 F D. A. heat treatments are equivalent and are substantially greater than that of specimens with the 1850 F anneal + 1360 F age heat treatment. Since little difference in tensile properties was observed from tests of specimens direct aged at 1360 F or at 1400 F, the 1360 F treatment was selected for use in the remainder of the program due to its slightly higher elongations and weld strengths.

6.2 Tensile Test Results

After the heat treatment had been selected, the Inconel 718 sheet material for Phase I was heat treated by Bendix Corporation. A series of tensile specimens, included with the flaw growth specimens during heat treatment, was then tested at room temperature and in liquid hydrogen. The results of these tensile tests are presented in Table 7. All welded specimens were tested with the weld bead on.

A comparison of the average tensile results of the preliminary tests for the 1360 F D. A. heat treatment and the Phase I material test results is presented in Table 8. No significant deviation in ultimate or yield strengths was noted between the two groups at either room temperature or -423 F.

TABLE 4. ROOM TEMPERATURE TENSILE RESULTS FOR THREE DIFFERENT HEAT TREATMENTS OF INCONEL 718 SHEET

| Specimen Number | Thickness, inch | Weld Thickness, inch | Width, inch | 0.2 Percent Yield Strength, psi | Ultimate Tensile Strength, psi | Elongation 1-Inch Gage Length, percent | Elongation 1.5-Inch Gage Length, percent |
|----------------------------------|-----------------|----------------------|-------------|---------------------------------|--------------------------------|--|--|
| <u>1400 F Direct Age</u> | | | | | | | |
| 9P | 0.1143 | -- | 0.499 | 176,000 | 207,000 | 25.0 | 20.0 |
| 10P | 0.115 | -- | 0.4985 | 177,000 | 206,000 | 22.0 | 18.5 |
| 11P | 0.115 | -- | 0.499 | 178,000 | 206,000 | 23.0 | 19.5 |
| Average | | | | 177,000 | 206,300 | 23.3 | 19.3 |
| 1W | 0.112 | 0.160 | 0.4995 | 165,000 | 200,000 | 7.0 | 5.5 |
| 2W | 0.112 | 0.160 | 0.501 | 165,000 | 203,000 | 9.0 | 7.5 |
| 3W | 0.112 | 0.160 | 0.4995 | 164,000 | 203,000 | 9.5 | 8.0 |
| Average | | | | 164,700 | 202,000 | 8.5 | 7.0 |
| <u>1360 F Direct Age</u> | | | | | | | |
| 15P | 0.1145 | -- | 0.499 | 176,000 | 204,000 | 26.0 | 20.0 |
| 3P | 0.1138 | -- | 0.499 | 178,000 | 202,000 | 26.0 | 20.0 |
| 24P | 0.1138 | -- | 0.4985 | 177,000 | 202,000 | 26.0 | 20.5 |
| Average | | | | 177,000 | 202,700 | 26.0 | 20.0 |
| 7W | 0.112 | 0.1655 | 0.4995 | 171,000 | 202,000 | 7.0 | 6.5 |
| 14W | 0.114 | 0.171 | 0.501 | 173,000 | 200,000 | 7.0 | 5.5 |
| 31W | 0.1133 | 0.169 | 0.500 | 175,000 | 207,000 | 11.0 | 13.5 |
| Average | | | | 173,000 | 203,000 | 8.3 | 8.5 |
| <u>1850 F Anneal, 1360 F Age</u> | | | | | | | |
| 28P | 0.114 | -- | 0.499 | 177,000 | 202,000 | 25.0 | 20.0 |
| 29P | 0.1138 | -- | 0.499 | 177,000 | 201,000 | 25.0 | 19.5 |
| 37P | 0.1135 | -- | 0.499 | 176,000 | 201,000 | 25.0 | 18.5 |
| Average | | | | 176,600 | 201,300 | 25.0 | 19.3 |
| 25W | 0.113 | 0.167 | 0.500 | 181,000 | 205,000 | 9.0 | 8.0 |
| 26W | 0.113 | 0.1673 | 0.500 | 180,000 | 205,000 | 12.0 | 10.0 |
| 27W | 0.1135 | 0.166 | 0.5005 | 179,000 | 204,000 | 12.0 | 10.0 |
| Average | | | | 180,000 | 204,700 | 11.0 | 9.3 |

Note: All weld metal stresses based on parent metal areas.

TABLE 5. LIQUID HYDROGEN (-423 F) TENSILE RESULTS FOR THREE DIFFERENT HEAT TREATMENTS OF INCONEL 718 SHEET

| Specimen Number | Thickness, inch | Weld Thickness, inch | Width, inch | 0.2 Percent Yield Strength, psi | Ultimate Tensile Strength, psi | Elongation 1-Inch Gage Length, percent | Elongation 1.5-Inch Gage Length, percent |
|----------------------------------|-----------------|----------------------|-------------|---------------------------------|--------------------------------|--|--|
| <u>1400 F Direct Age</u> | | | | | | | |
| 12P | 0.1150 | -- | 0.4995 | 207,600 | 281,150 | 17.5 | 16.6 |
| 13P | 0.1145 | -- | 0.4995 | 212,500 | 277,150 | 15 | 14 |
| 14P | 0.1149 | -- | 0.4995 | 206,900 | 283,150 | 21 | 18.6 |
| Average | | | | 209,000 | 280,500 | 17.8 | 16.4 |
| 4W | 0.1135 | 0.1610 | 0.5005 | 206,800 | 250,850 | 6 | 5.6 |
| 5W | 0.1140 | 0.1625 | 0.5005 | 188,400 | 246,250 | 5 | 4.6 |
| 6W | 0.1125 | 0.1615 | 0.5005 | 207,800 | 244,200 | 4 | 4 |
| Average | | | | 201,000 | 247,100 | 5 | 4.7 |
| <u>1360 F Direct Age</u> | | | | | | | |
| 25P | 0.1140 | -- | 0.4990 | 214,450 | 283,850 | 23 | 21.6 |
| 26P | 0.1140 | -- | 0.4990 | 215,300 | 283,850 | 24 | 22 |
| 27P | 0.1140 | -- | 0.4990 | 210,050 | 283,000 | 22 | 20 |
| Average | | | | 213,300 | 283,600 | 23 | 21.2 |
| 17W | 0.1137 | 0.1680 | 0.4997 | 215,600 | 252,550 | 5 | 3.3 |
| 18W | 0.1137 | 0.1700 | 0.5005 | 216,600 | 262,700 | 6 | 6 |
| 19W | 0.1140 | 0.1690 | 0.5005 | 205,900 | 247,100 | 4 | 3.3 |
| Average | | | | 212,700 | 254,100 | 5 | 4.2 |
| <u>1850 F Anneal, 1360 F Age</u> | | | | | | | |
| 38P | 0.1135 | -- | 0.4990 | 211,850 | 280,700 | 18.5 | 17.3 |
| 39P | 0.1140 | -- | 0.4992 | 210,850 | 282,000 | 24 | 21.3 |
| 40P | 0.1133 | -- | 0.4990 | 212,250 | 281,200 | 19.5 | 16.6 |
| Average | | | | 211,650 | 281,300 | 20.7 | 18.4 |
| 28W | 0.1135 | 0.1690 | 0.4997 | 215,100 | 261,800 | 6 | 5.3 |
| 29W | 0.1135 | 0.1660 | 0.4995 | 220,500 | 260,150 | 5.5 | 4.6 |
| 30W | 0.1135 | 0.1705 | 0.5007 | 224,350 | 258,650 | 5 | 4 |
| Average | | | | 220,000 | 260,200 | 5.5 | 4.6 |

Note: All weld metal stresses based on parent metal areas.

TABLE 6. PRELIMINARY INCONEL 718 WELD MATERIAL FRACTURE TEST RESULTS IN LIQUID HYDROGEN

| Spec. No. | Spec. Dim., Inch W | Area | Loads, kips | | | Stresses, ksi | | | Flaw Size, inch | | | Stress-Intensity Factors, ksi-sqrt (inch) | | | | | | | | | |
|------------------------------|-----------------------|-------|-------------|-------|-------|---------------|-------|------|-----------------|--------|--------|---|------|--------------|------|----------------|------|------|------|------|-------|
| | | | P1 | P2 | P3 | S1 | S2 | S3 | A | 2C | Area | PHI Correction | | Q Correction | | MSC Correction | | | | | |
| | | | | | | | | | | | | K1 | K2 | K3 | K1 | K2 | K3 | K1 | K2 | K3 | |
| 1360 F D. A. | | | | | | | | | | | | | | | | | | | | | |
| 138W | 0.167 | 1.000 | 0.1665 | 14.50 | 14.30 | 11.40 | 87.1 | 85.9 | 68.5 | 0.0979 | 0.4020 | 0.03091 | 44.2 | 43.6 | 34.7 | 44.7 | 44.1 | 35.0 | 50.3 | 49.6 | 39.3* |
| 139W | 0.165 | 0.999 | 0.1645 | 17.40 | 0.00 | 17.40 | 105.8 | 0.0 | 105.8 | 0.0910 | 0.3501 | 0.02502 | 50.8 | 0.0 | 50.8 | 51.7 | 0.0 | 51.7 | 57.0 | 0.0 | 57.0 |
| 140W | 0.163 | 1.000 | 0.1632 | 14.65 | 0.00 | 14.20 | 89.8 | 0.0 | 87.0 | 0.0984 | 0.4187 | 0.03236 | 46.0 | 0.0 | 44.6 | 46.7 | 0.0 | 45.2 | 53.0 | 0.0 | 51.3* |
| 1400 F D. A. | | | | | | | | | | | | | | | | | | | | | |
| 136W | 0.166 | 0.994 | 0.1651 | 17.35 | 0.00 | 17.00 | 105.1 | 0.0 | 103.0 | 0.0934 | 0.3634 | 0.02666 | 51.3 | 0.0 | 50.3 | 52.4 | 0.0 | 51.3 | 58.0 | 0.0 | 56.7 |
| 137W | 0.166 | 1.000 | 0.1657 | 14.75 | 11.35 | 14.65 | 89.0 | 68.5 | 88.4 | 0.0989 | 0.3735 | 0.02901 | 44.4 | 34.1 | 44.1 | 45.0 | 34.4 | 44.7 | 50.3 | 38.5 | 50.0* |
| 1800 F Anneal + 1360 F D. A. | | | | | | | | | | | | | | | | | | | | | |
| 142W | 0.162 | 1.000 | 0.1615 | 14.55 | 14.25 | 14.55 | 90.1 | 88.2 | 90.1 | 0.0808 | 0.3451 | 0.02190 | 41.9 | 41.0 | 41.9 | 42.4 | 41.6 | 42.4 | 46.2 | 45.2 | 46.2 |
| 143W | 0.161 | 0.999 | 0.1608 | 14.60 | 0.00 | 12.80 | 90.8 | 0.0 | 79.6 | 0.0908 | 0.3659 | 0.02609 | 44.1 | 0.0 | 38.7 | 44.7 | 0.0 | 39.1 | 49.7 | 0.0 | 43.4* |

*Secondary flaw.

TABLE 7. ROOM TEMPERATURE AND LIQUID HYDROGEN (-423 F) TENSILE RESULTS FOR INCONEL 718 SHEET MATERIAL

| Specimen Number | Thickness, Inch | Weld Thickness, Inch | 0.2 Percent* Yield Strength, psi | Ultimate* Tensile Strength, psi | Elongation in 1-Inch Gage Length, percent | Elongation in 1.5-Inch Gage Length, percent | Weld Specimen Failure Location |
|-----------------------------|-----------------|----------------------|----------------------------------|---------------------------------|---|---|--------------------------------|
| Results at Room Temperature | | | | | | | |
| 138P | 0.1128 | -- | 176,000 | 201,000 | 26 | 22 | -- |
| 139P | 0.1128 | -- | 176,000 | 202,000 | 26 | 22 | -- |
| 140P | 0.1121 | -- | 176,000 | 201,000 | 26 | 22 | -- |
| | | Average | 176,000 | 201,300 | 26 | 22 | |
| 173W | 0.1140 | 0.1680 | 170,000 | 196,000 | 4 | 3 | Weld center |
| 174W | 0.1140 | 0.1720 | 170,000 | 206,000 | 15** | 10 | Outside weld |
| 175W | 0.1160 | 0.1710 | 174,000 | 203,000 | 15 | 10 | Outside weld |
| | | Average | 171,300 | 201,700 | 11 | 12 | |
| Results in Liquid Hydrogen | | | | | | | |
| 135P | 0.1120 | -- | 210,000 | 284,000 | 28 | 26 | -- |
| 136P | 0.1128 | -- | 213,000 | 284,000 | *** | *** | -- |
| 137P | 0.1128 | -- | 210,000 | 283,000 | 29 | 28 | -- |
| | | Average | 211,000 | 283,700 | 28 | 27 | |
| 170W | 0.1138 | 0.1650 | 216,000 | 258,000 | 8 | 7 | Weld center |
| 171W | 0.1145 | 0.1670 | 212,000 | 221,000 | 3 | 2 | Weld center |
| 172W | 0.1140 | 0.1660 | 210,000 | 242,000 | 4 | 4 | Weld center |
| | | Average | 212,700 | 240,300 | 5 | 4 | |

*Base metal thickness used to compute weld specimen stresses.

**Failed near 1-inch gage mark, part of deformation outside mark.

***Piece broke out at fracture, no elongation measurements possible.

TABLE 8. COMPARISON OF AVERAGE TENSILE PROPERTIES FOR INCONEL 718 SHEET MATERIAL

| Material Data | 0.2 Percent Yield Strength, psi | Ultimate Tensile Strength, psi | Elongation in 1-Inch Gage Length, percent | Elongation in 1.5-Inch Gage Length, percent | |
|--------------------------|---------------------------------|--------------------------------|---|---|-----|
| Room Temperature Results | | | | | |
| Parent | Preliminary | 177,000 | 202,700 | 26 | 20 |
| | 1360 F D. A. Test Material | 176,000 | 201,300 | 26 | 22 |
| Weld | Preliminary | 173,000 | 203,000 | 8 | 8.5 |
| | 1360 F D. A. Test Material | 171,300 | 201,700 | 11 | 12 |
| Liquid Hydrogen | | | | | |
| Parent | Preliminary | 213,300 | 283,600 | 23 | 21 |
| | 1360 F D. A. Test Material | 211,000 | 283,700 | 28 | 27 |
| Weld | Preliminary | 212,700 | 254,100 | 5 | 4 |
| | 1360 F D. A. Test Material | 212,700 | 240,300 | 5 | 4 |

Special note should be made, however, of the elongation values and failure location in the welded material. For the room-temperature weld material tests, the preliminary 1360 F D. A. material failed either at the weld center or the weld fusion line, the specimens failing at the fusion line yielding higher elongation values. For the Phase I material at room temperature, two specimens failed in base metal well away from the weld and yielded elongation values of about 16 percent in 1.5 inches. The third specimen failed at the weld center with an elongation of 3 percent in a 1.5-inch gage length, as compared to 5.5 percent for the weld failure of the preliminary heat-treat material. Due to this variation in failure location and the resulting elongation, the average elongation values for the welded Phase I material are somewhat meaningless. The failure of the two specimens away from the weld would indicate a slightly stronger weld than previously noted. The low elongation of the specimen that failed in the weld, however, demonstrates the wide variation in weld tensile properties that may exist. Further tests are necessary for statistically meaningful room-temperature elongation values to be obtained.

The preliminary welded 1360 F D. A. specimens tests in liquid hydrogen failed in the weld or at the fusion line. All of the corresponding welded Phase I material specimens failed in the weld with elongations comparable to those obtained for the preliminary heat-treat material.

On the basis of these tests, no significant deviation in tensile properties at room temperature or in liquid hydrogen was observed which would indicate that the test material did not receive a typical 1360 F D. A. heat treatment.

At the request of Bendix and NASA-MS-C, an additional three specimens were tested in liquid nitrogen in the annealed condition with the weld bead on. The results are shown in Table 9.

TABLE 9. TENSILE TEST RESULTS FOR WELDED AND ANNEALED SHEET MATERIAL TESTED IN LIQUID NITROGEN

| Specimen Number | Thickness, inch | Weld Thickness, inch | Width, inch | 0.2 Percent Yield Strength, psi | Ultimate Strength, psi | Elongation in 1-Inch Gage Length, percent |
|-----------------|-----------------|----------------------|-------------|---------------------------------|------------------------|---|
| 212W | 0.1138 | 0.1460 | 0.5002 | 91,000 | 166,000 | 47 |
| 213W | 0.1140 | 0.1460 | 0.5005 | 80,600 | 159,000 | 34 |
| 214W | 0.1135 | 0.1465 | 0.5015 | 86,900 | 164,000 | 44 |

Note: Weld specimen stresses based on parent metal thickness.

6.3 Fracture Test Results

Fracture tests were conducted on parent and welded (flaw at the center of the weld) specimens submerged in Ucon 113 at room temperature, liquid nitrogen, liquid oxygen,

TABLE 10. INCONEL 718 PARENT MATERIAL FRACTURE RESULTS IN UCON 113, TYS = 177 KSI

| SPFC NO | SPEC. T | DIV. | INCH AREA | LOADS, KIPS | | | STRESSFS, KSI | FLAM SIZE, INCH | PHI CORRECTION | | | STRESS INTENSITY FACTORS, KSI-SQRT(INCH) | | | MSC CORRECTION | | | | | | |
|---------|---------|-------|-----------|-------------|------|-------|---------------|-----------------|----------------|-------|-------|--|------|-----|----------------|------|-----|------|-------|-----|------|
| | | | | P1 | P2 | P3 | | | A | K1 | K2 | K3 | D | K1 | K2 | K3 | D | K1 | K2 | K3 | |
| 61P | .114 | 1.000 | .1134 | 16.25 | 0.00 | 11.00 | 142.9 | 0.0 | 96.7 | .0733 | .4412 | .02560 | 67.7 | 0.0 | 45.9 | 71.9 | 0.0 | 47.1 | 85.5* | 0.0 | 56.0 |
| 62P | .114 | 1.000 | .1140 | 17.90 | 0.00 | 12.80 | 156.4 | 0.0 | 112.3 | .0698 | .3624 | .01987 | 69.7 | 0.0 | 50.7 | 74.4 | 0.0 | 52.4 | 86.2* | 0.0 | 60.7 |
| 63P | .114 | 1.000 | .1146 | 16.90 | 0.00 | 11.20 | 148.3 | 0.0 | 98.3 | .0725 | .4020 | .02289 | 69.0 | 0.0 | 45.7 | 73.4 | 0.0 | 46.9 | 86.4* | 0.0 | 55.3 |
| 121P | .114 | 1.000 | .1135 | 14.45 | 0.00 | 15.30 | 171.4 | 0.0 | 134.8 | .0572 | .2670 | .01199 | 68.5 | 0.0 | 53.9 | 74.1 | 0.0 | 56.5 | 81.2* | 0.0 | 61.9 |
| 123P | .113 | 1.002 | .1133 | 17.40 | 0.00 | 12.00 | 157.0 | 0.0 | 105.9 | .0660 | .3551 | .01851 | 69.3 | 0.0 | 46.7 | 74.3 | 0.0 | 48.2 | 85.2* | 0.0 | 55.2 |
| 125P | .113 | 1.000 | .1133 | 20.50 | 0.00 | 16.00 | 180.9 | 0.0 | 141.2 | .0463 | .1796 | .00653 | 62.2 | 0.0 | 48.5 | 0.0 | 0.0 | 50.9 | 0.0* | 0.0 | 53.3 |

TABLE 11. INCONEL 718 WELDED MATERIAL FRACTURE RESULTS IN UCON 113, TYS = 171 KSI

| SPFC NO | SPEC. T | DIV. | INCH AREA | LOADS, KIPS | | | STRESSFS, KSI | FLAM SIZE, INCH | PHI CORRECTION | | | STRESS INTENSITY FACTORS, KSI-SQRT(INCH) | | | MSC CORRECTION | | | | | | |
|---------|---------|------|-----------|-------------|------|------|---------------|-----------------|----------------|-------|-------|--|------|-----|----------------|------|-----|------|------|-----|------|
| | | | | P1 | P2 | P3 | | | A | K1 | K2 | K3 | D | K1 | K2 | K3 | D | K1 | K2 | K3 | |
| 44* | .102 | .993 | .1004 | 10.15 | 0.00 | 6.20 | 100.7 | 0.0 | 61.5 | .0686 | .3867 | .02083 | 45.7 | 0.0 | 27.9 | 47.1 | 0.0 | 28.2 | 56.6 | 0.0 | 33.9 |
| 44* | .103 | .994 | .1010 | 10.70 | 0.00 | 8.00 | 105.0 | 0.0 | 78.5 | .0647 | .3040 | .01585 | 44.7 | 0.0 | 33.4 | 46.0 | 0.0 | 34.0 | 53.4 | 0.0 | 39.4 |
| 47* | .104 | .994 | .1068 | 9.20 | 0.00 | 6.80 | 84.8 | 0.0 | 64.2 | .0756 | .4606 | .02735 | 41.9 | 0.0 | 31.0 | 42.9 | 0.0 | 31.3 | 53.1 | 0.0 | 38.8 |
| 150* | .100 | .997 | .1001 | 7.70 | 0.00 | 6.00 | 76.9 | 0.0 | 58.9 | .0717 | .4710 | .02652 | 36.5 | 0.0 | 28.5 | 37.2 | 0.0 | 28.8 | 46.5 | 0.0 | 36.0 |
| 151* | .100 | .997 | .0994 | 12.50 | 0.00 | 9.40 | 125.2 | 0.0 | 94.2 | .0453 | .1820 | .00648 | 42.9 | 0.0 | 32.3 | 44.7 | 0.0 | 33.0 | 47.6 | 0.0 | 35.1 |

TABLE 12. INCONEL 718 PARENT MATERIAL FRACTURE RESULTS IN LIQUID OXYGEN, TYS = 200 KSI

| SPFC NO | SPEC. T | DIV. | INCH AREA | LOADS, KIPS | | | STRESSFS, KSI | FLAM SIZE, INCH | PHI CORRECTION | | | STRESS INTENSITY FACTORS, KSI-SQRT(INCH) | | | MSC CORRECTION | | | | | | |
|---------|---------|-------|-----------|-------------|------|-------|---------------|-----------------|----------------|-------|-------|--|------|-----|----------------|------|-----|------|--------|-----|------|
| | | | | P1 | P2 | P3 | | | A | K1 | K2 | K3 | D | K1 | K2 | K3 | D | K1 | K2 | K3 | |
| 57P | .113 | 1.000 | .1124 | 17.45 | 0.00 | 12.00 | 158.3 | 0.0 | 106.4 | .0752 | .4336 | .02561 | 75.5 | 0.0 | 50.8 | 79.8 | 0.0 | 52.0 | 95.7* | 0.0 | 62.3 |
| 58P | .113 | 1.000 | .1120 | 14.50 | 0.00 | 12.60 | 172.8 | 0.0 | 111.6 | .0694 | .3837 | .02091 | 78.6 | 0.0 | 50.8 | 84.0 | 0.0 | 52.2 | 97.9* | 0.0 | 60.8 |
| 59P | .114 | 1.000 | .1134 | 10.95 | 0.00 | 13.80 | 175.3 | 0.0 | 171.3 | .0671 | .3447 | .01817 | 77.4 | 0.0 | 53.5 | 82.7 | 0.0 | 55.2 | 94.8* | 0.0 | 63.3 |
| 124P | .114 | 1.000 | .1137 | 23.70 | 0.00 | 18.50 | 208.4 | 0.0 | 162.7 | .0460 | .1735 | .00427 | 70.8 | 0.0 | 55.3 | 0.0 | 0.0 | 58.0 | 0.0* | 0.0 | 60.6 |
| 124P | .113 | 1.001 | .1135 | 19.40 | 0.00 | 13.20 | 171.0 | 0.0 | 116.3 | .0721 | .4063 | .02301 | 79.5 | 0.0 | 54.1 | 84.9 | 0.0 | 55.7 | 100.1* | 0.0 | 65.7 |
| 125P | .114 | 1.000 | .1136 | 23.40 | 0.00 | 18.20 | 206.0 | 0.0 | 160.2 | .0501 | .1937 | .00762 | 73.6 | 0.0 | 57.2 | 0.0 | 0.0 | 60.0 | 0.0* | 0.0 | 63.4 |

TABLE 13. INCONEL 718 WELDED MATERIAL FRACTURE RESULTS IN LIQUID OXYGEN, TYS = 200 KSI

| SPEC NO | Y | SPEC. DIV. | INCH AREA | LOADS, KIIPS | | | STRESSES, KSI | | | FLAM SIZE, INCH | PHI CORRECTION | STRESS INTENSITY FACTORS, KSI-SQRT(INCH) | | | | | | | | | |
|---------|------|------------|-----------|--------------|------|-------|---------------|-----|-------|-----------------|----------------|--|------|------|------|------|-----|------|------|-----|------|
| | | | | P1 | P2 | P3 | S1 | S2 | S3 | | | A | 2C | AREA | K1 | K2 | K3 | | | | |
| 424 | .107 | .990 | .1064 | 11.25 | 0.00 | 8.74 | 105.3 | 0.0 | 81.5 | .0637 | .3525 | .01764 | 45.9 | 0.0 | 35.5 | 47.0 | 0.0 | 36.0 | 54.3 | 0.0 | 41.6 |
| 434 | .103 | 1.001 | .1030 | 10.90 | 0.00 | 8.70 | 105.8 | 0.0 | 84.4 | .0652 | .3057 | .01565 | 45.2 | 0.0 | 35.1 | 46.2 | 0.0 | 36.6 | 53.6 | 0.0 | 42.4 |
| 514 | .104 | .993 | .1033 | 10.20 | 0.00 | 7.90 | 94.8 | 0.0 | 76.5 | .0705 | .4088 | .02264 | 44.7 | 0.0 | 35.3 | 45.7 | 0.0 | 35.8 | 55.1 | 0.0 | 43.2 |
| 1484 | .102 | .997 | .1021 | 8.15 | 0.00 | 7.20 | 79.8 | 0.0 | 70.5 | .0496 | .4647 | .02540 | 37.5 | 0.0 | 33.1 | 38.0 | 0.0 | 33.5 | 46.4 | 0.0 | 40.8 |
| 1494 | .102 | .997 | .1012 | 13.60 | 0.00 | 12.10 | 134.4 | 0.0 | 119.5 | .0496 | .1796 | .00700 | 46.9 | 0.0 | 41.7 | 48.4 | 0.0 | 42.8 | 51.8 | 0.0 | 45.8 |

TABLE 14. INCONEL 718 PARENT MATERIAL FRACTURE RESULTS IN LIQUID NITROGEN, TYS = 204.5 KSI

| SPEC NO | Y | SPEC. DIV. | INCH AREA | LOADS, KIIPS | | | STRESSES, KSI | | | FLAM SIZE, INCH | PHI CORRECTION | STRESS INTENSITY FACTORS, KSI-SQRT(INCH) | | | | | | | | | | |
|---------|------|------------|-----------|--------------|-------|-------|---------------|-------|-------|-----------------|----------------|--|------|------|------|------|------|------|-------|------|------|------|
| | | | | P1 | P2 | P3 | S1 | S2 | S3 | | | A | 2C | AREA | K1 | K2 | K3 | | | | | |
| 600 | .114 | 1.000 | .1140 | 21.17 | 0.00 | 17.44 | 145.7 | 0.0 | 153.1 | .0633 | .2970 | .01477 | 78.1 | 0.0 | 64.4 | 83.7 | 0.0 | 67.4 | 93.9 | 0.0 | 75.6 | |
| 640 | .114 | 1.000 | .1138 | 14.35 | 0.00 | 14.20 | 146.5 | 0.0 | 124.7 | .0713 | .4426 | .02479 | 78.2 | 0.0 | 58.6 | 83.1 | 0.0 | 60.6 | 98.3 | 0.0 | 71.6 | |
| 650 | .104 | 1.001 | .1038 | 19.44 | 11.20 | 14.80 | 147.7 | 107.9 | 142.6 | .0701 | .3936 | .02167 | 86.0 | 49.5 | 65.4 | 92.8 | 50.7 | 68.2 | 111.5 | 60.9 | 0.0 | 82.0 |
| 660 | .114 | 1.001 | .1134 | 18.80 | 0.00 | 19.50 | 174.3 | 0.0 | 171.7 | .0690 | .3427 | .01966 | 78.4 | 0.0 | 73.2 | 83.5 | 0.0 | 82.0 | 96.6 | 0.0 | 95.0 | |
| 1190 | .113 | 1.000 | .1132 | 23.95 | 0.00 | 21.20 | 211.6 | 0.0 | 187.3 | .0436 | .1806 | .00618 | 71.8 | 0.0 | 63.5 | 80.0 | 0.0 | 67.9 | 90.0 | 0.0 | 70.9 | |
| 1200 | .113 | 1.000 | .1132 | 23.17 | 0.00 | 19.00 | 204.7 | 0.0 | 167.9 | .0521 | .2091 | .00856 | 75.3 | 0.0 | 61.7 | 80.0 | 0.0 | 65.0 | 80.0 | 0.0 | 69.3 | |

TABLE 15. INCONEL 718 WELDED MATERIAL FRACTURE RESULTS IN LIQUID NITROGEN, TYS = 204.5 KSI

| SPEC NO | Y | SPEC. DIV. | INCH AREA | LOADS, KIIPS | | | STRESSES, KSI | | | FLAM SIZE, INCH | PHI CORRECTION | STRESS INTENSITY FACTORS, KSI-SQRT(INCH) | | | | | | | | | |
|---------|------|------------|-----------|--------------|------|-------|---------------|-----|-------|-----------------|----------------|--|------|------|------|------|-----|------|------|-----|------|
| | | | | P1 | P2 | P3 | S1 | S2 | S3 | | | A | 2C | AREA | K1 | K2 | K3 | | | | |
| 304 | .103 | .996 | .1022 | 11.10 | 0.00 | 8.60 | 108.6 | 0.0 | 84.1 | .0664 | .3887 | .02027 | 48.8 | 0.0 | 37.8 | 50.1 | 0.0 | 38.4 | 59.4 | 0.0 | 45.6 |
| 404 | .102 | .995 | .1016 | 11.94 | 0.00 | 10.10 | 117.8 | 0.0 | 94.4 | .0568 | .2929 | .01307 | 47.9 | 0.0 | 40.4 | 49.2 | 0.0 | 41.2 | 55.6 | 0.0 | 46.5 |
| 424 | .101 | .995 | .1006 | 14.60 | 0.00 | 12.60 | 143.4 | 0.0 | 125.5 | .0449 | .1812 | .00639 | 49.0 | 0.0 | 42.9 | 50.9 | 0.0 | 44.1 | 54.0 | 0.0 | 46.8 |
| 504 | .098 | .997 | .0970 | 8.95 | 0.00 | 8.00 | 91.4 | 0.0 | 81.7 | .0628 | .3048 | .01947 | 40.4 | 0.0 | 36.1 | 41.1 | 0.0 | 36.6 | 48.9 | 0.0 | 43.6 |
| 1464 | .101 | .997 | .1011 | 12.07 | 0.00 | 11.40 | 119.5 | 0.0 | 112.8 | .0556 | .1926 | .00841 | 43.5 | 0.0 | 41.1 | 44.6 | 0.0 | 42.0 | 48.5 | 0.0 | 45.7 |
| 1474 | .102 | .997 | .1013 | 7.82 | 0.00 | 7.50 | 77.3 | 0.0 | 74.0 | .0712 | .4792 | .02680 | 36.7 | 0.0 | 35.2 | 37.2 | 0.0 | 35.6 | 46.1 | 0.0 | 44.1 |

TABLE 16. INCONEL 718 PARENT MATERIAL FRACTURE RESULTS IN LIQUID HYDROGEN, TYS = 211 KSI

| SPEC NO | T | SPEC. DIV. | INCH AREA | LOADS, KIPS | | | STRESS, KSI | S1 | S2 | S3 | FLAW SIZE, INCH | | | PHI CORRECTION | | | D CORRECTION | | | MSC CORRECTION | | |
|---------|-----|------------|-----------|-------------|-------|-------|-------------|-------|-------|-------|-----------------|--------|------|----------------|------|------|--------------|-------|-------|----------------|-------|----|
| | | | | P1 | P2 | P3 | | | | | A | 2C | AREA | K1 | K2 | K3 | K1 | K2 | K3 | K1 | K2 | K3 |
| 519 | 112 | 1.002 | .1124 | 20.75 | 14.74 | 19.85 | 181.1 | 166.4 | 176.7 | .0482 | .3589 | .01922 | 80.9 | 78.4 | 78.9 | 86.3 | 74.5 | 83.9 | 99.9 | 90.9 | 97.1* | |
| 520 | 113 | 1.000 | .1133 | 20.55 | 16.35 | 181.3 | 144.3 | 144.3 | .0676 | .3614 | .01919 | 80.9 | 64.4 | 64.4 | 86.3 | 67.0 | 67.0 | 99.8 | 99.8 | 77.3 | 77.3 | |
| 530 | 114 | 1.000 | .1136 | 22.00 | 0.00 | 20.45 | 193.7 | 0.0 | 180.0 | .0614 | .2982 | .01428 | 80.7 | 0.0 | 75.0 | 86.7 | 0.0 | 79.8 | 96.8 | 0.0 | 89.0 | |
| 540 | 114 | 1.001 | .1136 | 23.00 | 0.00 | 20.80 | 202.5 | 0.0 | 183.1 | .0552 | .2386 | .01839 | 78.2 | 0.0 | 70.7 | 84.2 | 0.0 | 75.1 | 91.2 | 0.0 | 81.3 | |
| 550 | 114 | 1.000 | .1141 | 24.05 | 21.60 | 210.8 | 189.3 | 189.3 | .0449 | .1848 | .00652 | 77.4 | 65.1 | 65.1 | 78.4 | 69.3 | 69.3 | 82.0* | 82.0* | 72.5 | 72.5 | |
| 549 | 114 | 1.002 | .1143 | 14.65 | 0.00 | 17.50 | 141.4 | 0.0 | 153.1 | .0756 | .4395 | .02610 | 77.3 | 0.0 | 73.3 | 81.4 | 0.0 | 76.8 | 97.5 | 0.0 | 91.9 | |

TABLE 17. INCONEL 718 WELDED MATERIAL FRACTURE RESULTS IN LIQUID HYDROGEN, TYS = 212.7 KSI

| SPEC NO | T | SPEC. DIV. | INCH AREA | LOADS, KIPS | | | STRESS, KSI | S1 | S2 | S3 | FLAW SIZE, INCH | | | PHI CORRECTION | | | D CORRECTION | | | MSC CORRECTION | | |
|---------|-----|------------|-----------|-------------|-------|-------|-------------|-------|-------|-------|-----------------|--------|------|----------------|------|------|--------------|------|------|----------------|------|----|
| | | | | P1 | P2 | P3 | | | | | A | 2C | AREA | K1 | K2 | K3 | K1 | K2 | K3 | K1 | K2 | K3 |
| 374 | 105 | .996 | .1044 | 7.55 | 6.25 | 7.73 | 75.0 | 59.7 | 73.4 | .0747 | .4928 | .02891 | 36.4 | 29.0 | 35.7 | 36.8 | 29.2 | 36.1 | 45.9 | 36.4 | 45.0 | |
| 394 | 107 | .997 | .0884 | 9.95 | 0.00 | 9.80 | 114.7 | 0.0 | 117.9 | .0530 | .2917 | .01214 | 45.5 | 0.0 | 44.9 | 46.7 | 0.0 | 45.9 | 54.3 | 0.0 | 53.4 | |
| 414 | 107 | .998 | .0871 | 11.55 | 11.55 | 132.6 | 0.0 | 132.6 | .0453 | .1956 | .00696 | 46.3 | 0.0 | 46.3 | 47.7 | 0.0 | 47.7 | 52.4 | 0.0 | 52.4 | 0.0 | |
| 434 | 107 | .997 | .0864 | 9.45 | 8.25 | 8.75 | 102.0 | 85.4 | 90.6 | .0637 | .4009 | .02006 | 45.4 | 38.0 | 40.3 | 46.3 | 38.6 | 41.0 | 55.7 | 46.3 | 49.2 | |
| 1444 | 104 | .997 | .1036 | 9.05 | 0.00 | 8.80 | 96.1 | 0.0 | 85.0 | .0476 | .4005 | .02124 | 43.7 | 0.0 | 38.4 | 44.4 | 0.0 | 39.1 | 53.0 | 0.0 | 46.7 | |
| 1454 | 103 | .997 | .1034 | 13.75 | 0.00 | 13.75 | 126.8 | 0.0 | 126.8 | .0502 | .1992 | .00785 | 45.6 | 0.0 | 45.6 | 46.9 | 0.0 | 46.9 | 50.0 | 0.0 | 50.0 | |
| 1534 | 104 | .997 | .0934 | 9.95 | 0.00 | 9.10 | 106.1 | 0.0 | 97.1 | .0402 | .3016 | .01426 | 44.1 | 0.0 | 40.4 | 45.0 | 0.0 | 41.1 | 52.7 | 0.0 | 48.1 | |

TABLE 18. INCONEL 718 WELD (HAZ) MATERIAL FRACTURE RESULTS IN LIQUID NITROGEN, TYS = 204.5 KSI

| SPEC NO | SPEC. DIM. T | INCH AREA | LOADS, KIPS | | | STRESSES, KSI | | | FLAW SIZE, INCH | | | PHI CORRECTION | | | STRESS INTENSITY FACTORS, KSI-SQRT(INCH) | | | MSC CORRECTION | | |
|---------|--------------|-----------|-------------|------|-------|---------------|-----|-------|-----------------|-------|--------|----------------|-----|------|--|-----|------|----------------|-----|------|
| | | | P1 | P2 | P3 | S1 | S2 | S3 | A | 2C | AREA | K1 | K2 | K3 | K1 | K2 | K3 | K1 | K2 | K3 |
| 57W | .104 | .998 | 7.50 | 0.00 | 0.00 | 73.4 | 0.0 | 0.0 | .0700 | .3975 | .02185 | 33.7 | 0.0 | 0.0 | 34.1 | 0.0 | 0.0 | 40.9 | 0.0 | 0.0 |
| 58W | .103 | .997 | 11.75 | 0.00 | 10.24 | 115.0 | 0.0 | 100.2 | .0665 | .3534 | .01846 | 50.8 | 0.0 | 44.3 | 52.2 | 0.0 | 45.2 | 61.6 | 0.0 | 53.4 |
| 59W | .099 | .996 | 12.55 | 0.00 | 10.28 | 127.9 | 0.0 | 104.7 | .0658 | .3630 | .01876 | 55.6 | 0.0 | 46.4 | 58.6 | 0.0 | 47.4 | 70.0 | 0.0 | 56.7 |
| 60W | .105 | .998 | 10.05 | 0.00 | 0.00 | 105.7 | 0.0 | 0.0 | .0685 | .3985 | .02144 | 43.2 | 0.0 | 0.0 | 49.3 | 0.0 | 0.0 | 61.2 | 0.0 | 0.0 |

TABLE 19. INCONEL 718 WELD (HAZ) MATERIAL FRACTURE RESULTS IN LIQUID HYDROGEN, TYS = 212.7 KSI

| SPEC NO | SPEC. DIM. T | INCH AREA | LOADS, KIPS | | | STRESSES, KSI | | | FLAW SIZE, INCH | | | PHI CORRECTION | | | STRESS INTENSITY FACTORS, KSI-SQRT(INCH) | | | MSC CORRECTION | | |
|---------|--------------|-----------|-------------|------|-------|---------------|-----|-------|-----------------|-------|--------|----------------|-----|------|--|-----|------|----------------|-----|------|
| | | | P1 | P2 | P3 | S1 | S2 | S3 | A | 2C | AREA | K1 | K2 | K3 | K1 | K2 | K3 | K1 | K2 | K3 |
| 99W | .109 | .999 | 1.85 | 0.00 | 0.00 | 17.0 | 0.0 | 0.0 | .0800 | .5492 | .03451 | 9.6 | 0.0 | 0.0 | 9.6 | 0.0 | 0.0 | 10.9 | 0.0 | 0.0 |
| 160W | .094 | 1.002 | 11.75 | 0.00 | 11.00 | 124.2 | 0.0 | 116.3 | .0501 | .2284 | .00899 | 46.2 | 0.0 | 43.3 | 47.5 | 0.0 | 44.3 | 52.5 | 0.0 | 49.8 |
| 162W | .095 | 1.002 | 9.57 | 0.00 | 8.80 | 100.8 | 0.0 | 92.6 | .0602 | .3122 | .01876 | 42.2 | 0.0 | 38.8 | 43.0 | 0.0 | 39.4 | 50.3 | 0.0 | 46.1 |
| 166W | .106 | 1.001 | 11.70 | 0.00 | 10.80 | 110.6 | 0.0 | 102.1 | .0674 | .3595 | .01903 | 49.3 | 0.0 | 45.5 | 50.4 | 0.0 | 46.3 | 59.2 | 0.0 | 54.5 |

TABLE 20. INCONEL 718 AS-WELDED MATERIAL FRACTURE RESULTS IN LIQUID HYDROGEN, TYS = 212.7 KSI

| SPEC NO | SPEC. DIM. T | INCH AREA | LOADS, KIPS | | | STRESSES, KSI | | | FLAW SIZE, INCH | | | PHI CORRECTION | | | STRESS INTENSITY FACTORS, KSI-SQRT(INCH) | | | MSC CORRECTION | | |
|---------|--------------|-----------|-------------|------|------|---------------|-----|------|-----------------|-------|--------|----------------|-----|------|--|-----|------|----------------|-----|------|
| | | | P1 | P2 | P3 | S1 | S2 | S3 | A | 2C | AREA | K1 | K2 | K3 | K1 | K2 | K3 | K1 | K2 | K3 |
| 197W | .110 | 1.001 | 10.45 | 0.00 | 5.80 | 95.0 | 0.0 | 52.7 | .0555 | .2752 | .01200 | 37.9 | 0.0 | 21.0 | 38.5 | 0.0 | 21.1 | 42.3 | 0.0 | 23.2 |
| 199W | .109 | 1.002 | 9.90 | 0.00 | 5.60 | 90.6 | 0.0 | 51.3 | .0622 | .2984 | .01458 | 38.0 | 0.0 | 21.5 | 38.5 | 0.0 | 21.6 | 43.6 | 0.0 | 24.4 |
| 200W | .114 | .997 | 9.60 | 0.00 | 5.30 | 84.8 | 0.0 | 46.8 | .0637 | .3190 | .01596 | 36.3 | 0.0 | 20.0 | 36.7 | 0.0 | 20.1 | 41.5 | 0.0 | 22.7 |

or liquid hydrogen. The computations were made on a Control Data Model 6400 computer. The raw data for all of the fracture test results are presented as computer output in Tables 10 through 20.

A summary of the stress-intensity values based on fracture loads for specimens in the four environments is given in Table 21.

TABLE 21. SUMMARY OF FRACTURE TOUGHNESS RESULTS FOR PARENT AND WELD INCONEL 718 SHEET MATERIAL.

| Material | Environment | Temp., F | Flaw Location | Yield Strength 0.2 Percent Offset, ksi | Average Stress Intensity Factor, K_{Ic} , ksi $\sqrt{\text{in.}}$ | Ratio Stress Intensity Factor to 0.2 Percent Yield Strength, $\frac{K_{Ic}}{\sigma_y}$ |
|----------|-----------------|-------------|------------------|--|---|--|
| Parent | Ucon 113 | 80 | | 177.0 | 84.0 | 0.49 |
| | LO ₂ | -297 | | 200.0* | 97.1 | 0.48 |
| | LN ₂ | -320 | | 204.5* | 100.0 | 0.49 |
| | LH ₂ | -423 | | 211.0 | 94.5 | 0.445 |
| Weld | Ucon 113 | 80 | Weld Center | 171.0 | 51.4 | 0.300 |
| | LO ₂ | -297 | Ditto | 200.0* | 52.2 | 0.260 |
| | LN ₂ | -320 | " | 204.0* | 52.1 | 0.255 |
| | LH ₂ | -423 | " | 212.7 | 52.0 | 0.245 |

*Estimated values.

From Table 21, it can be seen that the critical flaw location is the weld center for all four environments. Fractographic examination of all of the welded specimens showed essentially a 100-percent flat fracture, indicating that plane-strain conditions had been achieved. For the parent material, however, some variation was noted in the critical stress-intensity factor with temperature, the values generally being higher at the lower temperatures. The fracture surface of the parent material specimens exhibited a mixture of modes varying from approximately 40 to 70 percent slant fracture mode. This indicates that, over the temperature range investigated, the parent material of this thickness is in the transition range between plane-stress and plane-strain conditions for fracture.

In order to determine the two most critical environments for fracture, both the values of K_{Ic} and the ratio of K_{Ic} to yield strength, σ_y , were examined. As shown in Table 21, the stress-intensity factors for welded material showed no significant variation with environment, i. e., with temperature. However, when the ratio K_{Ic}/σ_y is examined, the ratio is found to decrease with decreasing temperature. From a design standpoint, this means that for a given size flaw, a lower percentage of the yield strength can be employed as the temperature decreases. From the standpoint of the design function, then, it would appear that liquid nitrogen and liquid hydrogen were the two most severe environments. The parent material also indicates that on the basis of K_{Ic}/σ_y ratio, liquid hydrogen is a severe environment; the other three environments showing little variation. Thus, Bendix agreed that fracture tests with the flaw in the weld heat-affected zone would be conducted in liquid nitrogen and in liquid hydrogen to determine which flaw location was the most critical for fracture.

Some difficulty was experienced during precracking with the flaw in the heat-affected zone when cracks initiated at the center of the weld (no notch present) and grew to a size nearly equivalent to the crack produced at the EDM flaw in the heat-affected zone (HAZ). However, enough valid tests (no secondary flaws) were obtained to determine the value of K_{Ic} for the heat-affected zone in both liquid nitrogen and liquid hydrogen. The results of all the fracture tests are summarized in Table 22. As shown in Table 22, the center of the weld proved to be the most critical flaw location for both of the environments.

TABLE 22. SUMMARY OF THE AVERAGE FRACTURE RESULTS FOR INCONEL 718 SHEET MATERIAL

| Flaw Location | Environment | Average Stress-Intensity Factor, K_{Ic} , ksi $\sqrt{\text{in.}}$ |
|---|-----------------|---|
| Parent | Uncon 113 | 84.9 |
| Weld Center | | 51.4 |
| Parent | Liquid Oxygen | 97.1 |
| Weld Center | | 52.2 |
| Parent | Liquid Nitrogen | 100.1 |
| Weld Center | | 52.1 |
| Heat-Affected Zone | | 75.0 |
| Parent | Liquid Hydrogen | 94.5 |
| Weld Center | | 52.0 |
| Heat-Affected Zone | | 54.0 |
| No Postweld Heat Treatment; Weld Center | | 42.5 |

Also included in Table 22 is the average critical stress-intensity factor for three welded specimens with no postweld heat treatment (flaw at the center of the weld). The lack of heat treatment after welding lowered K_{Ic} from 52.0 ksi $\sqrt{\text{in.}}$ for the heat-treated weld to 42.5 ksi $\sqrt{\text{in.}}$ for the unheat-treated weld, thus showing the lack of adequate heat treatment after welding to be detrimental to the fracture strength of the weld.

6.4 Sustained-Load Flaw-Growth Results

Sustained-load flaw growth tests were initially conducted on specimens with the flaw located in parent material or at the center of the weld. The results of the tests in Ucon 113, liquid oxygen, and liquid nitrogen are presented in Tables 23 through 25 and shown graphically in Figures 11 through 16. A typical specimen that exhibited flaw growth during the sustained-load test is shown in Figure 17.

TABLE 23. SUSTAINED-LOAD FLAW GROWTH RESULTS FOR INCONEL 718 SHEET MATERIAL TESTED IN UCON 113 AT ROOM TEMPERATURE

| Specimen Number | Initial Stress Intensity Factor K_{II} , ksi $\sqrt{\text{in.}}$ | Ratio, K_{II}/K_{Ic} | Time at Load, t, hr | Comments |
|--|--|------------------------|---------------------|---|
| Parent Material Results, Average $K_{Ic} = 84.9$ ksi $\sqrt{\text{in.}}$ | | | | |
| 69P | 82.7 | 0.976 | <0.1 | Failed |
| 71P | 82.2 | 0.968 | 1.8 | Failed |
| 70P | 81.8 | 0.965 | 22.7 | Failed when adjacent specimen failed |
| 72P | 80.1 | 0.945 | 100.0 DNF* | Flaw growth, $\Delta a = 0.0088$ in. |
| 68P | 78.7 | 0.927 | 100.0 DNF | Flaw growth, $\Delta a = 0.0027$ in.** |
| 73P | 74.9 | 0.88 | 96.0 DNF | Flaw growth, $\Delta a = 0.0031$ in. |
| 74P | 68.4 | 0.805 | 90.0 DNF | Trace flaw growth, $\Delta a = <0.0010$ in. |
| 67P | 67.7 | 0.80 | 125.0 DNF | No growth |
| Weld Material Results, Average $K_{Ic} = 51.4$ ksi $\sqrt{\text{in.}}$ | | | | |
| 64W | 53.4 | 1.04 | <0.1 | Failed |
| 62W | 52.4 | 1.02 | <0.1 | Failed |
| 63W | 50.8 | 0.99 | 29.6 | Failed |
| 65W | 49.7 | 0.966 | 100.0 DNF | Flaw growth, $\Delta a = 0.0065$ in. |
| 66W | 47.9 | 0.93 | 114.0 DNF | Flaw growth, $\Delta a = 0.0078$ in. |
| 67W | 45.9 | 0.892 | 97.0 DNF | Flaw growth, $\Delta a = 0.0019$ in. |
| 68W | 40.4 | 0.785 | 70.0 DNF | Flaw growth, $\Delta a = 0.0064$ in. |
| 161W | 37.6 | 0.73 | 94.0 DNF | Flaw growth, $\Delta a = 0.0009$ in. |
| 85W | 33.3 | 0.646 | 97.0 DNF | Trace flaw growth, $\Delta a = <0.0010$ in. |

*DNF = did not fail, test discontinued.

** Δa = change in flaw depth during test.

TABLE 24. SUSTAINED-LOAD FLAW GROWTH RESULTS FOR INCONEL 718 SHEET MATERIAL TESTED IN LIQUID OXYGEN

| Specimen Number | Initial Stress Intensity Factor, K_{II} , ksi $\sqrt{\text{in.}}$ | Ratio, K_{II}/K_{Ic} | Time at Load, t, hr | Comments |
|--|---|------------------------|---------------------|--|
| Parent Material Results, Average $K_{Ic} = 97.1$ ksi $\sqrt{\text{in.}}$ | | | | |
| 75P | 100.5 | 1.03 | <0.1 | Failed |
| 81P | 95.1 | 0.98 | 1.0 | Failed |
| 76P | 90.0 | 0.93 | 5.25 DNF* | Flaw growth, $\Delta a = 0.0041$ in.** |
| 78P | 84.8 | 0.87 | 19.5 | Void |
| 77P | 79.9 | 0.82 | 6.0 DNF | Flaw growth, $\Delta a = 0.0025$ in. |
| 79P | 70.3 | 0.72 | 17.6 DNF | Flaw growth, $\Delta a = 0.0015$ in. |
| 80P | 63.0 | 0.65 | 93.1 DNF | No growth |
| 82P | 56.9 | 0.59 | 100.0 DNF | No growth |
| Weld Material Results, Average $K_{Ic} = 52.2$ ksi $\sqrt{\text{in.}}$ | | | | |
| 70W | 50.6 | 0.97 | <0.1 | Failed |
| 71W | 47.8 | 0.93 | 2.75 DNF | Flaw growth, $\Delta a = 0.0208$ in. |
| 72W | 41.8 | 0.80 | 3.0 DNF | Flaw growth, $\Delta a = 0.0107$ in. |
| 69W | 36.7 | 0.70 | <0.1 | Secondary flaw |
| 73W | 33.6 | 0.64 | 6.25 DNF | Flaw growth, $\Delta a = 0.0014$ in. |
| 167W | 34.8 | 0.64 | 17.1 | Void |
| 75W | 31.1 | 0.60 | 94.4 DNF | No growth |
| 74W | 29.1 | 0.56 | 29.5 DNF | No growth |

*DNF = did not fail, test discontinued.

** Δa = Change in flaw depth during test.

TABLE 25. SUSTAINED-LOAD FLAW GROWTH RESULTS FOR INCONEL 718 SHEET MATERIAL TESTED IN LIQUID NITROGEN

| Specimen Number | Initial Stress Intensity Factor, K_{II} , ksi $\sqrt{\text{in.}}$ | Ratio, K_{II}/K_{IC} | Time at Load, t, hr | Comments |
|---|---|------------------------|---------------------|---|
| Parent Material Results, Average $K_{IC} = 100.1$ ksi $\sqrt{\text{in.}}$ | | | | |
| 83P | 100.2 | 1.00 | <0.1 | Failed |
| 85P | 87.1 | 0.87 | 0.8 DNF* | Flaw growth, $\Delta a = 0.0013$ in.** |
| 90P | 84.7 | 0.85 | 78.5 DNF | Flaw growth, $\Delta a = 0.0012$ in. |
| 86P | 80.1 | 0.80 | 22.0 DNF | Flaw growth, $\Delta a = 0.0011$ in. |
| 88P | 75.9 | 0.76 | 95.9 DNF | Trace flaw growth, $\Delta a = <0.0010$ in. |
| 89P | 78.8 | 0.79 | 108.8 DNF | Trace flaw growth, $\Delta a = <0.0010$ in. |
| 87P | 73.3 | 0.73 | 21.5 DNF | No growth |
| 84P | -- | -- | -- | Liquid level malfunction, test void |
| Weld Material Results, Average $K_{IC} = 52.1$ ksi $\sqrt{\text{in.}}$ | | | | |
| 78W | 56.2 | 1.07 | 0.15 | Failed |
| 79W | 53.9 | 1.04 | 0.2 | Failed |
| 80W | 50.7 | 0.975 | 40.1 | Failed*** |
| 83W | 50.8 | 0.975 | <0.1 | Failed |
| 84W | 49.8 | 0.955 | 24.0 DNF | Flaw growth, $\Delta a = 0.0049$ in. |
| 164W | 45.8 | 0.88 | 24.5 | Failed*** |
| 165W | 41.2 | 0.792 | 100.0 DNF | Flaw growth, $\Delta a = 0.0012$ in. |
| 159W | 37.8 | 0.726 | 91.0 DNF | No growth |

*DNF = did not fail, test discontinued.

** Δa = change in flaw depth during test.

***Secondary flaws.

For the room-temperature Ucon 113, liquid nitrogen, and liquid oxygen tests, a run-out time of 100 hours was employed. The highest value of the stress-intensity factor at which flaw growth did not occur in 100 hours was defined as the threshold stress-intensity factor, K_{th} , for that combination of flaw location and environment. For example, for the parent material results in Ucon 113 (shown in Table 23) specimen 74P ($K_{II} = 68.4$ ksi $\sqrt{\text{in.}}$) exhibited a trace of flaw growth in 90 hours but specimen 67P ($K_{II} = 67.7$ ksi $\sqrt{\text{in.}}$) exhibited no flaw growth in 125 hours. Thus, the highest value of K_{II} that exists for parent material in room temperature Ucon 113 for no flaw growth lies between these two values, i. e., $67.7 < K_{th} < 68.4$ ksi $\sqrt{\text{in.}}$. For this case, the threshold stress-intensity factor for flaw growth is $K_{th} \approx 68$ ksi $\sqrt{\text{in.}}$.

For the liquid hydrogen test results, a slightly different analysis was necessary due to the quantity of liquid hydrogen available for each test that limited the run-out time to approximately 50 hours. For these results, the flaw-growth rate, $\Delta(a/Q)/\Delta t$ [where $\Delta(a/Q)$ is the change in the normalized flaw depth during the test and Δt is the time at load], was computed for each specimen as shown in Table 26. The flaw-growth rates then were plotted as a function of the ratio of initial to critical stress-intensity factor, K_{II}/K_{IC} , as shown in Figure 18. Finally, the flaw-growth rate was extrapolated to zero, the corresponding ratio of K_{II}/K_{IC} being defined as K_{th}/K_{IC} . As shown in Figure 18, $K_{th}/K_{IC} = 0.56$ or $K_{th} = 29.1$ ksi $\sqrt{\text{in.}}$ for the welded sheet material and $K_{th}/K_{IC} = 0.60$ or $K_{th} = 57$ ksi $\sqrt{\text{in.}}$ for the parent sheet material in liquid hydrogen.

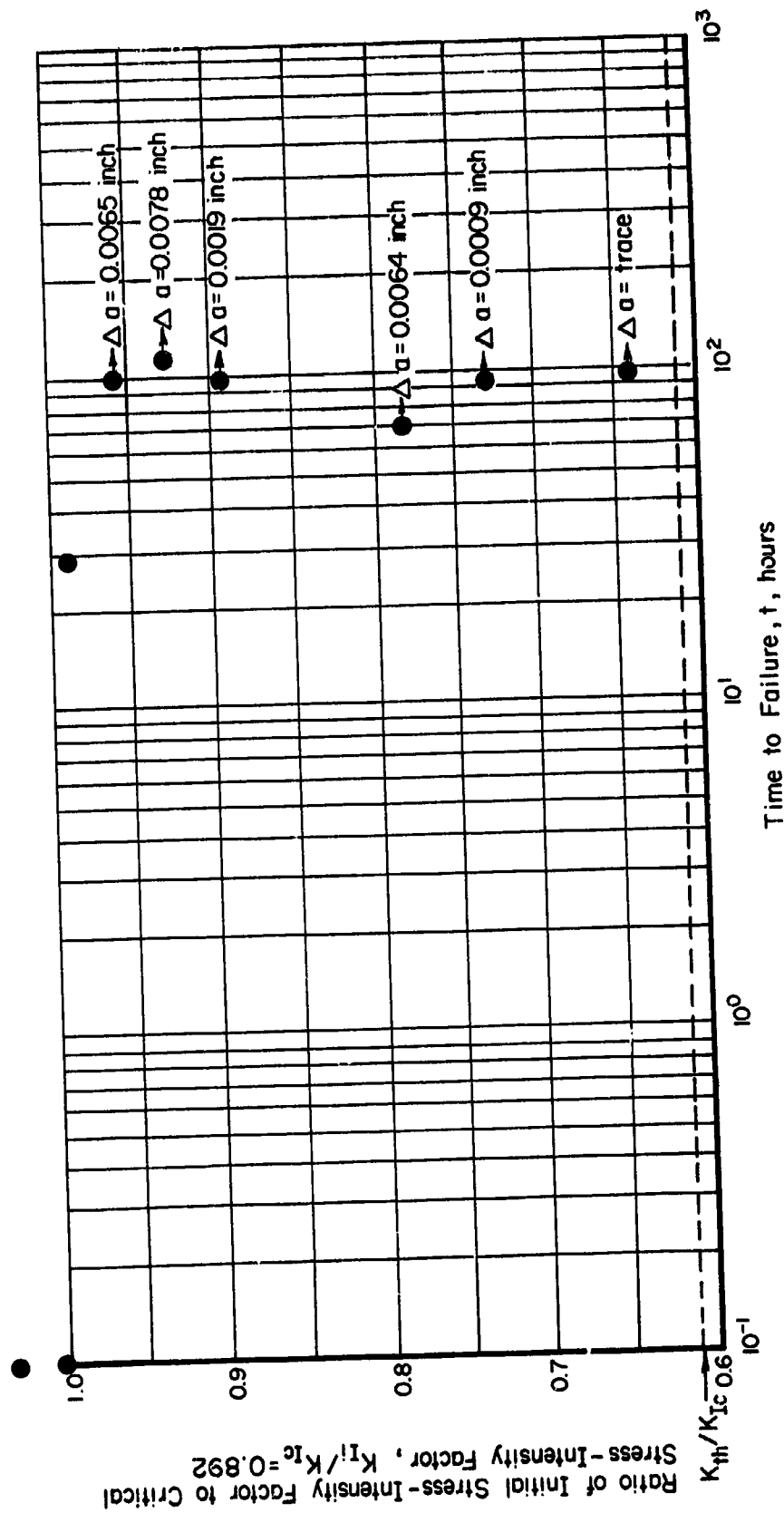


FIGURE 11. SUSTAINED LOAD TEST RESULTS FOR WELDED INCONEL 718 IN UCON 113 AT ROOM TEMPERATURE

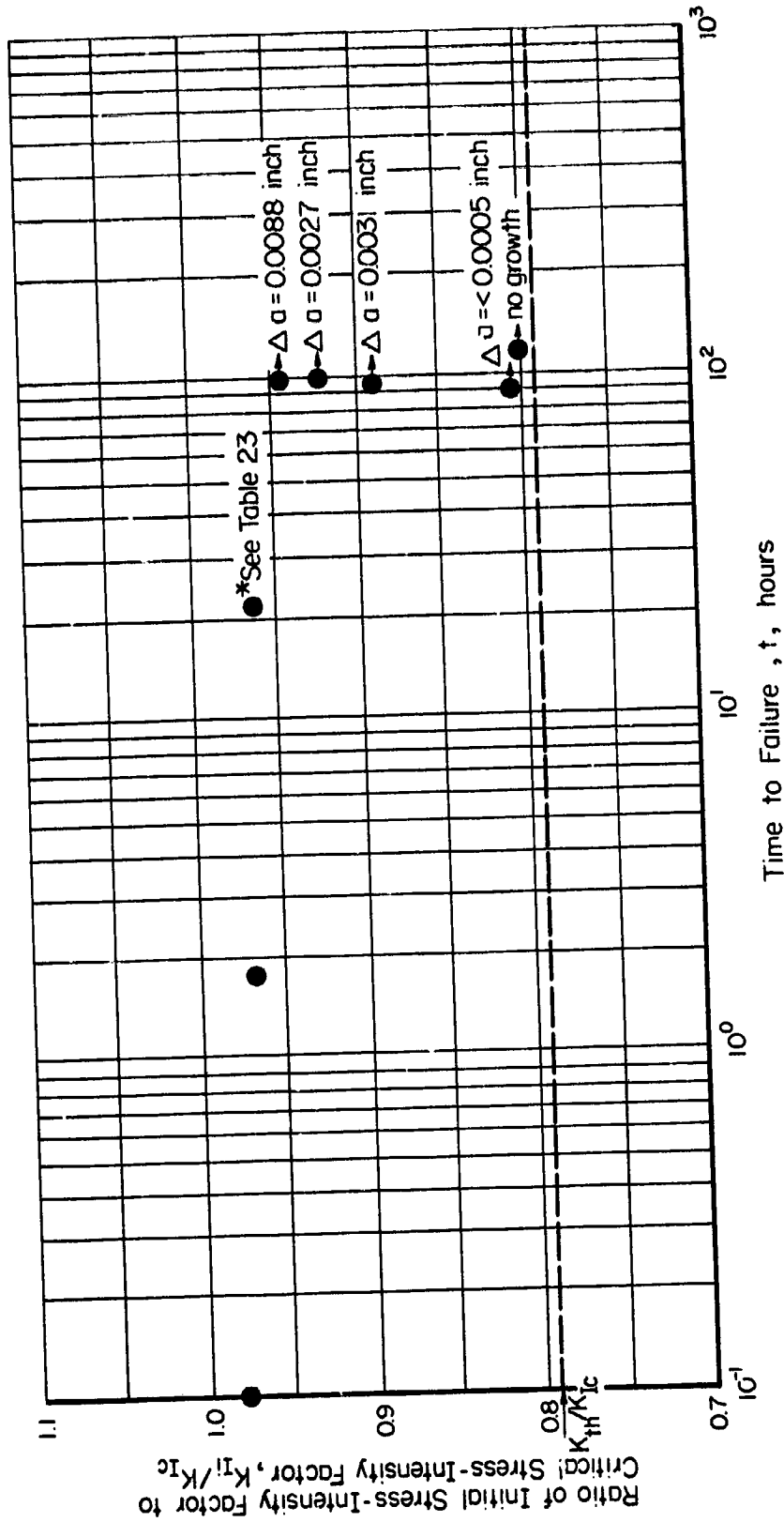


FIGURE 12. SUSTAINED-LOAD TEST RESULTS FOR PARENT INCONEL 718 IN UCON 113 AT ROOM TEMPERATURE

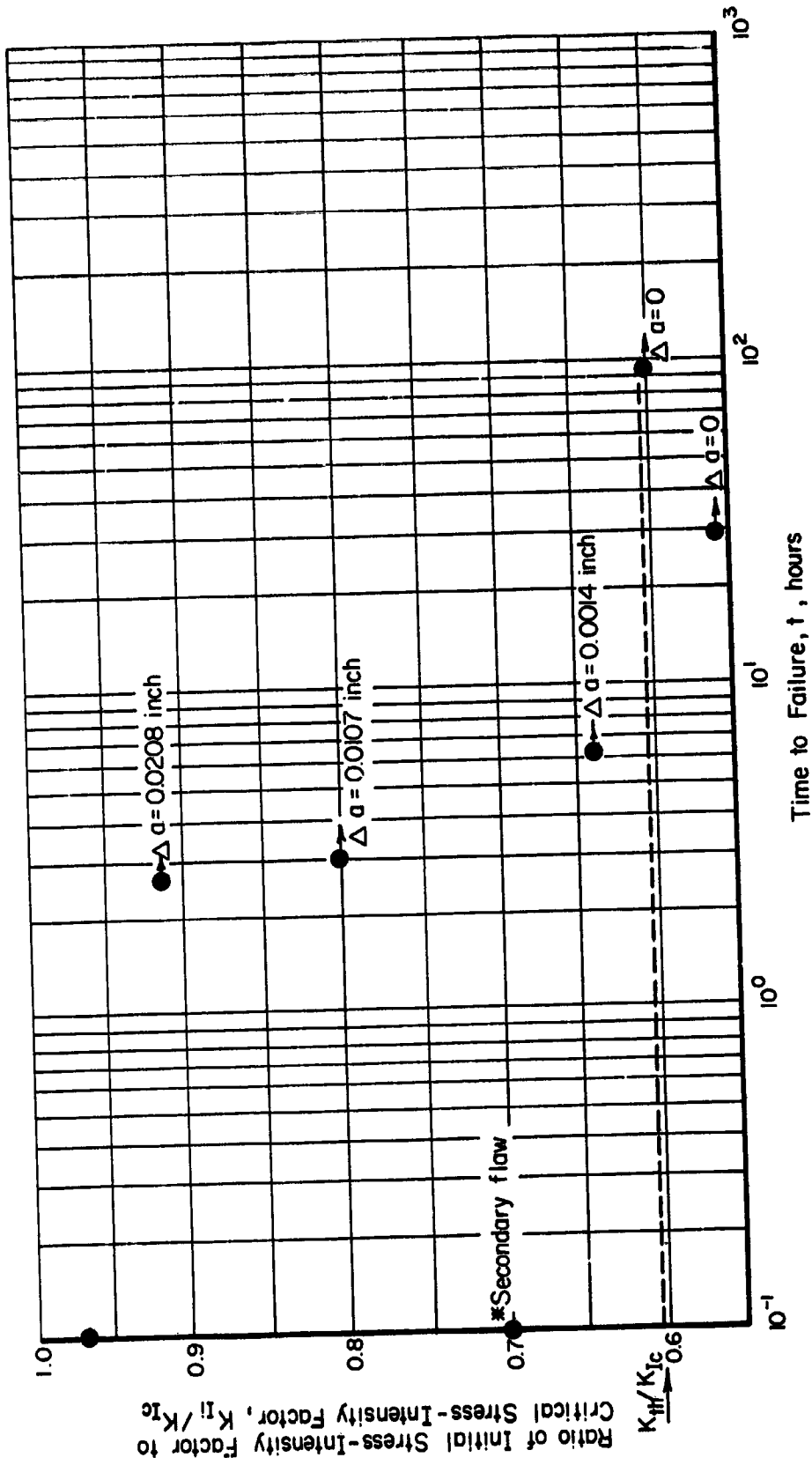


FIGURE 13. SUSTAINED-LOAD TEST RESULTS FOR WELDED INCONEL 718 IN LIQUID OXYGEN

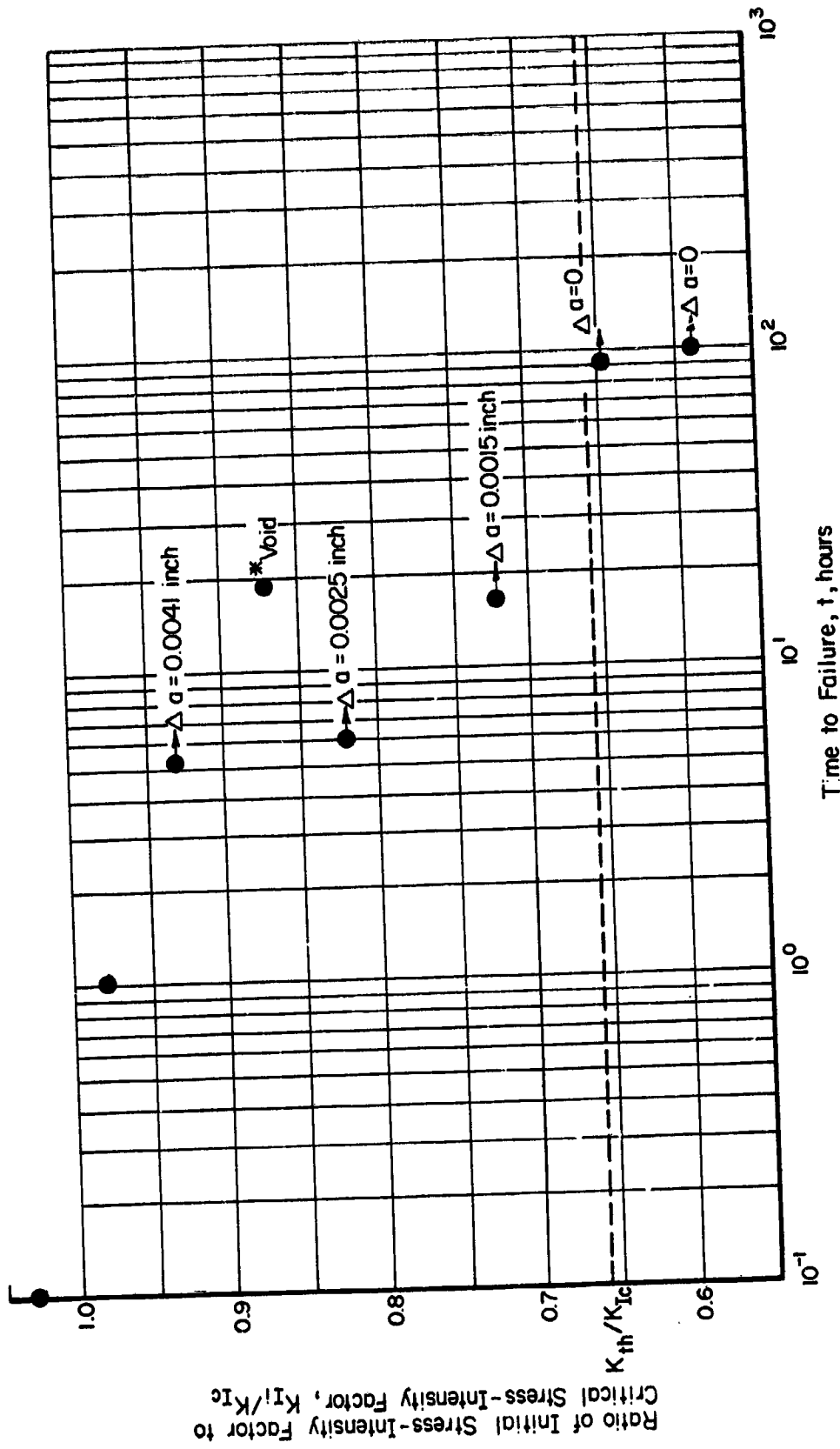


FIGURE 14. SUSTAINED-LOAD TEST RESULTS FOR PARENT INCONEL 718 IN LIQUID OXYGEN

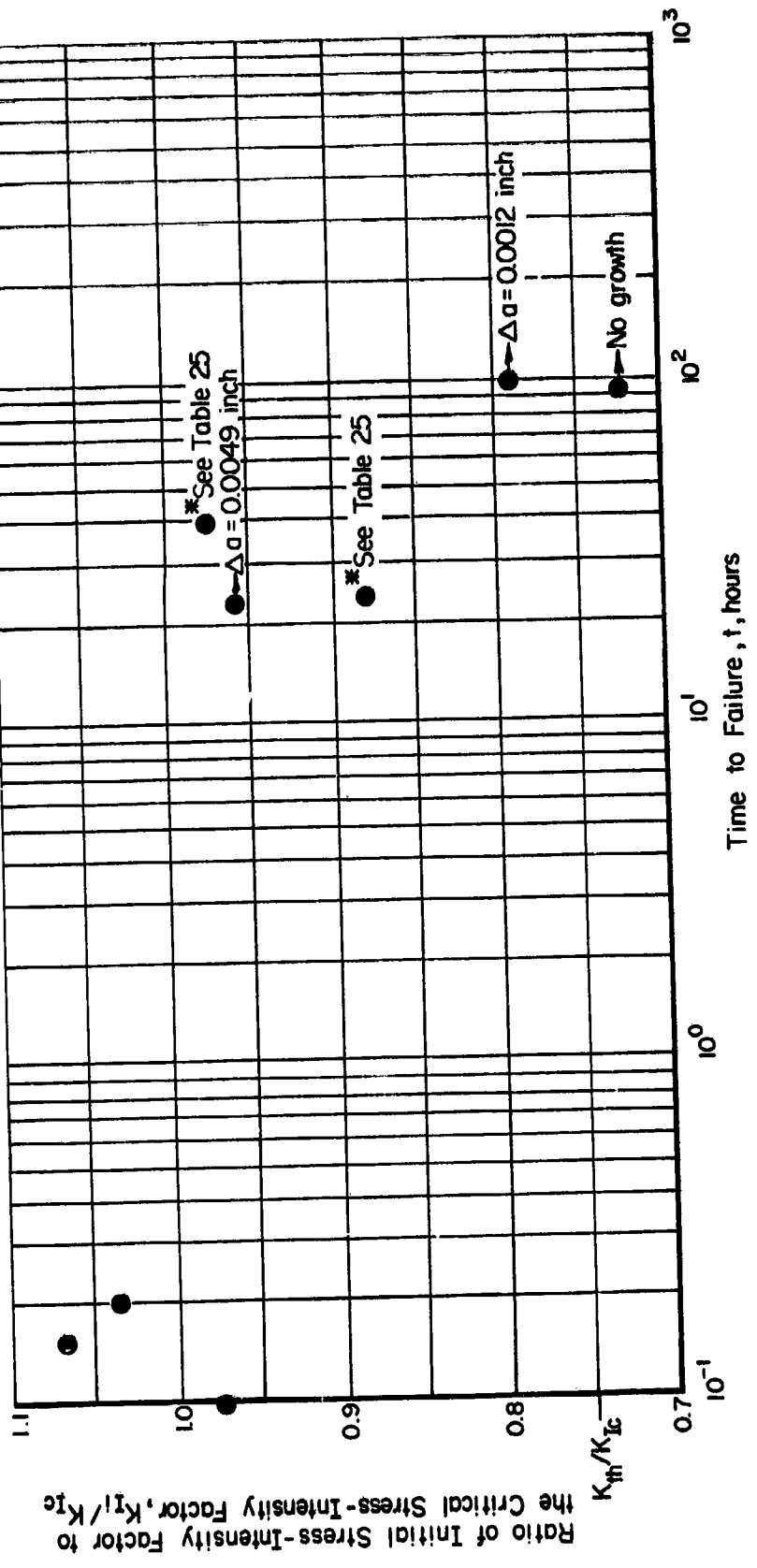


FIGURE 15. SUSTAINED-LOAD TEST RESULTS FOR WELDED INCONEL 718 IN LIQUID NITROGEN

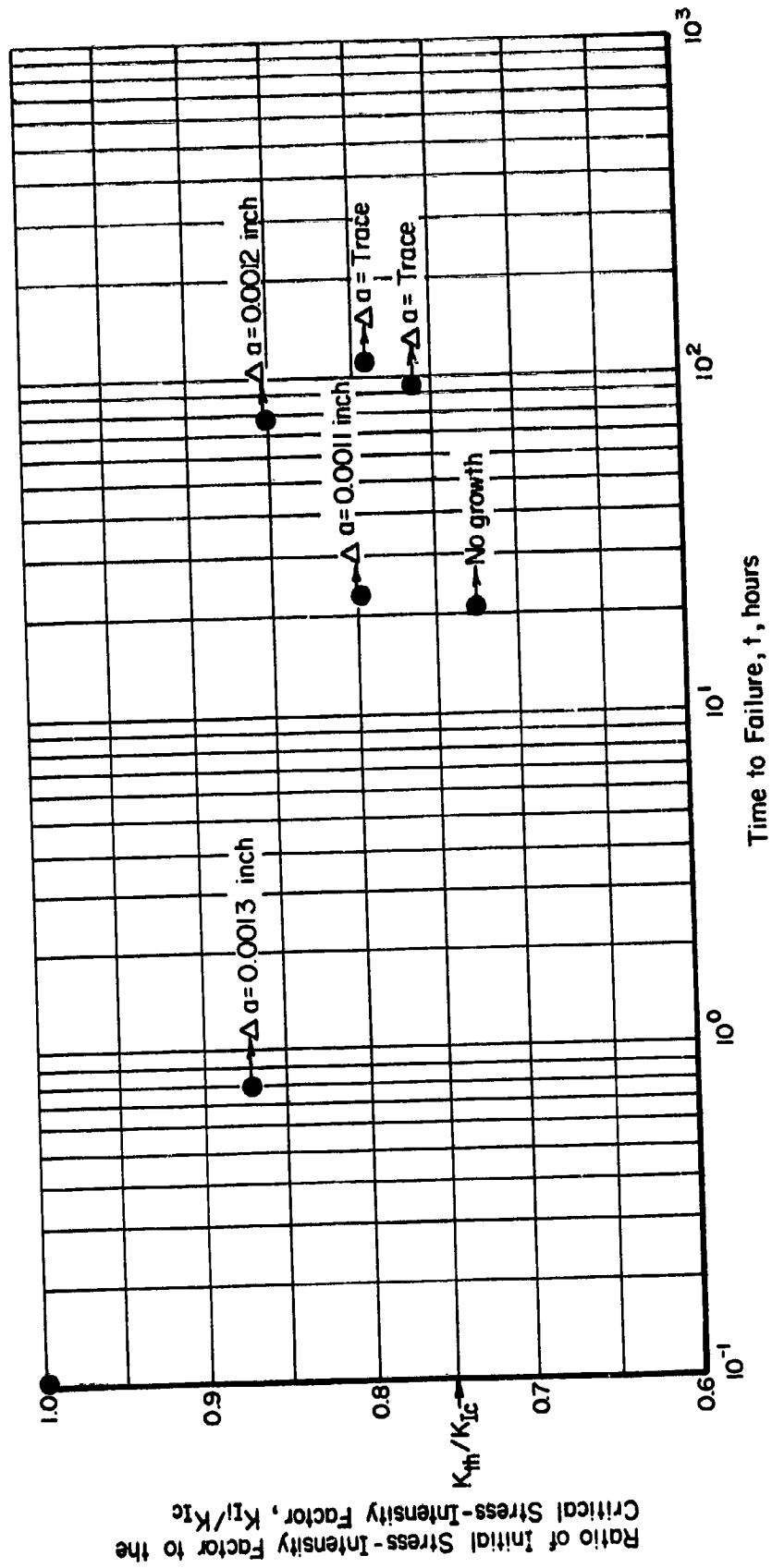
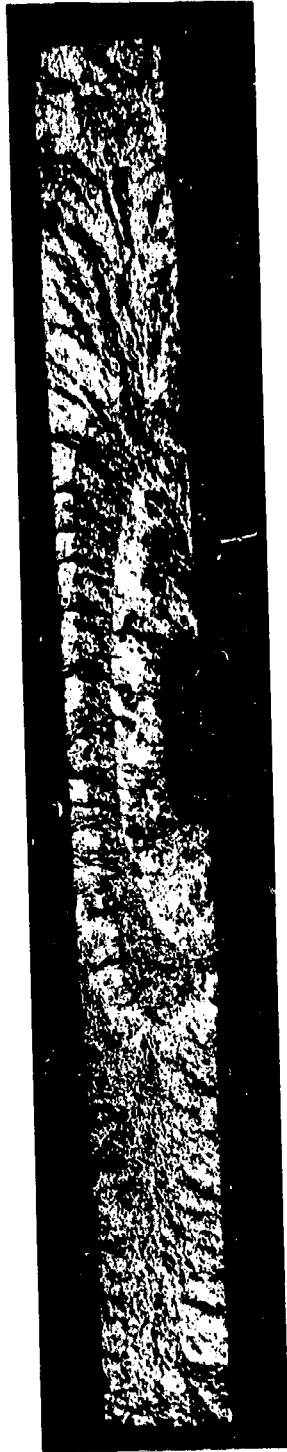


FIGURE 16. SUSTAINED-LOAD TEST RESULTS FOR PARENT INCONEL 718 IN LIQUID NITROGEN



6X

FIGURE 17. TYPICAL SUSTAINED-LOAD FLAW GROWTH SPECIMEN AFTER TESTING

Specimen No. 71W; Tested 2.75 Hours in Liquid Oxygen at a $K_{II}/K_{Ic} = 0.915$;
Did Not Fail.

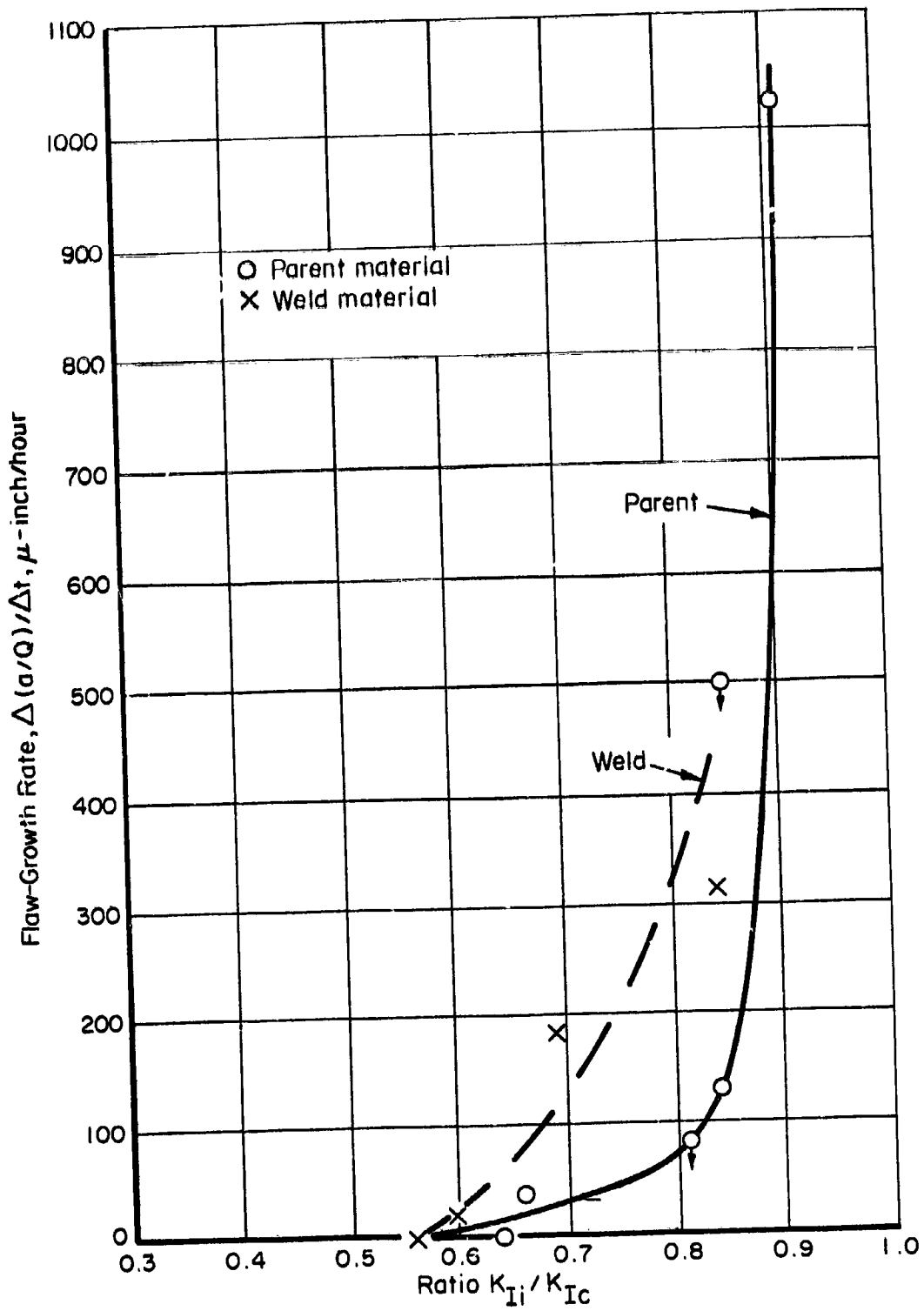


FIGURE 18. SUSTAINED-LOAD FLAW-GROWTH RATE FOR INCONEL 718 SHEET MATERIAL IN LIQUID HYDROGEN

TABLE 26. SUSTAINED-LOAD FLAW GROWTH RESULTS FOR INCONEL 718 SHEET MATERIAL IN LIQUID HYDROGEN

| Specimen Number | Initial Stress Intensity Factor, K_{II} , ksi $\sqrt{in.}$ | Ratio K_{II}/K_{IC} | Time at Load, t, hour | Flaw Growth Rate, $d(a/Q)/dt$ μ in./hr. | Comments |
|---|--|-----------------------|-----------------------|---|--|
| Parent Material, $K_{IC} = 94.5$ ksi $\sqrt{in.}$ | | | | | |
| 92P | 86.0 | 0.91 | 7.0 | 1,040 | Flaw growth, $\Delta a = 0.0085$ in. |
| 91P | 80.1 | 0.85 | 1.7 | <500 | Trace flaw growth, $\Delta a < 0.0010$ in. |
| 94P | 79.9 | 0.84 | 10.0 | 129 | Flaw growth, $\Delta a = 0.0015$ in. |
| 93P | 76.1 | 0.81 | 9.9 | <85 | Trace flaw growth, $\Delta a < 0.0010$ in. |
| 95P | 62.7 | 0.66 | 44.2 | 38 | Flaw growth, $\Delta a = 0.0023$ in. |
| 96P | 60.0 | 0.64 | 46.2 | 0 | No growth |
| Weld Material, $K_{IC} = 52.0$ ksi $\sqrt{in.}$ | | | | | |
| 87W | 43.7 | 0.84 | 3.37 | 312 | Flaw growth, $\Delta a = 0.0013$ in. |
| 88W | -- | -- | -- | -- | Void - secondary flaw |
| 86W | 36.0 | 0.69 | 4.35 | 188 | Flaw growth, $\Delta a = 0.0010$ in. |
| 108W | -- | -- | -- | -- | Void - secondary flaw |
| 91W | 30.7 | 0.59 | 51.5 | 19 | Flaw growth, $\Delta a = 0.0012$ in. |
| 92W | 29.8 | 0.57 | 45.0 | 18 | Trace flaw growth, $\Delta a < 0.0010$ in. |
| 90W | 29.3 | 0.56 | 25.0 | 0 | No growth |
| 89W | -- | -- | -- | -- | Void |

Once the values of K_{th} had been established for the flaws located in parent and weld material for the four environments, the two most critical sustained-load environments were determined. From Table 27 it is shown that both the value of K_{th} and the ratio of K_{th}/K_{IC} are lowest, for both the parent and weld flaw location, in the liquid oxygen and the liquid hydrogen environments. The low values of K_{th} and ratio of K_{th}/K_{IC} indicate that flaw growth under sustained load occurs readily in these environments. Thus, to determine the most severe flaw location for sustained-load flaw growth in these environments, a series of tests with the flaw in the weld heat-affected-zone (HAZ) was initiated.

TABLE 27. SUMMARY OF THE SUSTAINED-LOAD FLAW GROWTH RESULTS FOR INCONEL 718 SHEET MATERIAL

| Environment | Flaw Location | Threshold Stress-Intensity Factor, K_{th} , ksi $\sqrt{in.}$ | Ratio, K_{th}/K_{IC} |
|-----------------------------|---------------|--|------------------------|
| Ucon 113 (Room Temperature) | Parent | 68 | 0.79 |
| | | 75 | 0.75 |
| | | 64 | 0.66 |
| | | 57 | 0.60 |
| Ucon 113 (Room Temperature) | Weld Center | 32 | 0.62 |
| | | 39 | 0.75 |
| | | 31 | 0.60 |
| | | 29 | 0.56 |

The results of these tests in liquid oxygen on specimens with the flaw in the HAZ are presented in Table 28 and shown graphically in Figure 19. As was previously discussed, the two critical environments for the fracture tests were liquid nitrogen and liquid hydrogen, so no fracture results on specimens with the flaw in the HAZ were available in liquid oxygen. If Table 28 is examined, however, it is seen that specimen 98W failed within a short period of time (approximately 10 seconds) after the load was applied. Thus the value of K_{Ic} would be expected to be slightly greater than the recorded $K_{II} = 59.7 \text{ ksi}\sqrt{\text{in.}}$. Therefore, a value of $60 \text{ ksi}\sqrt{\text{in.}}$ was selected as a best estimate of K_{Ic} for this condition and was subsequently used to compute the ratios of K_{II}/K_{Ic} listed in Table 28 and shown in Figure 19.

TABLE 28. SUSTAINED-LOAD FLAW GROWTH RESULTS IN LIQUID OXYGEN FOR SPECIMENS WITH THE FLAW IN THE HEAT-AFFECTED ZONE

| Specimen Number | Initial Stress* Intensity Factor, | | Time at Load, t, hr | Comments |
|-----------------|------------------------------------|-------------------|---------------------|---|
| | K_{II} , ksi $\sqrt{\text{in.}}$ | K_{II}/K_{Ic} * | | |
| 95W | 59.0 | 0.98 | <0.1 | Void, secondary flaws |
| 98W | 59.7 | 0.99 | <0.1 | Failed |
| 97W | 53.3 | 0.89 | 88.1 DNF | Flaw growth, $\Delta a = 0.0106 \text{ in.}$ |
| 93W | 47.0 | 0.78 | 8.0 DNF | Void, secondary flaws |
| 100W | 42.0 | 0.70 | 96.2 DNF | Flaw growth, $\Delta a = 0.0039 \text{ in.}$ |
| 102W | 40.3 | 0.67 | 97.5 DNF | Trace of flaw growth, $\Delta a = 0.0010 \text{ in.}$ |
| 96W | 44.0 | 0.73 | <0.1 | Void, secondary flaws |

DNF = did not fail.

* $K_{Ic} = 60.0 \text{ ksi}\sqrt{\text{in.}}$; see text for discussion.

As shown in Table 28, some difficulty was experienced with secondary flaws. These secondary flaws generally occurred in the center of the weld, well away from the EDM flaw in the HAZ. However, enough valid data points were obtained to allow the threshold stress-intensity factor to be determined as $K_{th} = 39 \text{ ksi}\sqrt{\text{in.}}$ or $K_{th}/K_{Ic} = 0.65$. Thus, in liquid oxygen the weld center is the critical flaw location for sustained-load flaw growth.

For the liquid hydrogen environment, only one specimen was tested with the flaw in the HAZ. This test was conducted at a K_{II}/K_{Ic} ratio approximately equal to the threshold value ratio for specimens with the flaw at the weld center. The results of this test, as shown in Figure 20, show that the HAZ is not a significantly more critical flaw location than the weld center.

6.5 Fatigue-Crack Propagation Results (R = 0)

In the initial program, the fatigue tests were to be conducted at a stress ratio $R = 0$ and a maximum stress of 89.4 ksi. Initial flaw sizes were to be determined so that failure would occur between 1 and 500 cycles. This test schedule was followed for the

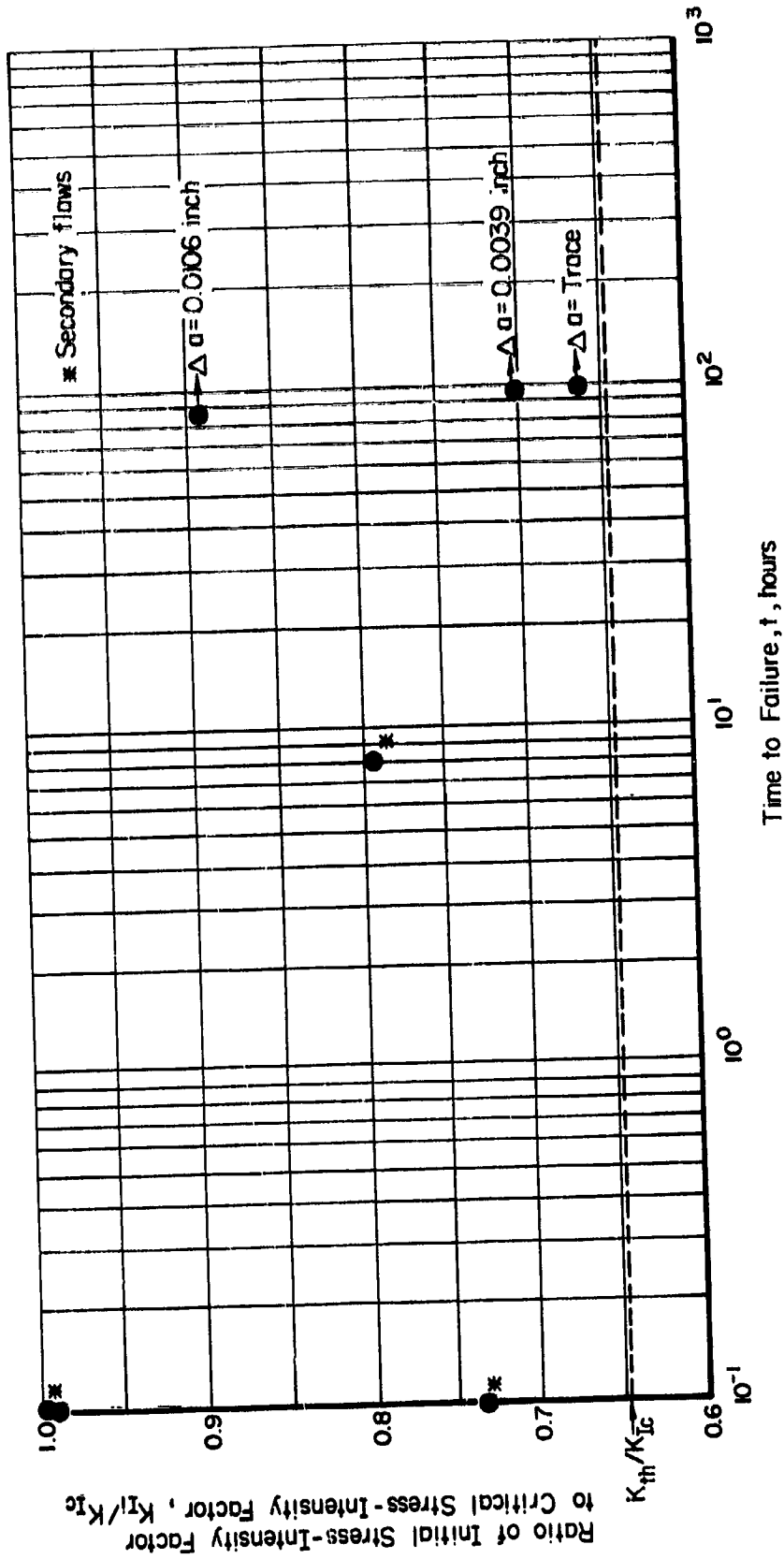


FIGURE 19. SUSTAINED-LOAD FLAW-GROWTH RESULTS FOR INCONEL 718 MATERIAL (HEAT-AFFECTED-ZONE) TESTED IN LIQUID OXYGEN

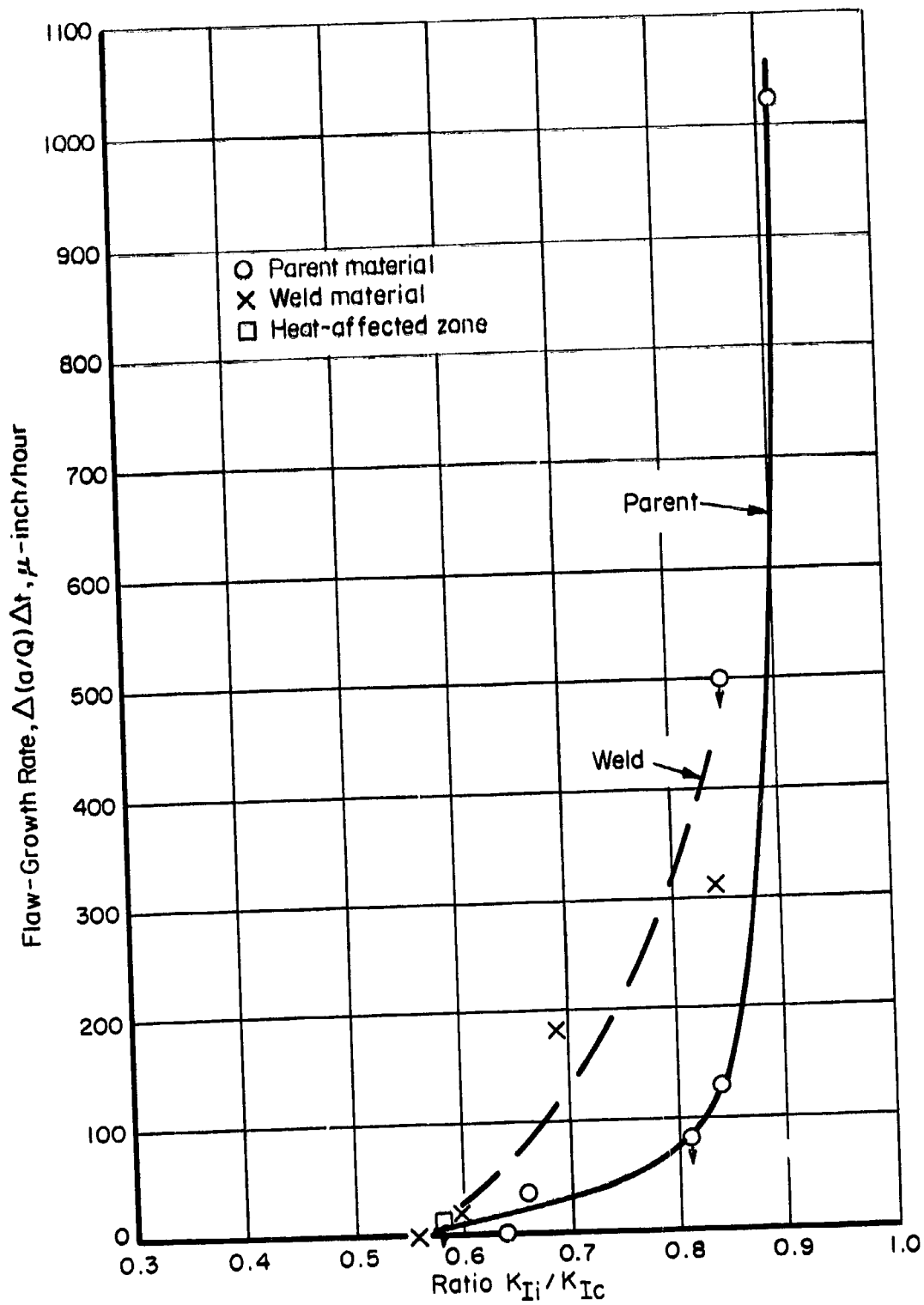


FIGURE 20. SUSTAINED-LOAD FLAW-GROWTH RATES FOR INCONEL 718 SHEET MATERIAL IN LIQUID HYDROGEN

welded specimens tested in liquid oxygen, the results of which are presented in Table 29 and shown graphically in Figure 21.

TABLE 29. WELDED INCONEL 718 SHEET MATERIAL FATIGUE RESULTS IN LIQUID OXYGEN,
AVERAGE $K_{Ic} = 52,2 \text{ ksi}\sqrt{\text{in.}}$

| Specimen Number | Initial Stress-Intensity Factor | | Cycles to Failure | Comments |
|-----------------|---|-----------------|-------------------|----------------|
| | K_{Ii} $\text{ksi}\sqrt{\text{in.}}$ | K_{Ii}/K_{Ic} | | |
| 115W | 52.0 | 1.0 | 1 | Secondary Flaw |
| 120W | 54.0 | 1.03 | 1 | |
| 109W | 48.8 | 0.935 | 92 | |
| 113W | 47.8 | 0.915 | 108 | |
| 110W | 46.2 | 0.885 | 120 | |
| 114W | 49.4 | 0.83 | 234 | |
| 111W | 44.0 | 0.84 | 282 | |
| 118W | 52.7 | 1.0 | 1 | Secondary Flaw |
| 116W | 39.3 | 0.755 | 408 | |
| 117W | 39.5 | 0.755 | 452 | |
| 119W | 37.7 | 0.72 | 481 | |
| 112W | 50.0 | 0.96 | 1 | Secondary Flaw |

Subsequent to the completion of these tests, the fatigue portion of the program was revised at the request of NASA-MSc personnel. The new test program involved fatigue cycling at the stress level ($R = 0$) necessary to produce an initial stress-intensity factor in the range $0.4 \leq K_{Ii}/K_{Ic} \leq 0.8$ for the liquid-oxygen tests and $0.2 \leq K_{Ii}/K_{Ic} \leq 0.4$ for the liquid-hydrogen tests. Due to the high toughness of this material, the flaw size and stress conditions necessary to achieve the relatively low values of K_{Ii} would result in the flaw propagating through the thickness prior to fracture. Therefore each specimen was cycled enough to produce from 0.005 to 0.010 inch of flaw growth in the thickness (a) direction at the desired K_{Ii} level. The specimen was then fractured, the growth measured and the average fatigue-crack propagation rate computed.

This change in the program allowed the average fatigue-crack propagation rates to be more accurately determined in the range of K_{Ii}/K_{Ic} ratios near and just below the threshold value for flaw growth under sustained-load in the test environments. The low range of $0.2 \leq K_{Ii}/K_{Ic} \leq 0.4$ for the liquid-hydrogen tests corresponded to the indicated threshold value for sustained-load flaw growth for Inconel 718 as determined by NASA-MSc in tests at ambient temperature and in an approximately 1,000 ps_i gaseous hydrogen environment.

The observed fatigue-crack propagation rates for parent material are presented in Tables 30 and 31 for the liquid-oxygen and liquid-hydrogen environments respectively. The weld material results in liquid hydrogen are presented in Table 32. The fatigue-crack propagation rates in Tables 30 through 32 are presented in terms of change in the normalized flaw depth, a/Q , per cycle. The measured crack-propagation rates, $\Delta(a/Q)/\Delta N$, are then listed in terms of the average stress-intensity factor, K_{Ii} , based on the average flaw size and the maximum load during the fatigue cycle. For the case of $R = 0$, the maximum stress-intensity factor is equivalent to the stress-intensity factor range, ΔK .

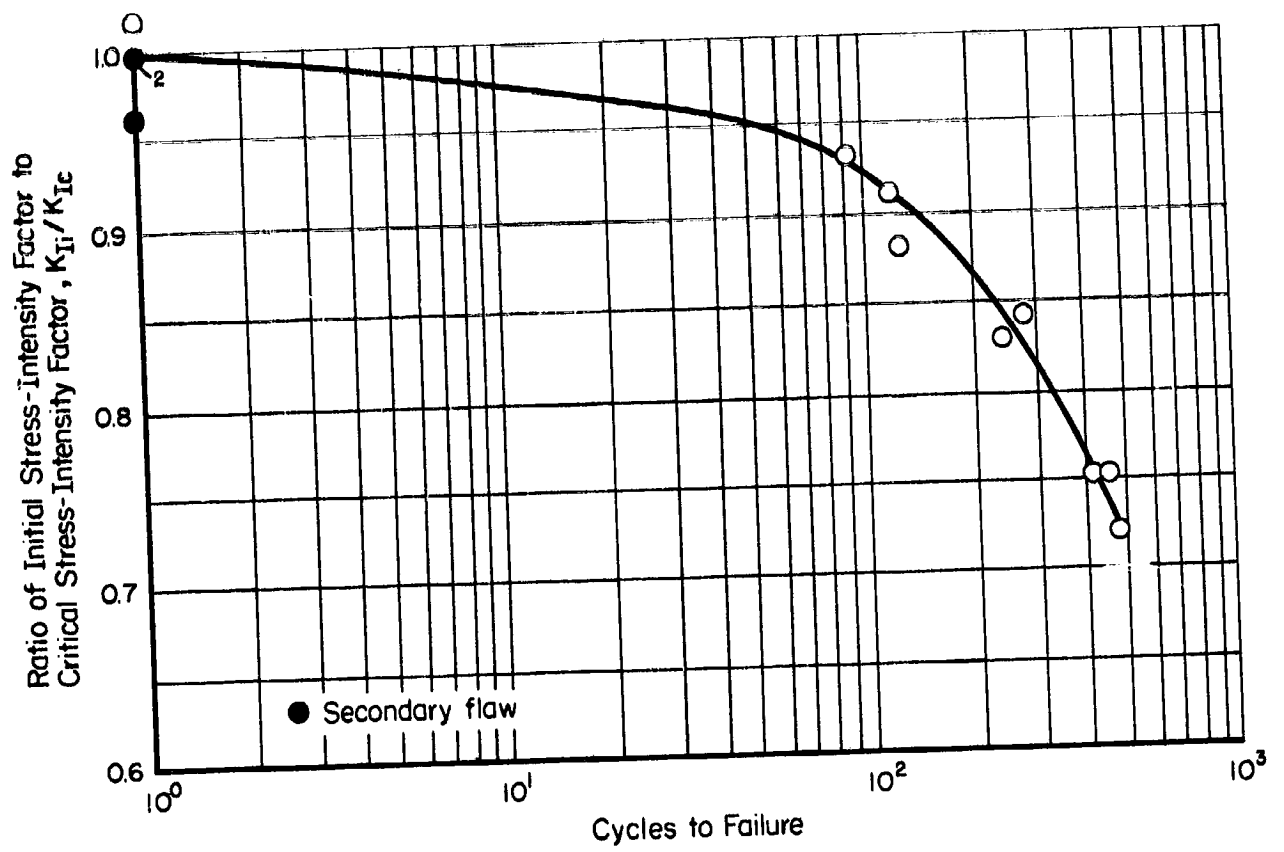


FIGURE 21. WELDED INCONEL 718 SHEET MATERIAL FATIGUE RESULTS IN LIQUID OXYGEN

TABLE 30. FATIGUE-CRACK PROPAGATION RESULTS FOR PARENT INCONEL 718
TESTED IN LIQUID OXYGEN, R = 0, $K_{Ic} = 97.1 \text{ ksi}\sqrt{\text{in.}}$

| Specimen Number | Maximum Test Stress Level, ksi | Average Initial Stress Intensity Factor ^a | | Measured Crack Propagation Rate, $\left \frac{d(a/Q)}{dN} \right $ $\mu\text{in./cycle}$ |
|--------------------|--------------------------------|--|-----------------------|---|
| | | \bar{K}_{II} , $\text{ksi}\sqrt{\text{in.}}$ | \bar{K}_{II}/K_{Ic} | |
| 101P | 89.4 | 46.6 | 0.480 | 7.3 |
| 103P | 89.4 | 46.1 | 0.475 | 7.9 |
| 100P ^{ba} | 120.0 | 45.8 | 0.471 | 7.4 |
| 102P | 120.0 | 44.0 | 0.454 | 4.1 |
| 105P | 120.0 | 46.6 | 0.480 | 5.4 |
| 104P | 120.0 | 53.7 | 0.554 | 7.6 |
| 3P | 120.0 | 59.0 | 0.608 | 17.8 |
| 2P | 120.0 | 60.4 | 0.621 | 18.2 |
| 4P | 120.0 | 64.1 | 0.661 | 21.7 |
| 106P | 120.0 | 66.6 | 0.686 | 30.8 |
| 1P | 120.0 | 68.0 | 0.701 | 39.0 |
| 107P | 120.0 | 72.6 | 0.749 | 63.0 |

^aBased on maximum stress of the fatigue cycle.

^{ba}Specimen buckled after cycling.

TABLE 31. FATIGUE-CRACK PROPAGATION RESULTS FOR PARENT INCONEL 718
TESTED IN LIQUID HYDROGEN, R = 0, $K_{Ic} = 94.5 \text{ ksi}\sqrt{\text{in.}}$

| Specimen Number | Maximum Test Stress Level, ksi | Average Initial Stress Intensity Factor ^a | | Measured Crack Propagation Rate, $\frac{d(a/Q)}{dN}$ $\mu\text{in./cycle}$ |
|-----------------|--------------------------------|--|-----------------------|--|
| | | \bar{K}_{II} , $\text{ksi}\sqrt{\text{in.}}$ | \bar{K}_{II}/K_{Ic} | |
| 118P | 68 | 37.4 | 0.396 | 4.80 |
| 117P | 68 | 36.6 | 0.386 | 2.50 |
| 127P | 64 | 32.2 | 0.342 | 1.40 |
| 116P | 68 | 31.6 | 0.335 | 0.98 |
| 114P | 64 | 26.6 | 0.281 | 0.47 |
| 113P | 68 | 26.0 | 0.274 | 0.32 |
| 112P | 50 | 29.8 | 0.315 | 0.70 |
| 111P | 50 | 28.2 | 0.298 | 0.86 |
| 110P | 50 | 24.2 | 0.256 | 0.39 |
| 109P | 50 | 21.2 | 0.224 | 0.18 |
| 108P | 50 | 18.0 | 0.190 | 0.14 |
| 129P | 50 | 19.4 | 0.206 | 0.22 |

^aBased on the maximum stress of the fatigue cycle.

TABLE 32. FATIGUE-CRACK PROPAGATION RESULTS FOR WELDED INCONEL 718
TESTED IN LIQUID HYDROGEN, R = 0, $K_{Ic} = 52.0 \text{ ksi} \sqrt{\text{in.}}$

| Specimen Number | Maximum Test Stress Level, ksi | Average Initial Stress Intensity Factor* \bar{K}_{II} , $\text{ksi} \sqrt{\text{in.}}$ | K_{II}/K_{Ic} | Measured Crack Propagation Rate, |
|-----------------|--------------------------------|--|-----------------|--|
| | | | | $\left \frac{d(a/Q)}{dN} \right $, $\mu\text{in./cycle}$ |
| 121W | 37 | 20.7 | 0.398 | 1.04 |
| 01W | 37 | 20.0 | 0.402 | 2.88 |
| 125W | 37 | 19.85 | 0.382 | 1.03 |
| 134W | 37 | 18.05 | 0.348 | 0.02 |
| 130W | 37 | 17.3 | 0.333 | 0.45 |
| 133W | 28 | 17.1 | 0.329 | 0.93 |
| 128W | 37 | 14.35 | 0.276 | 0.48 |
| 120W | 28 | 15.05 | 0.302 | 0.71 |
| 109W | 28 | 12.95 | 0.249 | 0.24 |
| 129W | 28 | 12.05 | 0.232 | 0.16 |
| 127W | 28 | 10.85 | 0.209 | 0.17 |
| 131W | 28 | Void, secondary flaw | | |

*Based on the maximum load of the fatigue cycle.

The method of analysis employed in this program was that proposed by Forman, Kearney, and Engle⁽¹⁾ in the form

$$\frac{d(a/Q)}{dN} = \frac{C(\Delta K_{II})^3}{(1-R)(K_{Ic}) - \Delta K_{II}} \quad (16)$$

where ΔK_{II} = stress-intensity factor range, $K_{max} - K_{min}$, $\text{ksi} \sqrt{\text{in.}}$

R = ratio K_{min} to $K_{max} = K_{min}/K_{max}$

K_{Ic} = critical stress-intensity factor, $\text{ksi} \sqrt{\text{in.}}$

C = constant = $5 \cdot 10^{-15}$ for Inconel 718.

This equation implies a unique relationship between the stress-intensity factor and the fatigue-crack propagation rate for a given environment and is therefore independent of the stress level per se.

To determine the validity of Equation 16, the data for the parent material tested in liquid hydrogen and in liquid oxygen were plotted as shown in Figure 22. Also shown in Figure 22 are the curves predicted by Equation 16 for the environments of liquid hydrogen ($K_{Ic} = 94.5 \text{ ksi} \sqrt{\text{in.}}$) and liquid oxygen ($K_{Ic} = 100.1 \text{ ksi} \sqrt{\text{in.}}$). From Figure 22,

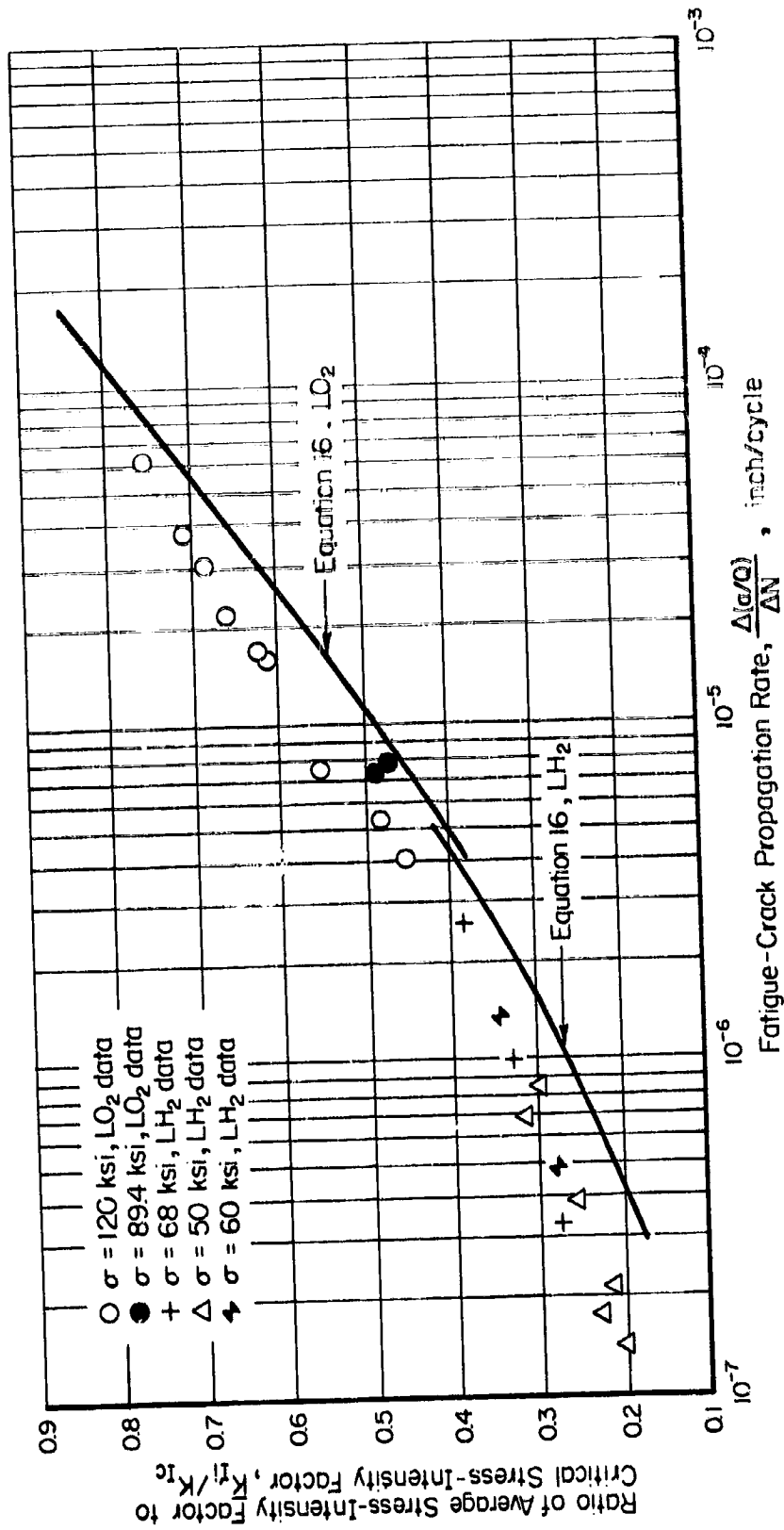


FIGURE 22. MEASURED FATIGUE-CRACK PROPAGATION RATES FOR PARENT INCONEL 718 TESTED IN LIQUID OXYGEN AND LIQUID HYDROGEN, $R = 0$

the predicted curves are found to parallel the basic parent material data over the entire range $0.2 \leq K_{II}/K_{IC} \leq 0.8$. While the fit of Equation 16 is generally good, the fact that the curve and the data are parallel indicate that a more precise determination of the experimental constant, C, will shift the curve to the left and further improve the accuracy of Equation 16. For example, a value of $C = 3 \cdot 10^{-15}$ would result in a better fit of Equation 16 to the parent material data. However, as will be shown in the following paragraphs, the constant $C = 5 \cdot 10^{-15}$ results in an excellent fit for the weld material data, so a change in the constant C does not appear warranted. Therefore, it can be stated that Equation 16 predicts conservative fatigue-crack propagation rates for the parent material.

As previously discussed, the weld material fatigue tests in liquid oxygen had been conducted at various ratios of K_{II}/K_{IC} so selected to produce failure in the range 1 to 500 cycles. The fatigue-crack propagation rate was determined by replotting the data from Table 21 as shown in Figure 23 where, instead of the ratio K_{II}/K_{IC} , the initial flaw size is plotted versus cycles to failure. The resulting curve was then differentiated at arbitrary values of a/Q , the slope, $\Delta(a/Q)/\Delta N$, being the fatigue-crack propagation rate for that particular initial value of a/Q . In order that these fatigue-crack propagation rates could be related to the appropriate K_{II}/K_{IC} value, the data in Table 21 was again plotted as the $\sqrt{a/Q}$ versus K_{II}/K_{IC} , as shown in Figure 24. Note that the value of K_{II}/K_{IC} , shown in Figure 24, includes the magnification factor, M_k . Thus, using Figure 24, the values of $\Delta(a/Q)/\Delta N$ obtained from Figure 23 could be related to K_{II}/K_{IC} for a specific initial value of a/Q . The results of such an analysis are presented in Table 33 for five arbitrary sets of a/Q values over the range of weld material data from the liquid oxygen tests.

TABLE 33. COMPUTED FATIGUE-CRACK PROPAGATION RATES FOR WELDED INCONEL 718 TESTED IN LIQUID OXYGEN, $R = 0$, $K_{IC} = 52.2 \text{ ksi}\sqrt{\text{in.}}$; MAXIMUM STRESS = 89.4 ksi

| Ratio Initial Stress-Intensity Factor to Critical Stress-Intensity Factor, K_{II}/K_{IC} | Fatigue Crack Propagation Rate as Determined From Figure 23, $\frac{\Delta(a/Q)}{\Delta N}$ $\mu\text{in./cycle}$ |
|--|---|
| 0.75 | 32.5 |
| 0.80 | 37.5 |
| 0.85 | 44.0 |
| 0.90 | 55.0 |
| 0.95 | 62.5 |

The fatigue-crack propagation rates for the weld material in liquid hydrogen and in liquid oxygen are plotted in Figure 25. Since $K_{IC} = 52.0 \text{ ksi}\sqrt{\text{in.}}$ in liquid oxygen and $52.2 \text{ ksi}\sqrt{\text{in.}}$ in liquid hydrogen, a value of $K_{IC} = 52.1 \text{ ksi}\sqrt{\text{in.}}$ was used in Equation 16 and a common curve was plotted for both the liquid-oxygen and liquid-hydrogen data. The agreement of the fatigue-crack propagation rates predicted by Equation 16 with those found experimentally is excellent. Therefore, it appears that Equation 16 is applicable for use in predicting the fatigue-crack propagation rates in welded and parent Inconel 718 sheet material tested in liquid hydrogen and in liquid oxygen.

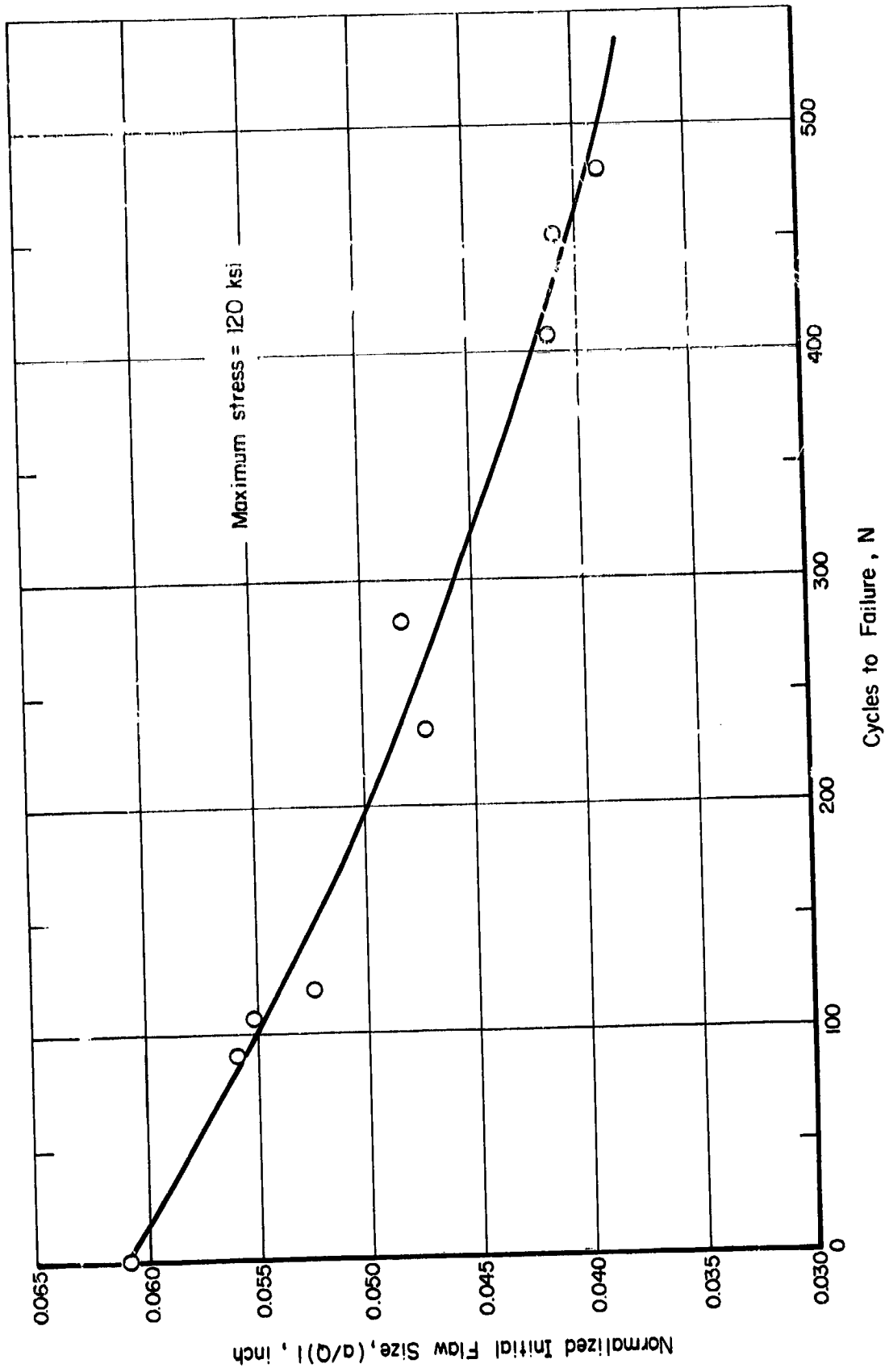


FIGURE 23. ALTERNATE PRESENTATION OF THE FATIGUE RESULTS FOR WELDED INCONEL 718 TESTED IN LIQUID OXYGEN, R = 0

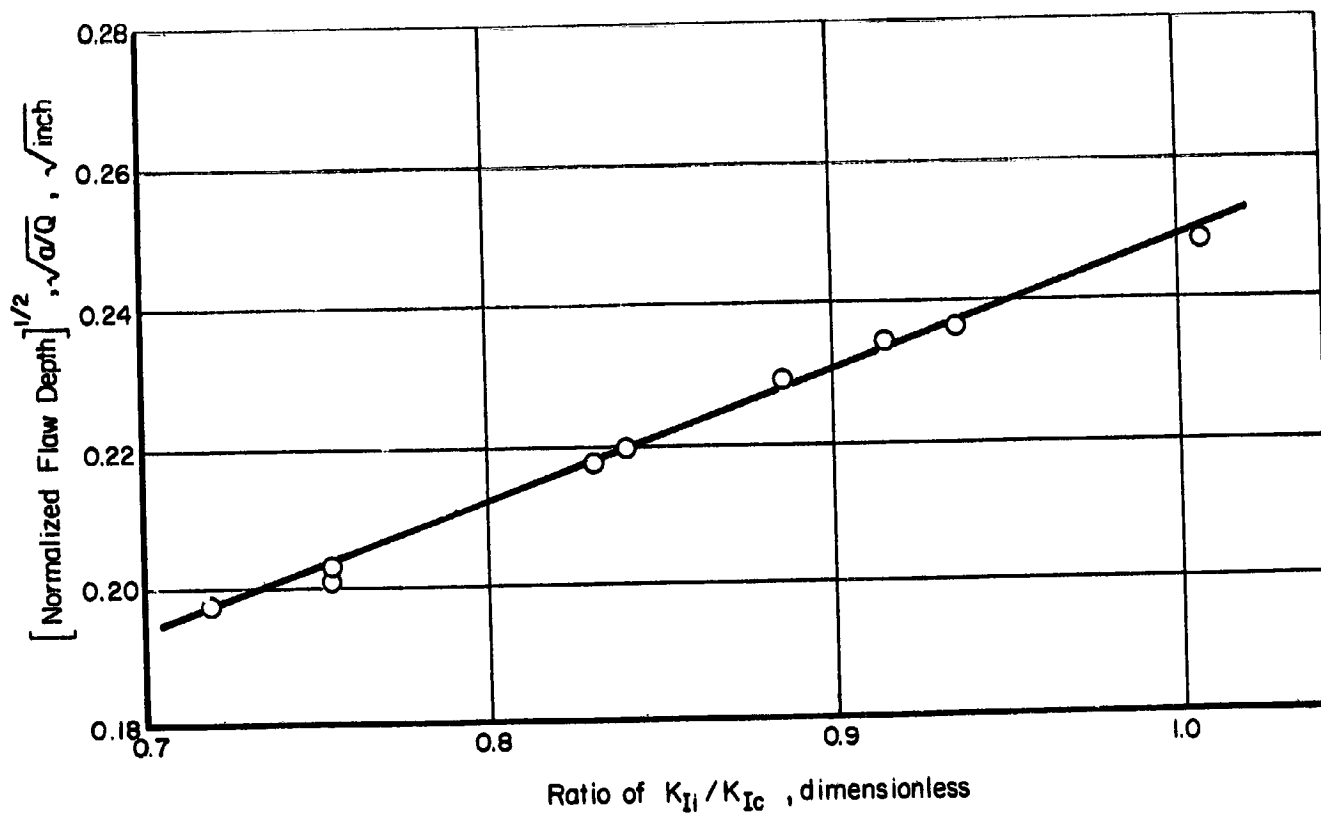


FIGURE 24. NORMALIZED FLAW DEPTH VERSUS K_{Ii}/K_{Ic} FOR WELDED INCONEL 718 SPECIMENS FATIGUE TESTED IN LIQUID OXYGEN

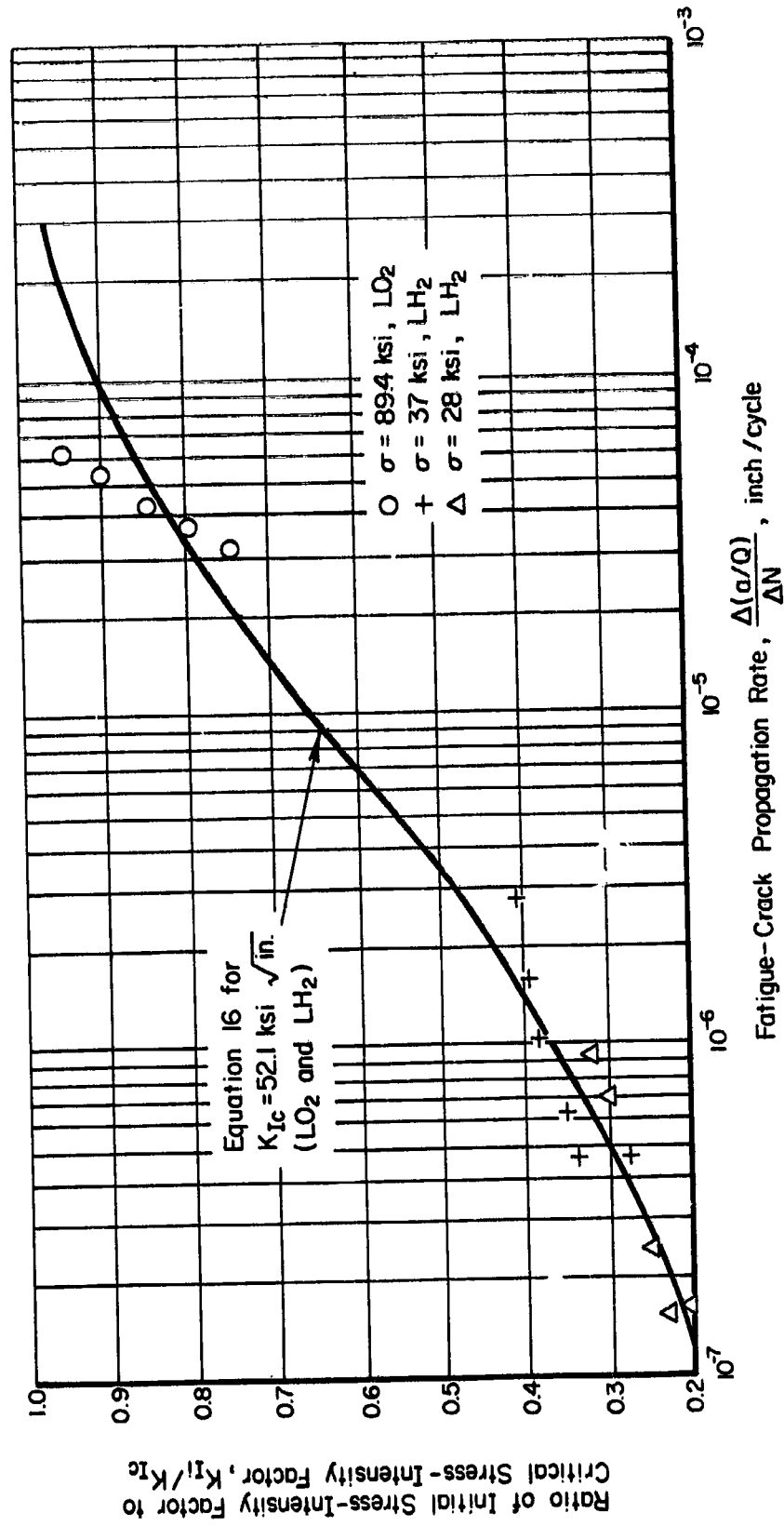


FIGURE 25. FATIGUE-CRACK PROPAGATION RATES FOR WELDED INCONEL 718 TESTED IN LIQUID OXYGEN AND LIQUID HYDROGEN, $R = 0$

6.6 Fatigue-Crack Propagation Rates Under High Mean-Stress Conditions

In this portion of the fatigue program, two welded specimens with the flaw at the center of weld were fatigue-cycled in liquid oxygen under the following conditions: stress = 72 ± 8 ksi, $0.55 \leq K_{II}/K_{IC} \leq 0.59$ (based on maximum load). These tests were designed to simulate the effect of pressure fluctuations in a pressure vessel on an initial flaw that is slightly below the size necessary for flaw growth under sustained load. The combination of sustained load and small superimposed cyclic load would provide a more realistic assessment of the true loading conditions on a vessel in service. Analysis of these data, shown in Table 34, yielded average fatigue-crack propagation rates of 7.5 and 3.5 μ inch/cycle. However, the fatigue-crack propagation rate predicted by Equation 16 for these conditions is only 0.21 μ inch/cycle. The higher measured fatigue-crack propagation rates indicate that pressure fluctuations near the operating pressure may produce significant flaw-growth during the life of the tank. A further study of the fatigue-crack propagation rates under high mean and small alternating loads is recommended to determine the severity of this problem.

TABLE 34. HIGH MEAN-LOAD FATIGUE-CRACK-PROPAGATION RESULTS
FOR WELDED INCONEL 718 TESTED IN LIQUID OXYGEN,
STRESS = 72 ± 8 ksi, $K_{IC} = 52.0$ ksi/ $\sqrt{\text{in.}}$

| Specimen Number | Average Maximum Stress- Intensity Factor,* | | Fatigue-Crack Propagation Rate, $\frac{\Delta(a/Q)}{\Delta N}$ |
|--------------------|--|-----------------------|--|
| | \bar{K}_{II} ksi/ $\sqrt{\text{in.}}$ | \bar{K}_{II}/K_{IC} | $\mu\text{in.}/\text{cycle}$ |
| 132W | 29.75 | 0.57 | 7.5 |
| 131W | 29.25 | 0.56 | 3.5 |

*Based on the maximum load during the fatigue cycle.

7.0 PHASE II TEST RESULTS

7.1 Tensile Tests Results

The parent material tensile specimens in Groups B and H were taken from a location 7 inches from the vessel pole, those in Groups C and G from a location 45 degrees from the pole, those in Groups D and F from a location 6 inches from the girth weld, and the welded specimens in Group E from the girth weld. All specimens were oriented parallel to a line from pole to pole of the vessel.

The results of the room-temperature and liquid-hydrogen tensile tests are presented in Tables 35 and 36, respectively. These tensile test results show no significant variation in the tensile properties for the specimens taken from various locations in the pressure vessel. However, the parent vessel material exhibits generally lower yield and ultimate strengths but higher elongations than had been observed for the sheet material. This is shown in the following tabulation:

| <u>Material</u> | <u>Temperature, F</u> | <u>Average Yield Strength, psi</u> | <u>Average Ultimate Strength, psi</u> | <u>Elongation in 1 Inch, percent</u> |
|-----------------|---------------------------|--|---|--|
| Parent Sheet | RT | 176,000 | 202,700 | 26.0 |
| Parent Vessel | RT | 167,000 | 197,300 | 27.7 |
| Parent Sheet | -423 | 211,000 | 283,700 | 28.0 |
| Parent Vessel | -423 | 207,800 | 279,700 | 30.5 |
| Welded Sheet | RT | 171,300 | 201,700 | 11.0 |
| Welded Vessel | RT | 151,000 | 194,200 | 7.2 |
| Welded Sheet | -423 | 212,700 | 240,300 | 5.0 |
| Welded Vessel | -423 | 213,000 | 272,300 | 6.0 |

Similarly, the room temperature yield strength, ultimate strength, and elongation are also significantly lower at room temperature for the welded vessel material than those found for the welded sheet material. However, in liquid hydrogen the ultimate strength of the welded vessel material is substantially higher than that of the welded sheet material, the yield strengths and elongations being approximately equal. These slight variations in tensile properties are not unexpected, however, considering the different type of mechanical working received by the vessel material during fabrication.

7.2 Fracture Test Results

The uncorrected fracture test data for the welded pressure vessel specimens tested in liquid oxygen and liquid hydrogen are presented in Tables 37 and 38. The fracture values corrected for the simple pin-end condition employed are presented in Table 39. Examination of Table 39 shows the average value of K_O (at the crack tip) of

TABLE 35. ROOM-TEMPERATURE TENSILE TEST RESULTS FOR PRESSURE VESSEL MATERIAL

| Specimen Number | Thickness, inch | Weld Thickness, inch | Width, inch | 0.2 Percent Yield Strength, psi | Ultimate Tensile Strength, psi | Elongation in 1-inch Gage Length, percent |
|-----------------|-----------------|----------------------|-------------|---------------------------------|--------------------------------|---|
| B-1 | 0.1340 | | 0.5000 | 163,000 | 198,000 | 29.0 |
| B-2 | 0.1360 | | 0.4995 | 163,000 | 197,000 | 28.0 |
| B-3 | 0.1360 | | 0.5000 | 164,000 | 197,000 | 30.0 |
| B-4 | 0.1350 | | 0.4995 | 166,000 | 197,000 | 28.0 |
| C-1 | 0.1395 | | 0.4995 | 172,000 | 200,000 | 28.0 |
| C-2 | 0.1385 | | 0.4990 | 164,000 | 195,000 | 32.5 |
| C-3 | 0.1385 | | 0.4990 | 167,000 | 198,000 | 30.0 |
| C-4 | 0.1370 | | 0.4995 | 166,000 | 197,000 | 27.0 |
| D-1 | 0.1290 | | 0.4990 | 178,000 | 199,000 | 27.0 |
| D-2 | 0.1245 | | 0.4990 | 169,000 | 195,000 | 23.0* |
| F-3 | 0.1280 | | 0.4996 | 164,000 | 196,000 | 27.0 |
| D-4 | 0.1275 | | 0.4990 | 175,000 | 198,000 | 28.0 |
| E-4 | 0.1410 | 0.1685 | 0.5000 | 165,000 | 199,000 | 8.0 |
| E-7 | 0.1415 | 0.1725 | 0.5000 | 150,000 | 199,000 | 10.0 |
| E-9 | 0.1410 | 0.1695 | 0.5000 | 138,000 | 190,000 | 6.0 |
| E-12 | 0.1390 | 0.1670 | 0.5003 | 151,000 | 189,000 | 5.0 |

Note: Weld specimen stresses based on parent metal areas.

*Specimen had measurable taper on thickness, failed at minimum section.

TABLE 36. TENSILE TEST RESULTS FOR PRESSURE VESSEL MATERIAL IN LIQUID HYDROGEN (-423 F)

| Specimen Number | Thickness, inch | Weld Thickness, inch | Width, inch | 0.2 Percent Yield Strength, psi | Ultimate Tensile Strength, psi | Elongation in 1-inch Gage Length, percent |
|-----------------|-----------------|----------------------|-------------|---------------------------------|--------------------------------|---|
| G-1 | 0.1310 | | 0.4982 | 201,000 | 281,000 | 30 |
| G-2 | 0.1325 | | 0.4988 | 208,000 | 280,000 | 30 |
| G-3 | 0.1332 | | 0.4982 | 211,000 | 280,000 | 30 |
| G-4 | 0.1320 | | 0.4990 | 204,000 | 280,000 | 32 |
| H-1 | 0.1365 | | 0.4978 | 203,000 | 281,000 | 35 |
| H-2 | 0.1335 | | 0.4975 | 205,000 | 281,000 | 30 |
| H-3 | 0.1365 | | 0.4995 | 205,000 | 280,000 | 30 |
| H-4 | 0.1362 | | 0.4975 | 206,000 | 280,000 | 34 |
| F-1 | 0.1220 | | 0.5002 | 217,000 | 285,000 | 20* |
| F-2 | 0.1265 | | 0.5000 | 212,000 | 278,000 | 27 |
| D-3 | 0.1270 | | 0.4994 | 212,000 | 284,000 | 29 |
| F-4 | 0.1290 | | 0.4970 | 209,000 | 266,000 | 20* |
| E-14 | 0.1140 | 0.1630 | 0.5005 | 215,000 | 274,000 | 5 |
| E-17 | 0.1150 | 0.1682 | 0.4990 | 206,000 | 287,000 | 7 |
| E-19 | 0.1160 | 0.1665 | 0.5012 | 218,000 | 286,000 | 6 |

Note: Weld specimen stresses based on parent metal thickness.

*Low elongation due to failure near gage length bench mark.

TABLE 37. UNCORRECTED INCONEL 718 VESSEL WELD MATERIAL FRACTURE RESULTS IN LIQUID OXYGEN

| Spec. No. | Spec. Dim., inch | | Loads, kips | | | Stresses, ksi | | | Flaw Size, inch | | Stress-Intensity Factors, ksi-sqrt (inch) | | | | | | | | | | |
|-----------|------------------|-------|-------------|-------|------|---------------|-------|-----|-----------------|--------|---|----------------|------|--------------|------|----------------|-----|------|------|-----|------|
| | T | W | P1 | P2 | P3 | S1 | S2 | S3 | A | 2C | Area | PHI Correction | | Q Correction | | MSC Correction | | | | | |
| | | | | | | | | | | | | K1 | K2 | K3 | K1 | K2 | K3 | | | | |
| 1E | 0.127 | 0.998 | 0.1268 | 16.55 | 0.00 | 10.75 | 130.5 | 0.0 | 84.8 | 0.0448 | 0.2114 | 0.00744 | 46.3 | 0.0 | 30.0 | 47.8 | 0.0 | 30.5 | 49.8 | 0.0 | 31.7 |
| 3E | 0.122 | 1.000 | 0.1220 | 12.05 | 0.00 | 8.10 | 98.8 | 0.0 | 66.4 | 0.0624 | 0.2927 | 0.01434 | 41.3 | 0.0 | 27.7 | 42.0 | 0.0 | 28.0 | 46.2 | 0.0 | 30.8 |
| 5E | 0.126 | 0.997 | 0.1259 | 13.00 | 0.00 | 8.75 | 103.3 | 0.0 | 69.5 | 0.0580 | 0.3238 | 0.01475 | 43.0 | 0.0 | 29.0 | 44.0 | 0.0 | 29.2 | 47.6 | 0.0 | 31.7 |

TABLE 38. UNCORRECTED INCONEL 718 VESSEL WELD MATERIAL FRACTURE RESULTS IN LIQUID HYDROGEN

| Spec. No. | Spec. Dim., inch | | Loads, kips | | | Stresses, ksi | | | Flaw Size, inch | | Stress-Intensity Factors, ksi-sqrt (inch) | | | | | | | | | | |
|-----------|------------------|-------|-------------|-------|------|---------------|-------|-----|-----------------|--------|---|----------------|------|--------------|------|----------------|-----|------|------|-----|------|
| | T | W | P1 | P2 | P3 | S1 | S2 | S3 | A | 2C | Area | PHI Correction | | Q Correction | | MSC Correction | | | | | |
| | | | | | | | | | | | | K1 | K2 | K3 | K1 | K2 | K3 | | | | |
| 6E | 0.124 | 0.902 | 0.1119 | 14.35 | 0.00 | 8.40 | 128.2 | 0.0 | 75.1 | 0.0491 | 0.2111 | 0.00814 | 46.6 | 0.0 | 27.3 | 47.9 | 0.0 | 27.5 | 50.2 | 0.0 | 28.9 |
| 20E | 0.117 | 0.997 | 0.1166 | 10.60 | 0.00 | 7.80 | 90.9 | 0.0 | 66.9 | 0.0629 | 0.3236 | 0.01599 | 38.8 | 0.0 | 28.6 | 39.4 | 0.0 | 28.8 | 44.1 | 0.0 | 32.2 |
| 8E | 0.119 | 0.999 | 0.1184 | 12.85 | 0.00 | 7.50 | 108.5 | 0.0 | 63.4 | 0.0599 | 0.2832 | 0.01332 | 44.5 | 0.0 | 26.0 | 45.4 | 0.0 | 26.2 | 49.9 | 0.0 | 28.7 |

TABLE 39. WELDED PRESSURE VESSEL MATERIAL FRACTURE RESULTS CORRECTED FOR CURVATURE

| Test Temperature | Specimen Number | Axial Stress, σ_A , ksi | Stress Ratio, σ_B/σ_A | Maximum Surface Stress, $\sqrt{A^2 + B^2}$, ksi | $K_{\pi/2}$ Corrected at Crack Tip, ksi $\sqrt{\text{in.}}$ | $K_{\pi/2}$ Corrected at Surface, ksi $\sqrt{\text{in.}}$ |
|------------------|-----------------|--------------------------------|-----------------------------------|--|---|---|
| -297 | 1E | 130.5 | 0.853 | 241.8 | 62.5 | 83.8 |
| -297 | 3E | 98.8 | 1.068 | 204.4 | 61.0 | 85.7 |
| -297 | 5E | 103.3 | 1.054 | 212.2 | 62.6 | 87.7 |
| -423 | 6E | 128.2 | 0.849 | 237.0 | 63.0 | 84.3 |
| -423 | 20E | 90.9 | 1.114 | 192.1 | 59.0 | 83.4 |
| -423 | 8E | 108.5 | 0.958 | 212.4 | 64.1 | 88.1 |

approximately $62 \text{ ksi}\sqrt{\text{in.}}$ and a $K_{\pi/2}$ (at the specimen surface) of approximately $85.5 \text{ ksi}\sqrt{\text{in.}}$ for both the liquid oxygen and the liquid hydrogen results. Both of these values are considerably higher than the value $K_{IC} = 52.1 \text{ ksi}\sqrt{\text{in.}}$ found for the welded sheet material specimens tested in liquid oxygen and in liquid hydrogen.

In evaluating the corrected data, it should be noted that, with one exception (Specimen No. 20E), the concave surface stresses at fracture are in excess of the material yield strength. Thus, a basic premise of fracture mechanics has been violated; namely, that nominally computed stresses be elastic, or that

$$\sigma_{\text{nominal}} \leq \sigma_{ys}$$

However, because of the apparent load-bearing capacity of these specimens with a flaw, there is considerable confidence that the pressure vessel welded material is of at least equivalent and probably superior fracture resistance to that of the welded sheet material.

7.3 Fatigue-Crack Propagation Results

The average fatigue-crack propagation rate was determined in a manner similar to that described in sub-section 6.5. Results are presented in Table 40. Since the normalized flaw depth, a/Q , is the parameter on which the crack growth rate was measured, the growth rates were examined in terms of the stress-intensity factors at the crack tip; i. e., in terms of K_{I0} . The resulting plot of (\bar{K}_{I0}/K_0) versus the measured crack-propagation rate, $\frac{\Delta(a/Q)}{\Delta N}$, is presented in Figure 26.

TABLE 40. FATIGUE-CRACK PROPAGATION RESULTS FOR WELDED VESSEL MATERIAL TESTED IN LIQUID OXYGEN (-297 F) AND IN LIQUID HYDROGEN (-423 F), $R = 0$

| Specimen Number | Temp, F | Maximum Nominal Stress σ , ksi | Average K_{I0} , Corrected at Crack Tip, $\text{ksi}\sqrt{\text{in.}}$ | Average $K_{I\pi/2}$, Corrected at Surface, $\text{ksi}\sqrt{\text{in.}}$ | \bar{K}_{I0}/K_0^* at Crack Tip | $\bar{K}_{I\pi/2}/K_{\pi/2}^{**}$ at Surface | Average Crack-Propagation Rate, $\frac{\Delta(a/Q)}{\Delta N}$, $\mu\text{in./cycle}$ |
|-----------------|---------|---------------------------------------|--|--|-----------------------------------|--|--|
| E-10 | -297 | 24 | 19.1 | 28.6 | 0.31 | 0.33 | 0.48 |
| E-13 | -297 | 41 | 32.0 | 46.7 | 0.52 | 0.55 | 1.67 |
| E-15 | -297 | 57 | 41.2 | 60.4 | 0.66 | 0.71 | 7.40 |
| E-11 | -423 | 28 | 22.0 | 32.7 | 0.36 | 0.38 | 0.42 |
| E-16 | -423 | 37 | 28.9 | 42.8 | 0.48 | 0.50 | 0.57 |
| E-18 | -423 | 16 | 12.0 | 17.6 | 0.19 | 0.21 | 0.06 |

*Using K_0 at crack tip = $62.0 \text{ ksi}\sqrt{\text{in.}}$ as average for both -297 F and -423 F.

**Using $K_{\pi/2}$ at surface = $85.5 \text{ ksi}\sqrt{\text{in.}}$ as average for both -297 F and -423 F.

As was previously shown, the welded sheet material fatigue-crack propagation rates were predicted quite closely by Equation (16). For comparison, Equation (16) is plotted in Figure 26 and shows the predicted growth rates to be slightly higher than those observed. Thus, the sheet material crack-propagation data and Equation (16) give a conservative estimate of the actual vessel material fatigue-crack propagation behavior. If the constant, C , is experimentally adjusted, a better fit of the vessel material data can be obtained for $C = 2 \cdot 10^{-15}$ as shown in Figure 26.

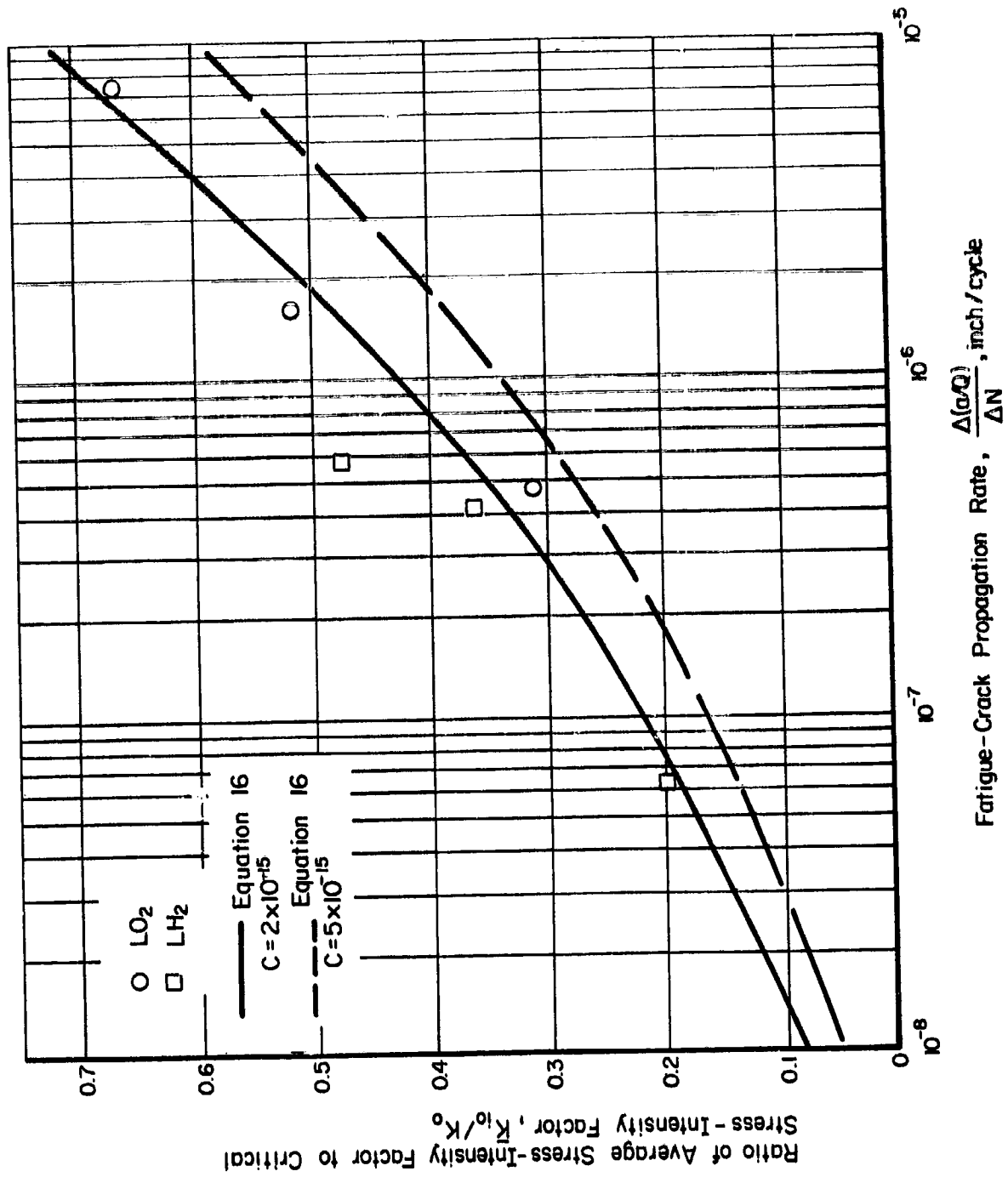


FIGURE 26. FATIGUE-CRACK PROPAGATION RATES FOR WELDED VESSEL MATERIAL BASED ON THE CORRECTED STRESS-INTENSITY FACTOR AT $\alpha = 0$, $K_0 = 62.0 \text{ ksi}\sqrt{\text{in.}}$.

8.0 CONCLUDING DISCUSSION

The results presented in Phase I provide the necessary fracture, fatigue-crack propagation, and sustained-load flaw growth data to allow a typical fracture mechanic analysis of a pressure vessel to be conducted based on the sheet material results. However, the spot-check results obtained in Phase II for actual vessel material raise one important question.

Normally the higher K_{Ic} values obtained for the vessel material fracture tests would be considered advantageous since it indicates a greater flaw tolerance in the vessel material. However, in the context of proof tests results, this greater flaw tolerance (higher K_{Ic}) exhibited by the vessel material is not as advantageous as it would first appear. For example, consider the weld material for the case of a proof test to a stress level σ_{proof} as shown in Figure 27. The higher value of K_{Ic} exhibited by the vessel material will result in a larger remaining flaw $(a/Q)_v$, than would be predicted from the sheet material results, $(a/Q)_s$. Thus, for a given proof cycle, a surviving vessel could contain a larger flaw than would be predicted by an analysis based on the sheet material results.

This problem may or may not be serious, depending upon the value of K_{th}/K_{Ic} that can be tolerated when the vessel enters service. If, for example, the ratio K_{th}/K_{Ic} is essentially equivalent for both the sheet and vessel material, then a larger flaw could be tolerated in the vessel material (higher K_{Ic}) than would be predicted from the sheet material results. In this case, the problem would not be too severe. However, as shown by the variation in tensile and fracture results for the vessel and sheet material, the difference in processing can have a significant effect on the properties. If, instead of the ratio K_{th}/K_{Ic} being constant, the value of K_{th} is a constant for the vessel and sheet material, then the flaw growth allowable during assembly and service would be affected.

This potential problem can only be resolved by conducting a spot check of the sheet material sustained-load flaw growth results with the vessel material. In this manner a consistent analysis based on vessel material results could be obtained.

It also should be pointed out, that the analysis presented here has not dealt with the possibility of slow flaw growth during the proof (or fracture) test. Such an occurrence has been shown to exist⁽⁵⁾ in other thin materials, and should be investigated for this material before the true significance of K_{Ic} values based on maximum load can be determined.

One additional factor also should be reiterated: the unexpectedly high fatigue-crack propagation rate observed under the high mean load condition. These results cast serious doubt on the validity of the assumption that pressure fluctuations in service would not produce significant flaw growth. This aspect should be studied further.

The results, comments, and recommendations presented in this report are intended to provide a more detailed insight into the flaw growth behavior of Inconel 718 sheet and vessel material. These results, combined with data from other sources will permit a detailed fracture mechanics analysis of Inconel 718 pressure vessels to be conducted by the controlling governmental agency. It is to this aim these results are presented.

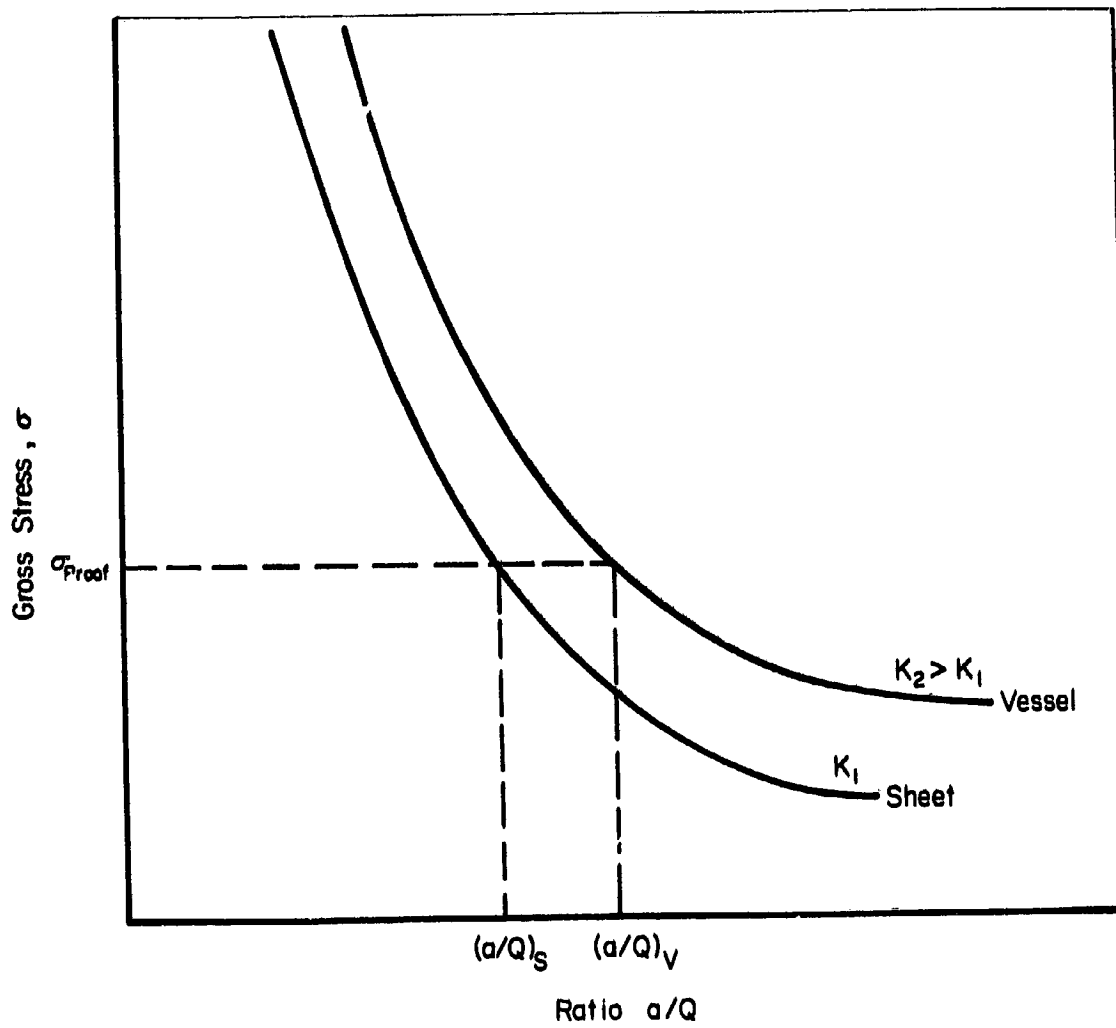


FIGURE 27. SCHEMATIC OF EFFECT OF THE CRITICAL STRESS-INTENSITY FACTOR ON THE MAXIMUM POSSIBLE FLAW SIZE AFTER PROOF

References

- (1) Forman, R. G., Kearney, V. E., and Engle, R. H., "Numerical Analysis of Crack Propagation in Cyclic-Loaded Structures", Transactions of the ASME, Journal of Basic Engineering, 459-464 (September, 1967).
- (2) Kobayashi, A. S., "On the Modification Factor of Deep Surface Flaws", Boeing SDRM No. 16 (December, 1965).
- (3) Glorioso, S. V., et al., "Lunar Module Pressure Vessel Operating Criteria Specification", SE-V-0024, NASA/MSC, Houston, Texas (October 25, 1968).
- (4) Smith F. W., "Stress Intensity Factors for a Semi-Elliptical Surface Flaw", Boeing SDRM No. 17 (August, 1966).
- (5) Hoepfner, D. W., Pettit, D. E., Feddersen, C. E., and Hylor, W. S., "Determination of Flaw Growth Characteristics of Ti-6Al-4V Sheet in the Solution-Treated and Aged Conditions", NASA CR-65811 (January 1, 1968).

APPENDIX A. ANALYSIS OF CURVATURE EFFECTS FOR
VESSEL-MATERIAL SPECIMENS

APPENDIX A. ANALYSIS OF CURVATURE EFFECTS FOR VESSEL-MATERIAL SPECIMENS

Introduction

Practical aspects of materials testing generally require that the test coupons cut from the curved surface of a pressure vessel be tested in uniaxial tension. Under axial loading of a coupon, the eccentricity inherent to curvature induces bending stress gradients through the thickness. These are greatly different from those relatively uniform, membrane hoop stresses anticipated in the design of the pressure vessels. Delineation of the stress gradient effects is made by evaluating the bending moment as an independent function of axial load and curvature. This dissociates axial and bending stresses as discrete components in evaluating specimen response. The bending stress component was verified by strain-differential measurement across the specimen thickness. Final application of the analysis was made by recoupling the axial and bending effects by superposition.

In the following paragraphs, an approximate analytical model is presented to relate the load, stress (or strain), and resultant material behavior observed in uniaxial curved-coupon tests with the corresponding behavior of the materials in a pressure vessel. The procedure was verified experimentally and then applied to the interpretation of the data from the tension and fracture tests and the related fatigue-crack growth results.

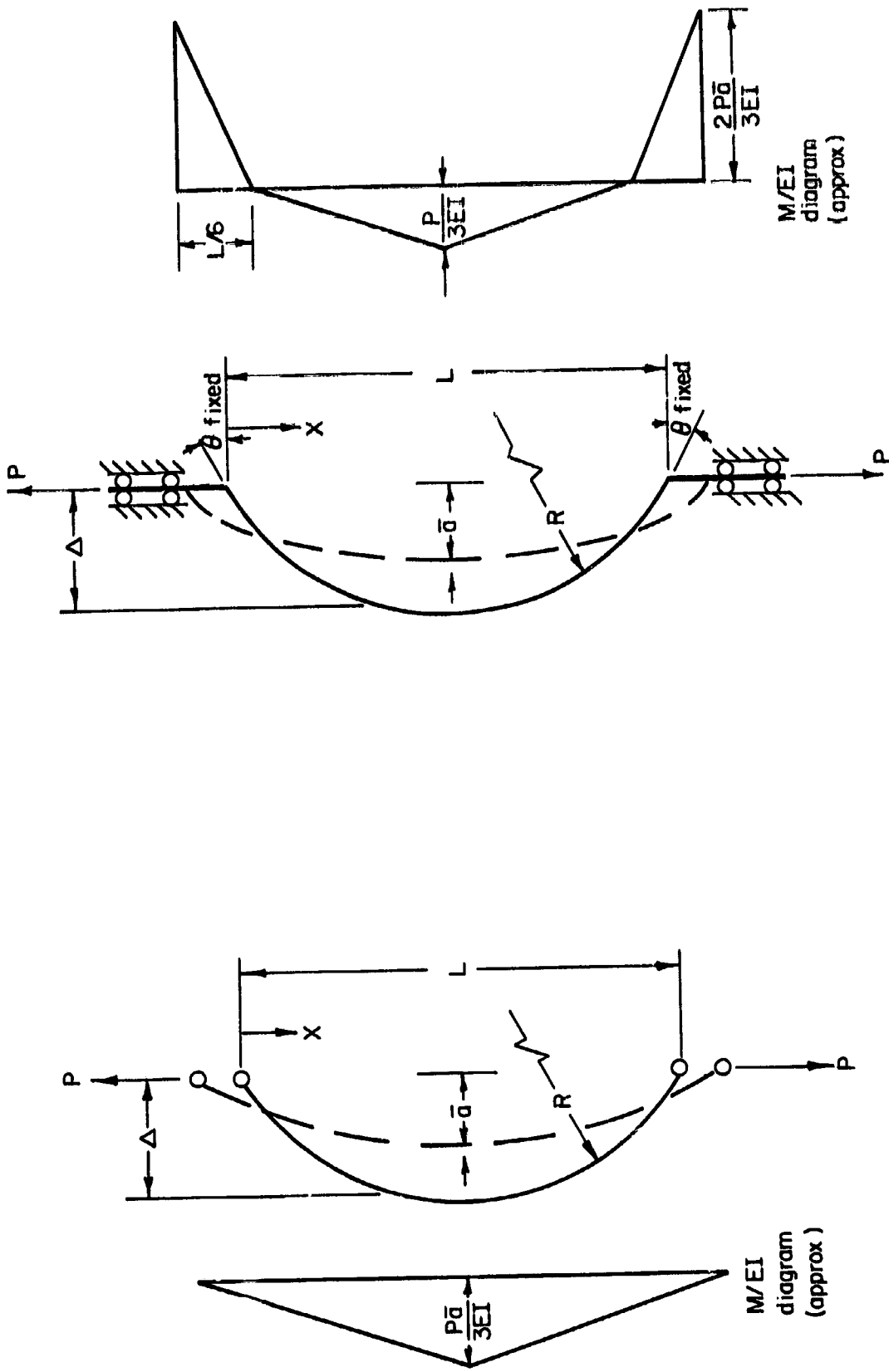
An Approximate Model of a Curved Tension Specimen

Consider the idealized tension specimens illustrated in Figure A-1. As the load is applied, the original specimen (solid line) extends to a configuration of less curvature (dashed line). The initial deflection, Δ , is reduced to an effective moment arm, \bar{a} . For a typical specimen of constant curvature, the initial deflection (load eccentricity, or "rise" of arc) can be approximated by

$$\Delta = L^2/8R \quad (A-1)$$

for small L/R ratios.

As the specimen extends under load, a lateral deflection occurs in which the mid-section of the specimen translates from an original position, Δ , to a new position, a , away from the load line. The resultant deflection ($\Delta - a$) is attributed to the bending distortion of the specimen, which may be evaluated by the moment-area theorems. Two cases typical of experimental fixturing conditions are illustrated in Figure A-1. Each has different end conditions and will be separately analyzed and verified in the following subsections.



(a) Free ends

(b) Rotationally fixed ends

FIGURE A-1. IDEALIZED FIXTURE ARRANGEMENTS FOR CURVED SPECIMENS

Case 1 - Free Ends

The free (or pin) ended curved coupon idealized in Figure A-1(a) is typical of the simplest method of tension testing. Since the specimen ends are free to rotate, there is no bending restraint at the fixture. Flexure in the specimen is proportional to the local displacement from the load line, and peaks at the midsection. Applying the moment-area theorem and assuming a linear M/EI distribution,

$$\Delta - a = \int_0^{L/2} \frac{Mx}{EI} dx \cong \int_0^{L/2} \frac{P(2ax/L)x}{EI} dx = \frac{(Pa)L^2}{12EI} , \quad (A-2)$$

where P = load
 M = moment
 E = Young's modulus
 I = moment of inertia of the section.

Since the assumption of linearity in the M/EI diagram is not precise, the numerical coefficient, 12, in the denominator is allowed to float at a value k_1 as an empirical fitting factor. Thus,

$$\Delta - \bar{a} = \frac{(Pa)L^2}{k_1 EI} .$$

Transposing and collecting terms, the effective moment arm at the midsection may be approximated as

$$\bar{a} = \Delta / \left(1 + \frac{PL^2}{k_1 EI} \right) \cong (L^2/8R) / \left(1 + \frac{PL^2}{k_1 EI} \right) . \quad (A-3)$$

It also follows that the maximum moment to be superimposed on the nominal axial loading is

$$M = P\bar{a} = (PL^2/8R) / (1 + PL^2/k_1 EI) . \quad (A-4)$$

Verification of this analytical model was obtained by measuring the strain differential through the thickness of tensile and fracture specimens. The total strain differential through the thickness may be calculated as twice the extreme fiber bending strain component,

$$2\epsilon_B = 2 \frac{Mc}{EI} = \frac{12M}{Ebt^2} = \frac{1.5/R}{\frac{Ebt^2}{PL^2} + \frac{12}{k_1 t}} . \quad (A-5)$$

Using Expression (A-5) with the geometric parameters,

| <u>Parameter</u> | <u>Specimen F-3</u> | <u>Specimen E-10</u> |
|----------------------|---------------------|----------------------|
| Modulus, E, psi | 29×10^6 | 29×10^6 |
| Width, b, inches | 0.996 | 0.9978 |
| Thickness, t, inches | 0.128 | 0.126 |
| Length, L, inches | 5.5 | 7.0 |
| Scalar factor, k_1 | 10.0 | 10.0 |

yields the following correlations:

| <u>Load, pounds</u> | <u>Strain Differential, microinches/inch</u> | | | |
|---------------------|--|-------------------|----------------------|-------------------|
| | <u>Specimen F-3</u> | | <u>Specimen E-10</u> | |
| | <u>Measured</u> | <u>Calculated</u> | <u>Measured</u> | <u>Calculated</u> |
| 500 | 3260 | 3067 | 2890 | 2720 |
| 1000 | 4540 | 4465 | -- | 4070 |
| 2000 | 5700 | 5783 | 5640 | 5412 |
| 4000 | 6660 | 6784 | 6660 | 6481 |
| 6000 | 7150 | 7200 | 6765 | 6938 |
| 8000 | 7520 | 7427 | 6715 | 7192 |

Note that the recorded strains represent the bending strains only as measured by the difference in strain readings between gages located on each side of the specimen.

For the case of a tensile specimen, the bending moment $M = Pa$ converges asymptotically to a value of $K_1 EI/8R$ as shown schematically in Figure A-2.

Beyond this convergence point, nonlinearities in the stress-strain curve must be attributed to the material behavior and not to specimen curvature. Thus, if after initial nonlinearities in the load record due to specimen straightening, there is a graphically detectable linear segment, as shown in Figure A-3, it can be stated that curvature effects have been bypassed or suppressed and the specimen is behaving in a linearly elastic fashion. It will continue to do so until the proportional limit is exceeded, at which time the nonlinearities that occur are due to material yielding. Thus, the 0.2 percent offset yield strength and the ultimate strength may be obtained in the conventional manner. Such a discernible segment was obtained in these tensile tests, the 80 percent convergence occurring at a nominal axial stress of $f_A = 50,000$ psi.

While much of this discussion has been implicitly based on an ideal elastic-plastic concept of material behavior, it is recognized that there are some second-order effects due to the strain hardening which have been neglected. However, the analysis presented here, while conservative, is meaningful. Further consideration of these second-order effects is considered beyond the scope of this program.

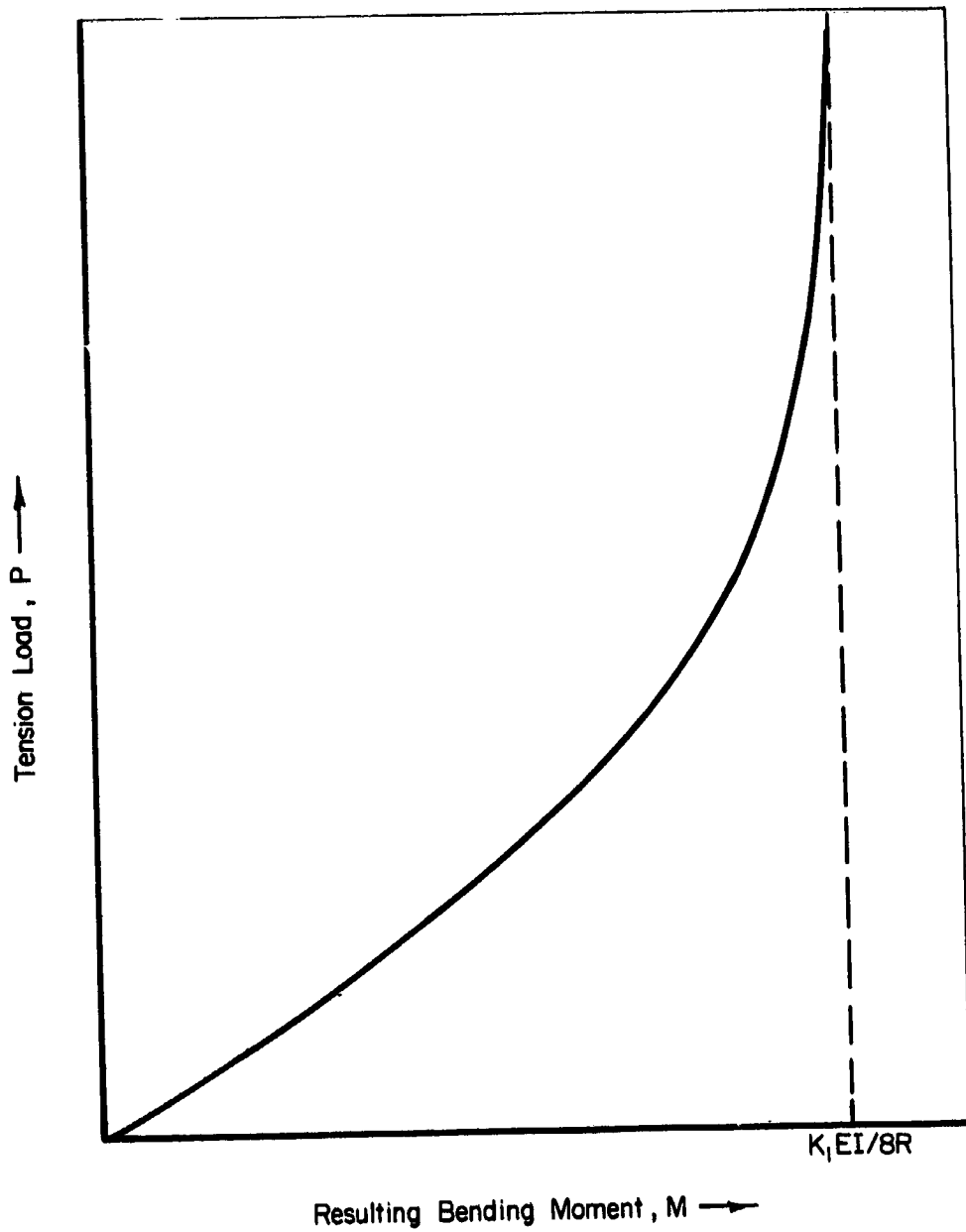


FIGURE A-2. RESULTING BENDING MOMENT IN A CURVED SPECIMEN
SUBJECTED TO TENSION LOADING

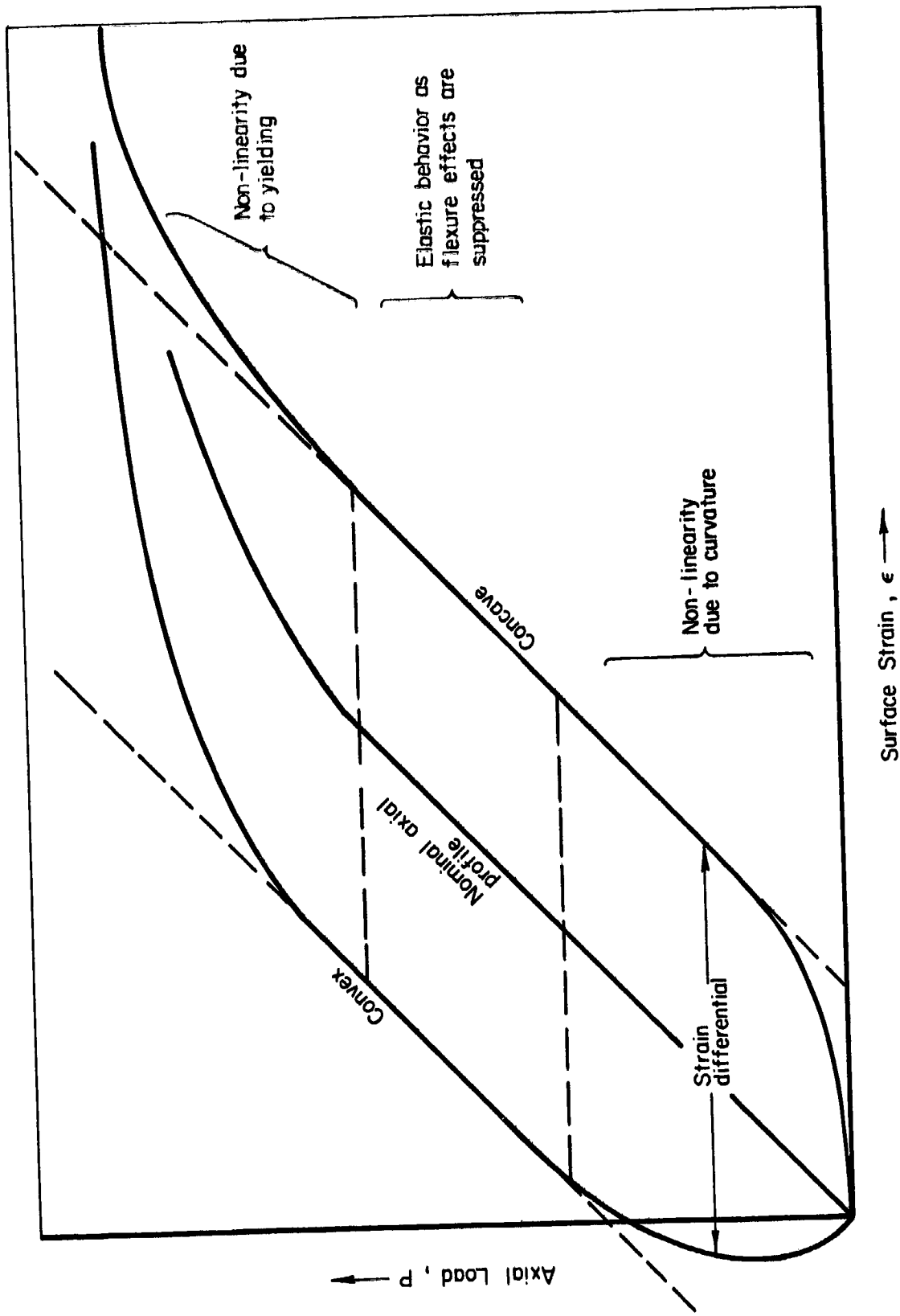


FIGURE A-3. LOAD-STRAIN PROFILE FOR CURVED SPECIMENS UNDER TENSION LOADING

Case 2 - Rotational Restraint at Ends

Fatigue-test specimens are usually tightly clamped in their gripping fixtures to avoid localized fretting. As a result, rotational restraint at the ends occurs as illustrated in Figure A-1(b). Again applying the moment-area theorem,

$$\Delta - \bar{a} = \int_0^{L/2} \frac{Mx}{EI} dx \approx \frac{PaL^2}{54EI} \quad (\text{A-6})$$

or approximately one-half of that obtained in Case 1. Again, recognizing that the assumption of discrete linearity in the M/EI diagram is not precise, a fitting factor, k_2 , is permitted for final empirical correlation such that

$$\Delta - \bar{a} \equiv \frac{PaL^2}{k_2EI} .$$

Transposing and collecting terms,

$$\bar{a} = \Delta / \left(1 + \frac{PL^2}{k_2EI} \right) = (L^2/8R) / \left(1 + \frac{PL^2}{k_2EI} \right) . \quad (\text{A-7})$$

Verification of this model was also obtained experimentally. Recalling that

$$M = \frac{P\bar{a}}{3}$$

at the midsection, the total strain gradient through the thickness is given by

$$2\epsilon_B = 2 \frac{Mc}{EI} = \frac{12M}{Ebt^2} = \frac{0.5/R}{\frac{Ebt^2}{PL^2} + \frac{12}{k_2t}} . \quad (\text{A-8})$$

Using this expression with the following geometry of Specimen E-10:

Modulus, $E = 29 \times 10^6$ psi

Width, $b = 0.9978$ inches

Thickness, $t = 0.126$ inches

Length, $L = 3.5$ inches (between grips in fatigue fixturing)

Scalar factor, $K_2 = 20$ (empirically selected for data fit),

the following correlation is obtained:

| <u>Load,</u> <u>pounds</u> | <u>Strain Differential,</u> <u>microinches/inch</u> | |
|-------------------------------|--|-------------------|
| | <u>Measured</u> | <u>Calculated</u> |
| 200 | 90 | 120 |
| 1200 | 935 | 637 |
| 2200 | 1075 | 1051 |
| 4200 | 1725 | 1675 |
| 6200 | 2180 | 2121 |

Thus the two models proposed here generally show good agreement with the experimentally measured strains.

APPENDIX B. LIST OF SYMBOLS

APPENDIX B. LIST OF SYMBOLS

- a = flaw depth
- σ = gross stress
- Q = Irwin plasticity correction = $\Phi^2 - 0.212 \left\{ \frac{\sigma}{\sigma_y} \right\}^2$
- Φ = elliptic integral of the second kind
- σ_y = 0.2 percent yield stress
- M_{kf} = Kobayashi's magnification factor for flaw depth
- M_{kp} = Kobayashi's plasticity correction.
- 2c = surface crack length of flaw
- t = specimen thickness
- M_k' = current NASA/MSK magnification factor
- M_k = prior NASA/MSK magnification factor
- P_1 = maximum load
- P_2 = pop-in load
- P_3 = 5 percent secant offset load
- K_{Ic} = critical stress-intensity factor based on maximum load
- K_a = axial load stress-intensity factor
- K_b = bending moment stress-intensity factor
- α = polar angle measured from the flaw axis of symmetry
- M_b = bending magnification factor
- σ_b = extreme fiber bending stress component
- σ_a = axial stress component
- E = modulus of elasticity
- K_{th} = threshold stress-intensity factor for sustained-load flaw growth
- K_{II} = stress intensity at the start of a test
- ΔK_{II} = stress-intensity factor range, $K_{max} - K_{min}$, ksi $\sqrt{in.}$
- R = ratio K_{min} to $K_{max} = K_{min}/K_{max}$
- C = constant
- K_o = stress-intensity factor to maximum flaw depth for curved specimen
- $K_{\pi/2}$ = stress-intensity factor at the surface for curved specimen
- \bar{K} = average stress intensity factor for a small amount of fatigue-crack growth
- Δ = initial deflection in a curved specimen under load
- \bar{a} = effective movement arm
- L = effective specimen length
- R = radius of curvature